DOCTOR OF PHILOSOPHY

Development of Novel Compact Laser Sources for Bio-Medical Applications

Alhazime, Ali

Award date:
2014

Awarding institution:
University of Dundee

DOCTOR OF PHILOSOPHY

Development of Novel Compact Laser Sources for Bio-Medical Applications

Ali Alhazime

2014

University of Dundee

-

Development of Novel Compact Laser Sources for Bio-Medical Applications

Ali Ahmed Alhazime

April 2014

A thesis submitted for the degree of Doctor of Philosophy, University of Dundee,

School of Engineering, Physics and Mathematics

For my parents and my wife

Table Contents

List of Figures

List of Tables

Acknowledgements

While working towards my PhD degree, I have been supported by many people without whom it work would not have been completed.

First and foremost I wish to thank my supervisor Professor Edik Rafailov for allowing me the opportunity to work in his group in Dundee and for his guidance, availability, advice, support and encouragement throughout these years.

Special thanks should go to Dr Ying Ding, whose lab I worked in. His support and friendship were invaluable to me and his knowledge of ultrafast quantum dot optical devices was a major driving force of this research. Thanks should also go to Gurmeet Kanda for his invaluable help.

Every member of the Photonics and Nanoscience research group in the School of Engineering, Physics and Mathematics, University of Dundee, contributed in many different ways to this work. Especially I want to make mention of Dr Daniil Nikitichev, Dr Ksenia Fedorova, Dr Mantas Butkus and Dr Ross Leyman.

Next, appreciative thanks go to the technical team of Gary Callon, Grant Kydd and Callum Moore.

As I was involved in an international project I had the opportunity to meet, to work with and to learn from the researchers from III-V lab, Innolume and the University of Sheffield.

I acknowledge the financial support of the EU "FAST-DOT" project.

On a personal note I wish to thank my parents and my wife for their unwavering support.

Declaration

I, Ali Alhazime, hereby certify that this thesis, which is approximately thirty three thousand words in length, has been written by me, that it is the record of work carried out by me and that it has not been submitted in any previous application for a higher degree.

Date Signature of candidate

I hereby certify that the candidate has fulfilled the conditions of the Resolution and Regulations appropriate for the degree of Doctor of Philosophy in the University of Dundee and that the candidate is qualified to submit this thesis in application for that degree.

Date Signature of supervisor

Abstract

The focus of this thesis relates to the development and characterisation of novel semiconductor based lasers sources tunable in the broad spectral ranges that are unattainable by conventional lasers due to a lack of suitable laser gain materials.

Within the first part, the broad gain spectrum from quantum dot (QD) materials is seen to be an appealing feature for the development of broadly tunable lasers, broadband amplifiers and ultra short pulse generation. As has been previously shown quantum-dot external-cavity passively mode-locked lasers (QD-ECMLLs) are excellent candidates for versatile ultra short pulse generation. This is due to the flexibility that anexternal-cavity mode-locking configuration can offer in terme of a broad tunability for both repetition rate and wavelength which could be achieved. Similarly quantum-dot semiconductor optical amplifiers (QD-SOA) are suitable for the broadband pulse power amplification.

Furthermore, master oscillator power amplifier (MOPA) picosecond optical pulse sources using all chirped QD structures were investigated using the MOPA system consisting of two parts, firstly QD-ECMLL and secondly a tilted taper QD-SOA. A further investigation involved a comparison between 1^{st}-order diffraction grating and 2^{nd}-order diffraction grating for this tunable QD-MOPA. The result found was the maximum fundamental

mode-locking (FML) wavelength tuning range. Nearly 100 nm (from 1187nm to 1283nm) wavelength tuning range was achieved under a 900 mA current applied to the gain chip with a 2^{nd}-order grating diffraction. Furthermore it was also demonstrated that the peak power spectral density achieved with the 2^{nd}-order diffraction (max; 31.4dBm/nm) is much higher (2-4dB) than that from the 1^{st}-order diffraction under similar conditions. The narrowest optical spectrum width was achieved from the 2^{nd}-order diffraction and the narrowest pulse of 13 ps was found for the setup with the 1^{st}-order diffraction grating. The wavelength tuning range from both orders can be amplified by increasing the injection current of the gain chip without deteriorating the stability of FML.

The second part of this thesis focussed on experimental testing of EP-VECSELs, also known as electrically-pumped semiconductor disc lasers (SDLs), which produce high multi watt output power with diffraction limited output beam profile. EP-VECSELs have great potential within the applications where the watt level CW output power and mode-locked light with picosecond pulses sources are required.

List of Abbreviations

Abbreviation	Meaning
AR	anti reflective
AUT	autocorrelator
DH	double heterostructure
ECDL	external cavity diode laser
ES	excited state
F	fibre
FS	fibre splitter
GaAs	gallium arsenide
GaInNaAsSb	gallium indium sodium arsenic antimony
GS	ground state
HR	high reflective
HWP	half wave plate
InAs	indium arsenide
InGaAsP	indium gallium arsenide phosphorus

Abbreviation	Meaning
L	lens
LED	light emitting diodes
ML	mode-locked
OI	optical isolator
OS	optical spectrometer
OSC	oscilloscope
PM	power meter
PS	power supply
QD	quantum dot
QW	quantum well
QWR	quantum wire
RFSA	RF spectrum analyzer
SESAM	semiconductor saturable absorber mirror
SHG	second harmonic generation
TBWP	time bandwidth product
TC	temperature controller

Abbreviation	Meaning
UV	ultraviolet
VCSELs	vertical-cavity surface-emitting laser diodes
µm	micrometre
Å	Angstrom
dBm	power ratio in decibels
E	energy
F	frequency
Fs	femtosecond
GHz	gigahertz
MHz	megahertz
mW	milliwatt
Nm	nanometre
PAV	average power
PPEAK	peak power
Ps	picosecond
FWHM	full width at half maximum

Abbreviation	Meaning
MOPA	master oscillator power amplifier
DG	diffraction grating
QD-ECMLLs	quantum-dot external-cavity passively mode-locked lasers
QD-SOA	quantum-dot semiconductor optical amplifier
SDLs	semiconductor disk lasers
MBE	molecular beam epitaxy
OP-VECSELs	optically pumped vertical external cavity surface emitting lasers
EP-VECSELs	electrically pumped vertical external cavity surface emitting lasers
DBR	distributed bragg reflector
SESAM	sdemiconductor saturable absorber mirror

List of Publications

1- Y. Y. Ding, **A. Alhazime**, D. Nikitichev, K. Fedorova, M. Ruiz, M. Tran, Y. Robert, A. Kapsalis, H. Simos, C. Mesaritakis, T. Xu, P. Bardella, M. Rossetti, I. Krestnikov, D. Livshits, I. Montrosset, D. Syvridis, M. A. Cataluna, M. Krakowski, and E. Rafailov, "Tunable Master-Oscillator Power-Amplifier Based on Chirped Quantum-Dot Structures *IEEE Photon. Tech. Lett.*, 24 (20), 1841-1844 (2012).

2- D. I. Nikitichev, K. A. Fedorova, Y. Ding, **A. Alhazime**, A. Able, W. Kaenders, I. Krestnikov, D. Livshits, E. U. Rafailov, "Broad wavelength tunability from external cavity quantum-dot mode-locked laser," *Appl. Phys. Lett.*, . 101, 121107 (2012).

3- **A. Alhazime**, Y. Ding, D. Nikitichev, K. Fedorova, and E. Rafailov, "Broadly tunable quantum-dot based ultrashort pulse laser system with different diffraction grating orders," *Electronics Letters*, 49 (5), 364-366 (2013).

4- **A. Alhazime**, M. Butkus, C.J. Hamilton, E. U. Rafailov, "216 MHz repetition rate passively mode-locked electrically-pumped VECSEL," submitted to–*Optics Letters* - 2014.

List of Conference Contributions

1- **A. Alhazime**, Y. Ding, D. Nikitichev, K. Fedorova, and E. Rafailov, "Broadly Tunable Ultrashort pulse Quantum-Dot Based Laser with Different Diffraction Grating Orders," Photon 12, Durham, U.K. (2012).

2- Y. Ding, **A. Alhazime**, D. Nikitichev, K. Fedorova, M. Ruiz, M. Tran, Y. Robert, A. Kapsalis, H. Simos, C. Mesaritakis, T. Xu, P. Bardella, M. Rossetti, I. Krestnikov, D. Livshits, I. Montrosset, D. Syvridis, M. A. Cataluna, M. Krakowski, and E. Rafailov, "Tunable Master-Oscillator Power-Amplifier Using All Chirped Quantum-Dot Structures," CLEO: 2012, San Jose, CA, USA (2012).

3- D. I. Nikitichev, K. A. Fedorova, Y. Ding, **A. Alhazime**, A. Able, W. Kaenders, I. Krestnikov, D. Livshits, E. U. Rafailov, "Broadly tunable picosecond pulses quantum-dot mode-locked laser," Laser Optics 2012, St. Pertersburg, Russia (2012).

4- **A. Alhazime**, M. Butkus, C.J. Hamilton, E. U. Rafailov, “216 MHz repetition rate passively mode-locked electrically-pumped VECSEL,” SPIE LASE: 2014, San Jose, CA, USA (2014).

Chapter 1. **Introduction**

1.1 Development of Semiconductor Lasers

In 1953, von Neumann had the idea of manufacturing a semiconductor laser and identified the materials required to do so [1]. A few years later (1956) Aigrain considered the concept of a semiconductor laser. His preliminary notes were made public in the summer of 1958 [2] along with Basov's ideas regarding population inversion in semiconductors [3] In 1957, the Japanese scientist, Nishizawa, filed patents for semiconductor masers and [4] and by 1960 Boyle and Thomas had patented a semiconductor laser [5].

The practical outcome of this early work on semiconductor lasers actually mattered little because of the subsequent development of improved materials. Unfortunately, in most of the early papers no obvious materials were identified in the fabrication of semiconductor lasers. Research continued, however, even when the use of GaAs and GaAsP was identified from reports in 1962 of highly efficient electroluminescence from forward-based GaAs p-n junctions [6-7].

In 1963, Alferov, Holonyak and Kroemer independently took a significant step forward when they suggested that a double heterostructure laser consisting of a lower bandgap layer surrounded by higher bandgap semiconductor materials could result in low (room) temperature and threshold current lasing [8-13]. Another stage was reached in the 1970s when Dingle and C.H. Henry predicted that by reducing the dimensionality of the active region a significant improvement of semiconductor optical source performance would follow [14]. Thus ensued the development of new growth techniques such as metal organic chemical vapour deposition and molecular beam epitaxy [15-16], amongst

others, which enabled control on an atomic scale and led to the growth of quantum well [15, 17-20] and quantum dot laser structures [21]. This made it possible for semiconductor lasers to operate at very low threshold currents with higher efficiency [17]. Presently, both types of lasers are of great research interest [22] and this has led to diode lasers being widely used as compact, cheap light sources for a wide range of applications such as medical applications and telecommunications.

1.2 Double Heterostructures

In classical double heterostructures that is, in which the heterostructure layers are wider than the De Broglie wavelength of electrons (this typically means at least a few tens of nm) several fundamental physical phenomena take place such as the super-injection (that is, the situation in which the quasi-Fermi level enters into the conduction band and valence band because of heterostructure) of carriers, optical confinement along with electron confinement, wide gap window effect, and diffusion (Figure 1-1) [23]. The resultant significant advances deriving from these physical phenomena led to the award of the Nobel Prize in Physics to Alferov and Kroemer for developing semiconductor heterostructures for use in high-speed optoelectronics [24].

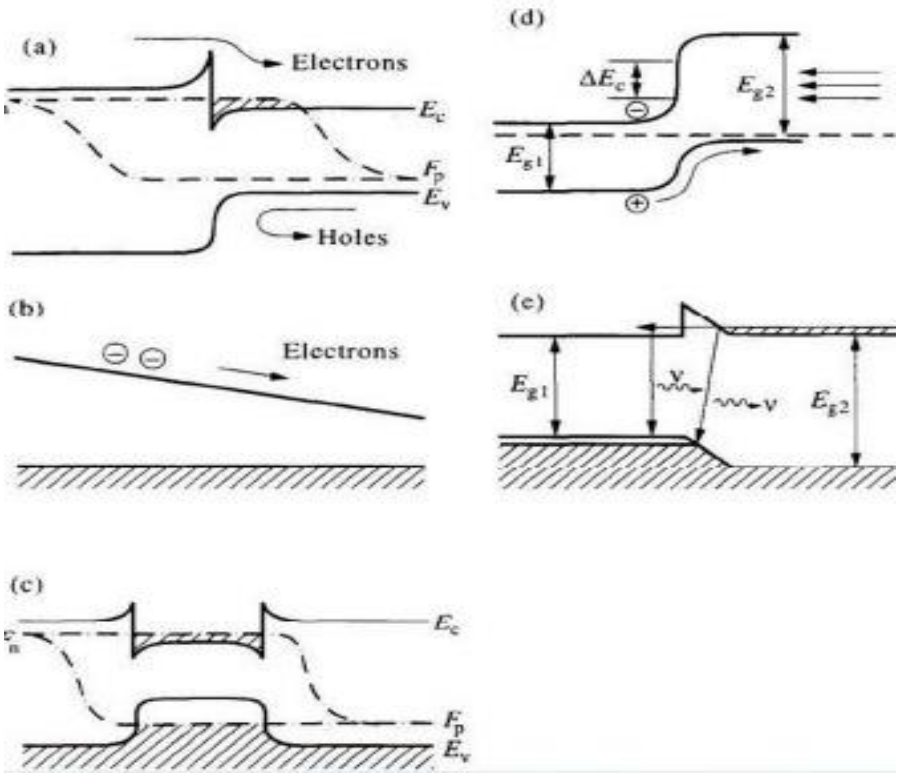

Figure 1-1 Main physical phenomena in classical heterostructures: (a) One-side injection and superinjection; (b) drift in built-in quasi-electric field; (c) electron and optical confinement; (d) wide-gap window effect; (e) diagonal tunnelling through heterostructure interface [24].

It is undeniable that contemporary solid state physics would not be as advanced as it is today but for the availability of semiconductor heterostructures and double heterostructures. Structures such as quantum wells, quantum wires and quantum dots attract overwhelming interest in the research community [25]. With the development of the fundamental physics and technology of semiconductor heterostructures, applications are plentiful: notably, telecommunication systems, heterostructure-based light-emitting diodes and low-noise high electron mobility transistors for high-frequency applications such as satellite TV [25]

The continual progression of lasers thanks to heterostructure has led to the development of many domestic applications; most notably in the form of compact disc technology where a laser is used to ‘read’ digital information from an optical disc [26]. Another prominent application of the heterostructure technology is solar cells and in fact the Mir space station utilised AlGaAs heterostructure solar cells during its 15-year orbit [25].

1.3 Dimensionality in Semiconductor Materials

Semiconductor lasers are a low cost source for the generation of light with a broad wavelength range. The added flexibility in the choice of semiconductor material compounds results in the ability to tune the emission wavelength over a wide spectral range; i.e., from visible to infrared [27]. The characteristics of semi conductor diode lasers can be optimised by the use of artificial structures and have been found to be strongly connected to the band structure of their active region. Quantum size effect occurs when the thickness of an active semiconductor region is reduced to the de Broglie wavelength as given by:

$$\lambda_B = \frac{h}{p} \tag{1.1}$$

where h is Planck’s constant and p is the electron momentum. By constraining the dimensions of the semiconductor it is possible to realise lower dimensionalities in the active region of the laser; i.e., from bulk (three-dimensional), to a thin epitaxial layer, i.e., a quantum well (two-dimensional), to an elongated tube, i.e., a quantum wire (one-dimensional), and finally to an isolated area, i.e., a quantum dot (zero-dimensional) [28].

A quantum well structure is commonly found in semiconductor lasers and also in optical amplifiers. The quantum wire is a one-dimensional confined structure where carrier movement is free in one dimension and confined in two others. Possibly the most important zero-dimensionally confined structure, one of zero-dimensionality, from the laser device perspective is the quantum dot [29].

Quantum dots exhibit electron and hole confinement in all three dimensions and their tiny clusters of semiconductor material are confined in such a way. The charge carriers occupy a restricted set of energy levels, similarly to atoms, which explains the use of the description of the quantum dot as an artificial atom [26, 30]. Pragmatically, different energy momentum relations in the direction of confinement result in the spatial confinement of the carriers in lower-dimensional semiconductors - compare this with the bulk case (see Figure 1-2).

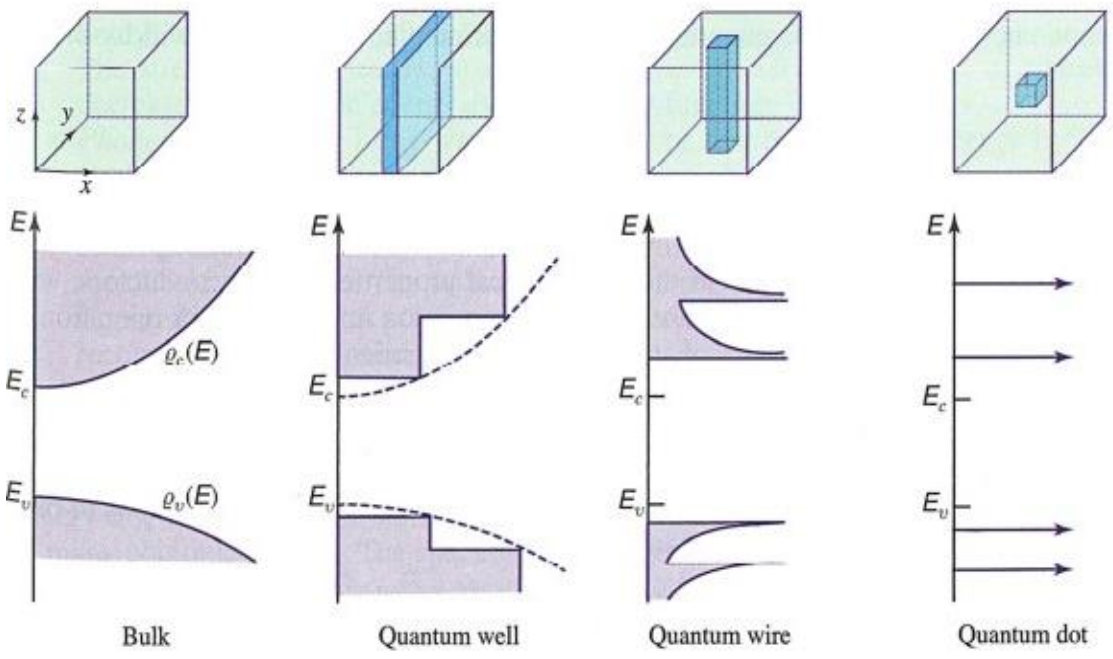

Figure 1-2 Schematic morphology and density of states in bulk (3-D), quantum well (2-D), quantum wire (1-D) and quantum dot (0-D) material. The quantum dot case is for real dots which are not identical in size and exhibit size fluctuations leading to a broadening in energy level structure [31].

In comparison with higher-dimensional structures, the density of states (DOS) function in QDs is more advantageous for applications in photonics where allowed energy states alone correspond to discrete quantum levels in QDs. The density of states (DOS) shows how many energy states are available within unit energy intervals in a crystal of unit volume. In other words it demonstrates just how many states excited electrons of certain energies can occupy. In other words, the number of carriers necessary to fill these states is decreased, because of a delta-shaped density of states thus reducing the threshold value of QD-based lasers and at the same time increasing the gain at a given carrier density [29, 32]. Decreased dimensionality of carriers' confinement causes a reduction in threshold current in laser diodes (Figure 1-3) [33].

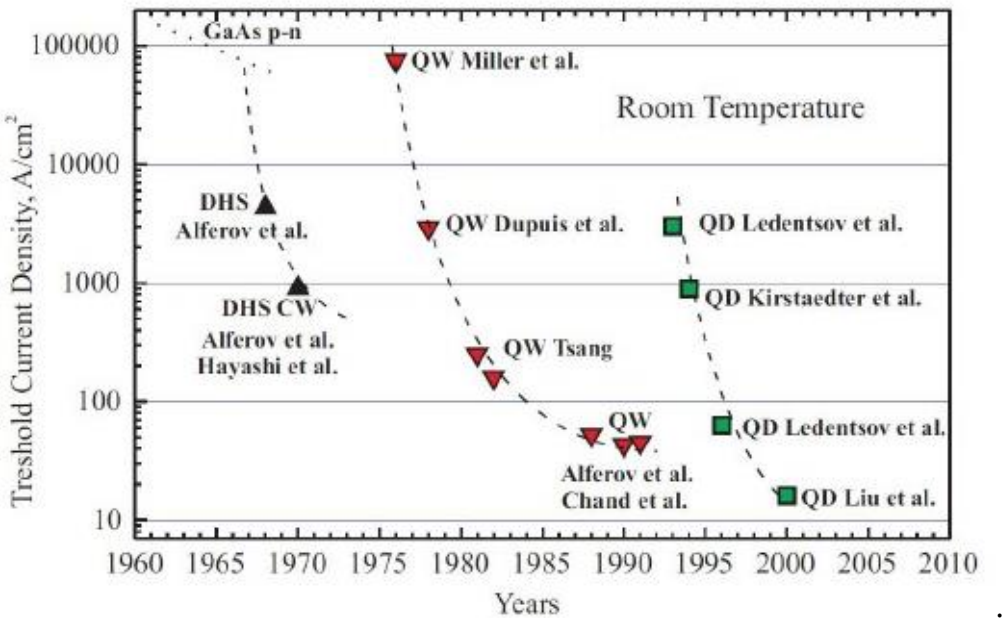

Figure 1-3 The reduction of threshold current density in laser diodes over time using different semiconductors. [33]

Low-dimensional lasers exhibit a reduced sensitivity to temperature which is highly advantageous in practice for all semiconductor lasers (see Figure 1-4). As far as QDs are concerned a (practically) infinite characteristic temperature has been predicted.

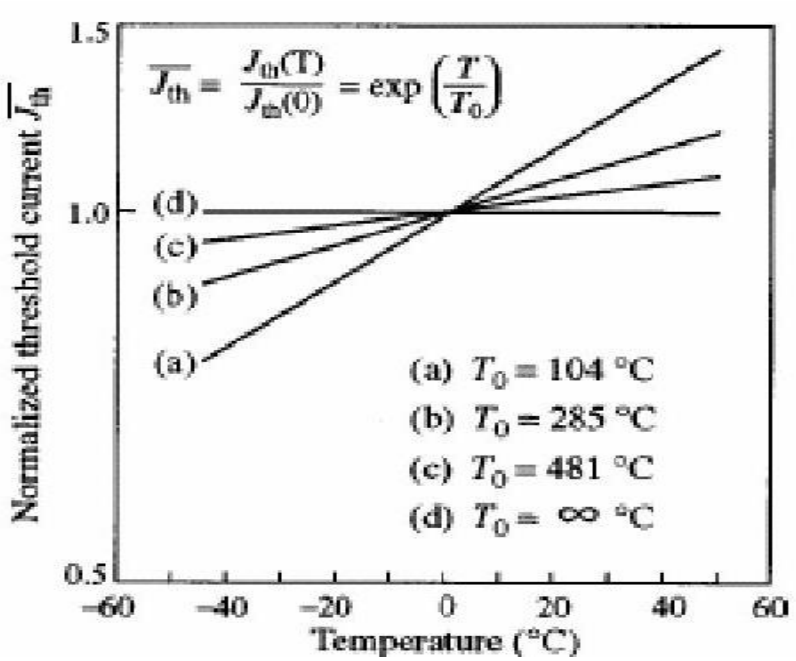

Figure 1-4 A theoretical simulation of threshold current dependence on the temperature for different carrier confinement configurations: (a) bulk; (b) with quantum wells; (c) with quantum wires; (d) with quantum dots [26].

In 1982, Y. Arakawa and H. Sakaki theoretically considered certain effects in lasers based on heterostructures with size quantization in one, two and three directions. They stated that the threshold current of such a laser is likely to be far less sensitive than that of a conventional laser reflecting the reduced dimensionality of the electronic state. Their experimental studies focussed on a QW laser in a magnetic field directed perpendicular to the QW plane then demonstrated an increase in the characteristic temperature which described the exponential growth of the threshold current, the characteristic temperature increased in the magnetic field from 144 to 313°C. This indicated the possibility of weakening the threshold current dependence on temperature for QW ;lasers and full temperature stability for QD lasers [28].

1.4 Quantum Dots (QDs) Fabrication

This thesis will mainly consider QD lasers. A QD is a nano-scale crystal made of semiconductor materials, small enough to exhibit significant quantum mechanical properties especially when considered in all three spatial dimensions. Particular promise has been shown by a group of quantum dot materials based on III-V QD epitaxially grown on a semiconductor substrate. An example of this is InGaAs/InAs QD on a GaAs on a substrate, which emits in the 1.1 μm - 1.3 μm wavelength range and can be extended to 1.55 μm. As an alternative, InGaAs/InAs QD can be grown on an InP substrate covering the 1.4 μm - 1.9 μm wavelength range [28].

As a consequence these recent achievements in QD epitaxial growth have enabled the fabrication of QD lasers where the most effective method for the fabrication of QDs is the strained -layer epitaxial growth in the Stranski-Krastanow mechanisation [34-36]. In this growth mode, when a film is epitaxially grown over a substrate the growth is initially when growth is layer by layer. However, beyond a particular critical thickness three dimensional islands start to form on top of a continuous film called the wetting layer. Crucial to this technique is the lattice constant of the deposited material which is larger than that of the substrate so that the additional strain leads to the formation of dots [32]. An example is found in the InAs film with a lattice constant of 6.06 Å deposited on a GaAs substrate (lattice constant of 5.64 Å)when the advantage is that such films can be grown using molecular beam epitaxy (MBE) and metal organic chemical vapour deposition (MOCVD), the beneficiaries being the science of QDs with all knowledge acquired previously. Importantly manufacturers have no need for investment into the new epitaxy equipment to fabricate these structures.

The lateral positions of QD growth in a plane surface are random and there is no standard way of arranging the dots in a planar order (Figure 1-5a). Typical sizes of QDs

are 15 nm - 20 nm in diameter and around 5 nm in height. The dot size, the shape and the surface density are dependent on growth temperature and other growth conditions. However, changing the thickness of the capping layer leads to variations in the size of the QDs. For example being the average size of the QDs capped with a thicker layer is larger so that by changing the thickness of the capping layers for different groups of QD layers, a broad spectral emission can be achieved [37-38]. The physical size of these QDs is between 5 nm and 50 nm and they are defined by etching on two-dimensional electron gases in semiconductor heterostructures. The electronic properties lie between those of bulk semiconductors and discrete molecules [39-41].

Materials grown using molecular beam epitaxy (MBE) techniques have become the standard for fabrication of III-V semiconductor quantum dots. They enable many degrees of parameter control and thus epitaxial deposition of high structural quality and high purity in semiconductor layers with few angstroms precision is possible. Self formation of QDs mainly employs an artificially created strain between deposited layers [28]. Epitaxial growth free of defects can be performed when the lattice constants are the same, and even a small variation that results in an approximate match is possible. An example of this can be found in the growth of GaAs/AIAs heterostructures where the lattice mismatch is about 0.1 %. When many III-V material compositions have a much higher mismatch, however, this will result in defects forming to reduce the strain when QWs are grown [42]. Although this may be well managed, it does limit the material usage of certain spectral ranges. Unlike in the growth of QWs, the widening of elastic strain energy is the driving force in the formation of QDs [43].

There are two outcomes from such fluctuations during growth. Firstly, there is a distribution of dot size, height and composition and, secondly, epitaxy techniques potentially reduce the amount of fluctuation of these parameters to as little as a few percent. When dots are grown on a planar surface, their lateral positions will be random,

as evidenced in Figure 1-5 below. In the self-assembly process, there is no standard way of arranging the dots in a planar ordered way unless they are encouraged to grow in particular positions over a pre-patterned substrate [44-45].

The density of QDs is between 10^9 cm^{-2} and 10^{11} cm^{-2} but the sparse distribution of QDs produces little gain. Such levels may not be sufficient for the optimal efficiency of a laser. Therefore, to avoid this problem QDs can be grown in stacks allowing an increase in the modal gain without increasing the internal optical mode loss. TEM images of the real view of InAs-grown QDs along with a cross-section of a multilayer InGaAs QD sample [46] are shown in Figure 1-5b.

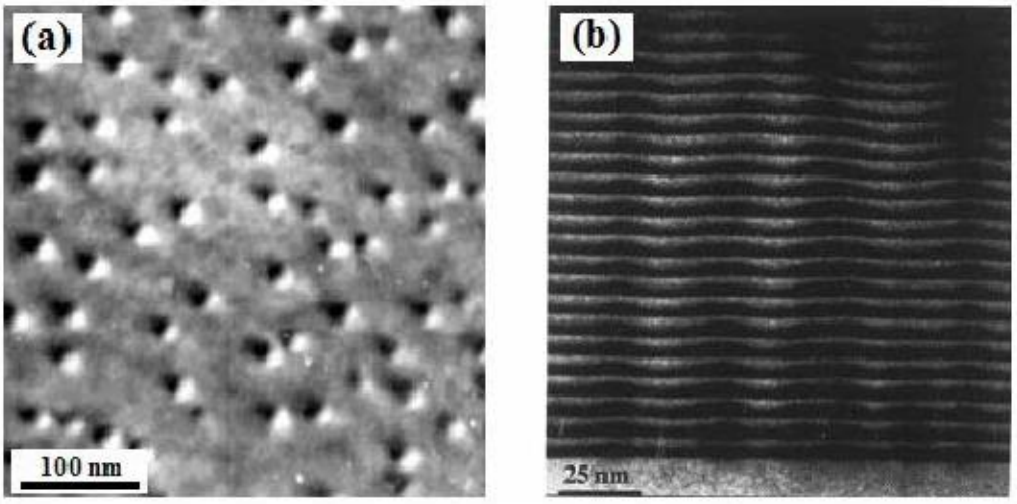

Figure 1-5 TEM images of quantum dots: (a) Single sheet of InAs quantum dots grown on GaAs and (b) cross-section of a 25-layer thick stack of InGaAs quantum dots (thicker dark regions) grown on GaAs substrate (lighter area in the bottom of the picture and surrounding the InGaAs layers). The QDs are connected within the layers by the wetting layers (thin dark regions) [47].

1.5 Optical Properties of QDs

Research into QDs has been carried out for only approximately 10 years and so is a relatively new field of research. This section will discuss fundamental properties which that affect performance in complete devices such as energy levels, gain, emission, wavelength and others, particularly InGaAs QDs in GaAs, the area of interest in this study. QDs have certain energetic levels, resulting in optical transitions that are determined by the arrangement of several factors: atoms, lattice strain and surrounding material.

A QD-based laser ideally should be temperature-insensitive, generating single frequency emission with a low threshold current density, but in fact such lasers offer a broader spectral bandwidth. The difference here relates to the size variations of QDs which brings about a disconnection in the broadening of energy levels. The clustering of QDs during MBE growth is the reason for a Gaussian size distribution with a corresponding distribution of emission frequencies [29, 48]. Figure 1-6 shows a comparison between the schematic morphology and density of the states for charge carriers in an ideal QD and real QD-based material with inhomogeneous broadening effect [49]. The demonstration of how inhomogeneous broadening impacts significantly on the shape of the density state functions for QDs by broadening the gain bandwidth and the emission spectrum of the structure can be seen in Figure 1-6.

The effect of inhomogeneous broadening is a disadvantage from the reduced dimensionality perspective, the reason being that states of energy are not Delta function-like anymore. The result is that there is an increase in the threshold of lasing at the same time as a reduction in modal and differential gain and gain saturation value [50-51]. Conversely, a broad gain bandwidth has the potential for being advantageous for short pulse generation, but so far the potential has not been realised in terms of a significant

advantage for ultra-short pulse generation in mode-locked devices and wavelength tuning [52].

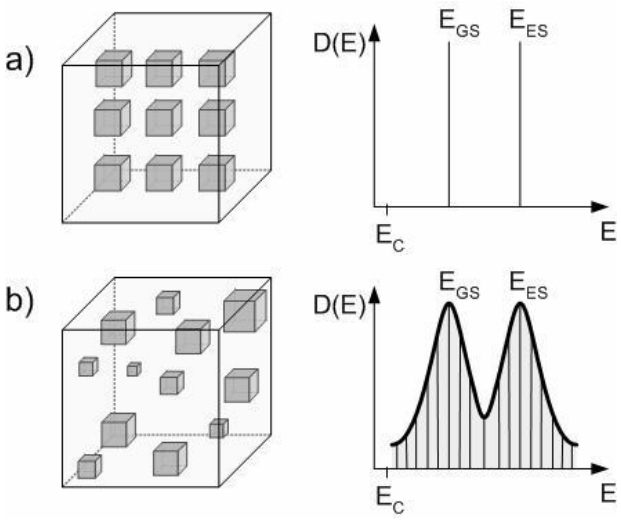

Figure 1-6 Schematic morphology and density of states for charge carriers in: (a) An ideal quantum-dot system and (b) a real quantum-dot system, where inhomogeneous broadening is illustrated [52].

1.6 Tunable External Cavity Diode Lasers

In 1964, Crowe and Craig demonstrated the first laser diode coupled to an external cavity and some years later several papers based on the same system were published by two Soviet groups [53-56]. Later in 1972 Ludeke and Harris [57] reported the tunability of CW radiation from a GaAs injection laser where an external dispersive cavity is found over a range of 15nm about the centre wavelength of 825.5 nm at a temperature of 77 K. In a single mode operation with CW output power as large as 17 mW with a line width of 350 MHz was observed. In 1981 Fleming and Mooradian [58] were the first to study the spectral ECDLs in detail. There were further developments in the early to mid-1980s by British Telecom Research Laboratories which suggested the application of such lasers in transmitters and local oscillators in coherent optical

telecommunications [59-60]. At the same time, much research was carried out at AT&T Bell Laboratories and in France, at the Centre National d'Etudes des Telecommunications [61]. By the end of the 1980s and the beginning of the 1990s ECDLs excited a growing interest as a coherent radiation source for spectroscopic research and in commercial fibre optic test and measurement equipment [62]. Nowadays, broadly tunable compact and low cost ECDLs are in the developmental stage for applications in telecommunications and wavelength division multiplexing systems (WDM) [63].

Recently, there has been a growing interest in the development of broadly-swept tunable laser sources for optical coherence tomography thanks to their high spectral bandwidth and output power [64-66]. Tunable external cavity diode laser systems consist of semiconductor diode lasers with or without antireflection coatings on one or two facets; a collimator for coupling the output of a diode laser and additionally an external mode selection filter. Generally speaking, significant differences can be found in the operational features of a diode laser in an external cavity depending on several factors; the length of the external cavity, diffraction grating, optical power and diode laser parameters [67]. The diffraction grating reflects different wavelengths at slightly different angles, similar to a prism, spatially separating the light by wavelength. Littman-Metcalf and Littrow cavity configurations are typically used for the implementation of tunable ECDLs. In both configurations, a diffraction grating is used to control the emission wavelength and the selection of a single longitudinal mode of laser oscillation [67-69] and the tuning of the wavelength over the entire range of gain bandwidth by moving and rotating the grating position.

1.6.1 Litrow Configurations.

In a Littrow configuration the diffraction grating (DG) is used as the end mirror reflecting the first order diffraction beam back to the laser and providing optical feedback of zeroth order when the diffraction beam is coupled out of the laser, Figure 1-7.

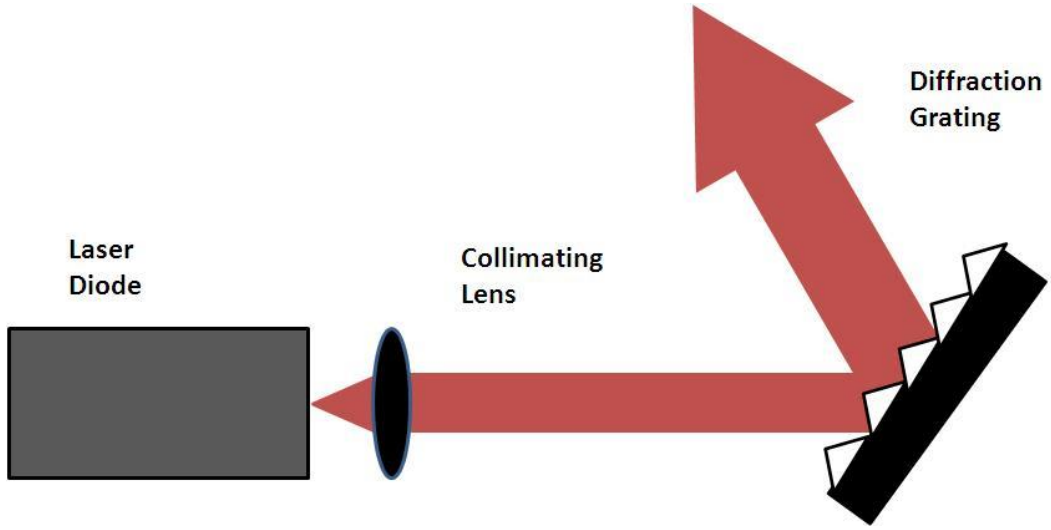

Figure 1-7 Schematic diagram of External-Cavity Diode Laser in Littrow configuration.

By changing the incidence angle of the diffraction grating an emission wavelength can be tuned. The diffraction equation for this type of configuration is given by:

$$m\lambda = d(\sin\alpha + \sin\beta) \qquad 1.2$$

where m is the diffraction order, λ is the wavelength, d is the line spacing, α is the incidence angle, and β is the diffraction angle.

This configuration has both an advantage and a disadvantage. The benefit is that there is a possibility of achieving a significantly higher output than in the case of the Littman-Metcalf configuration. The downside is that there is a shift in position of the beam as wavelength tuning is achieved due to a change in the incidence angle of the diffraction grating [70].

1.6.2 Littman-Metcalf Configurations

In the Littman-Metcalf configuration the DG reflects the first order diffraction beam towards the tuning mirror which in turn reflects it back to the laser. However the emission wavelength can be tuned by rotating this mirror. Thus the zeroth order diffraction beam is coupled out of the laser Figure 1-8.

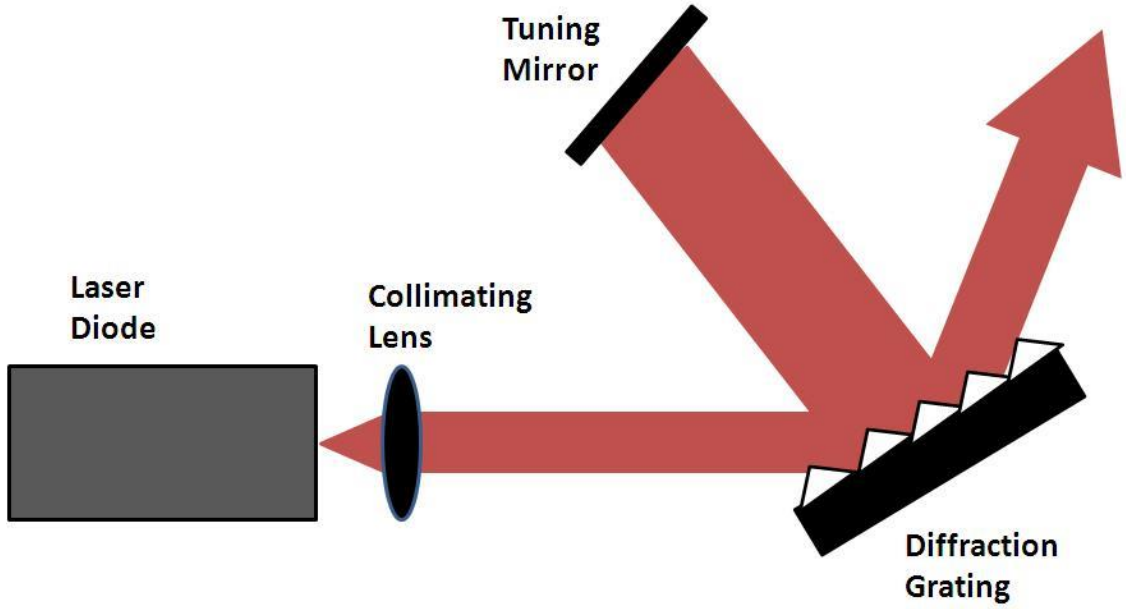

Figure 1-8 Schematic diagram of External-Cavity Diode Laser in Littman-Metcalf configuration.

An advantage of the above configuration is that the position of the output beam remains fixed during the rotation of the tuning mirror. A second benefit is that the line width is smaller because the wavelength selectivity is stronger. There are two disadvantages, the main one being that the zeroth order reflection of the beam reflected by the tuning mirror is lost resulting in lower output power. Secondly with the resulting higher losses in this configuration there is a resultant reduction in tuning range [70].

1.7 References

[1] J. v. Neumann, "Notes on the photon-disequilibrium-amplification scheme (JvN), September 16, 1953," *IEEE Journal of Quantum Electronics*, vol. 23, pp. 659-673, 1987.

[2] P. Aigrain, "Masers à Semi-Conducteurs," in *Quantum Electronics*, p. 1761, 1964.

[3] N. Basov, B. Vul, and Y. M. Popov, "Quantum-mechanical semiconductor generators and amplifiers of electromagnetic oscillations," *Sov. Phys. JETP*, vol. 10, p. 416, 1959.

[4] J. Nishizawa, "Semiconductor Maser," *Japanese Patent*, vol. 273217, 1957.

[5] W. S. Boyle and D. G. Thomas, "Optical maser," ed: US Patent 3,059,117, 1962.

[6] R. Keyes and T. Quist, "Recombination radiation emitted by gallium arsenide," *Proc. IRE*, vol. 50, pp. 1822-1823, 1962.

[7] J. Pankove and M. Massoulie, "Injection luminescence in gallium arsenide," in *Journal of the Electroctrochemical Society*, 1962, pp. C67-C67.

[8] Z. I. Alferov, V. M. Andreev, V. I. Korol'kov, D. N. Tret'yakov, and V. M. Tuchkevich, "High-voltage p-n junctions in GaxAl1−xAs crystals," *Sov. Phys.*, vol. 1, pp. 1313-1314 1968.

[9] Z. I. Alferov, V. M. Andreev, E. L. Portnoi, and M. K. Trukan, "AlAs-GaAs heterojunction injection lasers with a low room-temperature threshold," *Sov. Phys*, vol. 3, pp. 1107-1110 1970.

[10] I. Hayashi, M. Panish, P. Foy, and S. Sumski, "Junction lasers which operate continuously at room temperature," *Applied Physics Letters*, vol. 17, pp. 109-111, 1970.

[11] J. N. Holonyak and S. Bevacqua, "Coherent (visible) light emission from Ga(As1-xPx) junctions," *Appl. Phys*, vol. 1(4), pp. 82-83 1962.

[12] H. Kroemer, "A proposed class of heterojunction injection lasers," *Proc. IEEE,* vol. 51(12), pp. 1782–1783 1963.

[13] M. I. Nathan, W. P. Dumke, G. Burns, F. H. Dill Jr, and G. J. Lasher, "Stimulated emission of radiation from GaAs p-n junctions," *Appl. Phys,* vol. 1(3), pp. 62-64, 1962.

[14] R. Dingle and C. H. Henry, "Quantum effects in heterostructure lasers," *U.S.*, vol. Patent 3982207 Sept. 1976.

[15] R. D. Dupuis, "AlGaAs-GaAs lasers grown by metelorganic chemical vapor deposition - A review," *J. Crystal Growth*,vol. 55, pp. 213-221, 1981.

[16] M. A. Herman and H. Sitter, *Molecular Beam Epitaxy*,Berlin: Springer-Verlag, 1989.

[17] Z. I. Alferov, S. V. Ivanov, P. S. Kop'ev, N. N. Ledentsov, M. E. Lutsenko, M. I. Nemenov, B. Y. Meltser, V. M. Ustinov , and S. V. Shaposhnikov, "Spreading and surface recombination in quantum well (Al,Ga)As double heterostructure separate confinement lasers with a broad stripe," *Sov. Phys. Semicond,* vol. 24, pp. 92-95 1990.

[18] Z. I. Alferov, A. M. Vasiliev, S. V. Ivanov, P. S. Kop'ev, N. N. Ledentsov, B. Y. Mel’tser, and V. M. Ustinov, "Reduction of the threshold current density (52A/cm-2, 300K) in SCH GaAs-AlGaAs lasers by using a quantum well confined by a variable-step short-period superlattice," *Sov. Phys.: Tech. Phys*, vol. Lett. 14, p. 782, 1988.

[19] R. C. Miller, R. Dingle, A. C. Gossard, R. A. Logan, A. Nordland, and W. J. W., "Laser oscillation with optically pumped very thin GaAs-AlxGa1−xAs multilayer structures and conventional double heterostructures " *J.Appl. Phys,* vol. 47, p. 4509, 1976.

[20] W. T. Tsang, "Extremely low threshold (AlGa)As modified multi-quantum well heterostructure lasers grown by molecular beam epitaxy," *Appl. Phys,* vol. Lett. 39, pp. 786-788 1981.

[21] D. Z. Garbuzov, Antonishkis.N.Y, Bondarev.A.D, Gulakov.A.B., Zhigulin.S.D, Katsavets.N.I, Kochergin.A.V, and Rafailov.E.U, "High power λ =0.81μm InGaAsP/GaAs SCH SQW lasers," *IEEE Journal of Quantum Electronics,* vol. 27(6), p. 1531, 1991.

[22] G. Park, O. B. Schekin, D. L. Huffaker, and D. G. Deppe, "1.3-μm quantum-dot laser," *IEEE PhotonTech. Lett.,* vol. 12, pp. 230-232 2000.

[23] V. Lutskii, "Quantum size effect–-present state and perspectives of experimental investigations," *Physica Status Solidi (a),* vol. 1, pp. 199-220, 1970.

[24] Z. I. Alferov, V. Andreev, D. Garbuzov, Y. V. Zhilyaev, E. Morozov, E. Portnoi, and V. Trofim, "Investigation of the influence of the AlAs-GaAs heterostructure parameters on the laser threshold current and the realization of continuous emission at room temperature," *Sov. Phys. Semicond,* vol. 4, pp. 1573-1575, 1971.

[25] Z. I. Alferov, "Classical heterostructures paved the way," *III-Vs Review,* vol. 11, pp. 26-31, 1998.

[26] Z. I. Alferov, "Nobel Lecture: The double heterostructure concept and its applications in physics, electronics, and technology," *Reviews of Modern Physics,* vol. 73, pp. 767-782, 2001.

[27] E. e. Kapon, "Semiconductor *Lasers: Materials and Structures*,Academic Press, San Diego, 1999.

[28] V. M. Ustinov, A. Zhukov, A. Y. Egorov, and N. Maleev, *Quantum Dot Lasers*: Oxford University Press., New York, 2003.

[29] V. M. Ustinov, *Quantum Dot Lasers* (*vol. 11*), Oxford University Press: New York, 2003.

[30] B. E. Saleh and M. C. Teich, *Fundamentals of Photonics*, New York, NY: Wiley, 1991.

[31] B. E. Saleh and M. C. Teich, *Fundamentals of Photonics*,New York: Wiley, 2007.

[32] E. U. Rafailov, M. A. Cataluna, and E. A. Avrutin, *Ultrafast Lasers Based on Quantum Dot Structures: Physics and Devices*,New York: Wiley, 2011.

[33] N. N. Ledentsov, "The way to quantum dot lasers," *Window to Microworld*, vol. 1(5), pp. 17-25 2002. http://wmw-magazine.ru/uploads/volumes/05/17.pdf.

[34] L. Goldstein, F. Glas, J. Marzin, M. Charasse, and G. Le Roux, "Growth by molecular beam epitaxy and characterization of InAs/GaAs strained-layer superlattices," *Applied Physics Letters*, vol. 47, pp. 1099-1101, 1985.

[35] M. Grundmann, *Nano-optoelectronics: Concepts, Physics and Devices*: Springer-Verlag, Berlin, 2002.

[36] D. Leonard, K. Pond, and P. Petroff, "Critical layer thickness for self-assembled InAs islands on GaAs," *Physical Review B*, vol. 50, p. 11687, 1994.

[37] A. Ekimov and A. Onushchenko, "Quantum size effect in three-dimensional microscopic semiconductor crystals," *ZhETF Pis ma Redaktsiiu*, vol. 34, p. 363, 1981.

[38] M. Reed, J. Randall, R. Aggarwal, R. Matyi, and T. Moore, "Observation of discrete electronic states in a zero-dimensional semiconductor nanostructure," *Physical Review Letters*, vol. 60, pp. 535-537, 1988.

[39] L. E. Brus, "Chemistry and physics of semiconductor nanocrystals," *Columbia University*, 2007.

[40] C. B. Murray, C. Kagan, and M. Bawendi, "Synthesis and characterization of monodisperse nanocrystals and close-packed nanocrystal assemblies," *Annual Review of Materials Science,* vol. 30, pp. 545-610, 2000.

[41] D. J. Norris, "Measurement and assignment of the size-dependent optical spectrum in cadmium selenide (CdSe) quantum dots," Ph.D. thesis,Massachusetts Institute of Technology, 1995.

[42] S. Vetter, J. Hastie, V.-M. Korpijarvi, J. Puustinen, M. Guina, O. Okhotnikov, S. Calvez, and M. Dawson, "Short-wavelength GaInNAs/GaAs semiconductor disk lasers," *Electronics Letters,* vol. 44, pp. 1069-1070, 2008.

[43] N. Ledentsov, V. Shchukin, M. e. Grundmann, N. Kirstaedter, J. Böhrer, O. Schmidt, D. Bimberg, V. Ustinov, A. Y. Egorov, and A. Zhukov, "Direct formation of vertically coupled quantum dots in Stranski-Krastanow growth," *Physical Review B,* vol. 54, p. 8743, 1996.

[44] A. Y. Egorov, A. Zhukov, P. Kop'ev, N. Ledentsov, M. Maksimov, and V. Ustinov, "Effect of deposition conditions on the formation of (In, Ga) As quantum clusters in a GaAs matrix," *Semiconductors,* vol. 28, pp. 809-811, 1994.

[45] D. Leonard, G. Medeirosribeiro, H. Drexler, K. Pond, W. Hansen, J. P. Kotthaus, and P. M. Petroff, "Progress In Self-Assembled Quantum Dots Of InxGa1-xAs on GaAs," *in Compound Semiconductors 1994,* H. Goronkin and U. Mishra, (Eds.),~~ed~~ Bristol: Iop Publishing Ltd,pp. 819-824~~.~~, 1995.

[46] P. Y. Yu and M. Cardona, "Fundamentals of Semiconductors: physics and materials properties," *3rd ed. Heidelberg: Springer-Verlag,* 2001.

[47] D. Bimberg, M. Grundmann, and N. Ledentsov, "Growth, spectroscopy, and laser application of self-ordered III-V quantum dots," *MRS Bulletin,* vol. 23, pp. 31-34, 1998.

[48] O. Stier, M. Grundmann, and D. Bimberg, "Electronic and optical properties of strained quantum dots modeled by 8-band k· p theory," *Physical Review B,* vol. 59, p. 5688, 1999.

[49] S. Nalivko, V. Kononenko, and I. Manak, "Design and characteristics of widely tunable quantum-well heterostructure lasers in the Littman and Metcalf cavity configuration," in *International Conf Transparent Optical Networks.*, 1999, pp. 215-218.

[50] H. Dery and G. Eisenstein, "The impact of energy band diagram and inhomogeneous broadening on the optical differential gain in nanostructure lasers," *International Conf. on Quantum Electronics,* vol. 41, pp. 26-35, 2005.

[51] O. Qasaimeh, "Effect of inhomogeneous line broadening on gain and differential gain of quantum dot lasers," *IEEE Transactions on Electron Devices,* vol. 50, pp. 1575-1581, 2003.

[52] M. A. Cataluna, "Ultrashort-pulse generation from quantum-dot semiconductor diode lasers," Ph.D. thesis,University of St Andrews, 2008.

[53] A. Bogatov, P. G. Eliseev, L. Ivanov, A. Logginov, M. Manko, and K. Senatorov, "Study of the single-mode injection laser," *IEEE Journal of Quantum Electronics, IEEE Journal of,* vol. 9, pp. 392-394, 1973.

[54] O. Bogdankevich, B. Vasil'ev, A. Nasibov, A. Z. Obidin, A. Pechenov, and M. Zverev, "Investigation of the dynamics of emission from a" radiating mirror" semiconductor laser with an external resonator," *Quantum Electronics,* vol. 4, pp. 84-85, 1974.

[55] S. Darznek, M. Zverev, and V. Ushakhin, "Investigation of a multielement electron-beam-pumped semiconductor laser with an external mirror," *Quantum Electronics,* vol. 4, pp. 1272-1274, 1975.

[56] P. G. Eliseev, I. Ismailov, and Y. F. Fedorov, "Injection lasers for multichannel optical communication," *IEEE J. Quantum Electronics,* vol. QE-6(1). pp.38-41, 1970.

[57] R. Ludeke and E. Harris, "Tunable GaAs laser in an external dispersive cavity," *Applied Physics Letters,* vol. 20, pp. 499-500, 1972.

[58] M. Fleming and A. Mooradian, "Spectral characteristics of external-cavity controlled semiconductor lasers," *IEEE Journal of Quantum Electronics, IEEE Journal of,* vol. 17, pp. 44-59, 1981.

[59] M. Bagley, R. Wyatt, D. Elton, H. Wickes, P. Spurdens, C. Seltzer, D. Cooper, and W. Devlin, "242 nm continuous tuning from a GRIN-SC-MQW-BH InGaAsP laser in an extended cavity," *Electronics Letters,* vol. 26, pp. 267-269, 1990.

[60] R. Wyatt and W. Devlin, "10 kHz linewidth 1.5 μm InGaAsP external cavity laser with 55 nm tuning range," *Electronics Letters,* vol. 19, pp. 110-112, 1983.

[61] F. Favre, D. Le Guen, J. Simon, and B. Landousies, "External-cavity semiconductor laser with 15 nm continuous tuning range," *Electronics Letters,* vol. 22, pp. 795-796, 1986.

[62] F. Favre and D. Le Guen, "82 nm of continuous tunability for an external cavity semiconductor laser," *Electronics Letters,* vol. 27, pp. 183-184, 1991.

[63] S. B. Yoo, "Wavelength conversion technologies for WDM network applications," *Journal of Lightwave Technology,*vol. 14, pp. 955-966, 1996.

[64] N. Krstajic, D. T. Childs, S. Matcher, D. Livshits, A. Shkolnik, I. Krestnikov, and R. Hogg, "Swept-Source Laser Based on Quantum-Dot Semiconductor Optical Amplifier—Applications in Optical Coherence Tomography," IEEE *Photonics Technology Letters, IEEE,* vol. 23, pp. 739-741, 2011.

[65] B. Stevens, D. Childs, K. Groom, M. Hopkinson, and R. Hogg, "All semiconductor swept laser source utilizing quantum dots," *Applied Physics Letters*, vol. 91, pp. 121119-121119-3, 2007.

[66] S. H. Yun, C. Boudoux, G. J. Tearney, and B. E. Bouma, "High-speed wavelength-swept semiconductor laser with a polygon-scanner-based wavelength filter," *Opt. Lett.*, vol. 28(20), pp. 1981–1983, 2003.

[67] C. Hawthorn, K. Weber, and R. Scholten, "Littrow configuration tunable external cavity diode laser with fixed direction output beam," *Review of Scientific Instruments*, vol. 72, pp. 4477-4479, 2001.

[68] M. G. Littman and H. J. Metcalf, "Spectrally narrow pulsed dye laser without beam expander," *Applied Optics*, vol. 17, pp. 2224-2227, 1978.

[69] K. Liu and M. G. Littman, "Novel geometry for single-mode scanning of tunable lasers," *Optics Letters*, vol. 6, pp. 117-118, 1981.

[70] K. A. Fedorova, "Novel semiconductor based broadly tunable light sources," Ph.D. thesis, University of Dundee, 2011.

Chapter 2. **Bio-Medical Applications**

2.1 Introduction

The field of ultrafast optics, and its applications in biomedicine, emerged from pioneering mode-locking studies of organic dye and solid-state lasers in the 1960s and early 1970s. A good deal of the early work on ultrashort pulse duration technology focused on dye lasers, the gain bandwidth of which allows for pulse durations of the order of 10 fs; however, these lasers suffer from a number of disadvantages. They have a limited power output, degrade quickly during operation, require continuous pumping, and, most seriously, involve the handling of toxic and even carcinogenic substances. For these reasons, where ultrashort pulses were needed, solid-state lasers, notably Ti:sapphire lasers, and, later, fibre and semiconductor lasers, superseded dye lasers, for the most part, as soon as their level of their development allowed [1-2].

Femtosecond lasers have found a wide diversity of uses within biological and medical research, diagnosis, and treatment. Their low average power serves to restrict the degree of thermal damage they cause to living tissue, while their intensity and peak power are sufficiently high to enable nonlinear processes for a variety of medical applications from high-resolution microscopy to precise or complex surgical procedures. For example, they make possible the study, or highly-targeted removal, of tissue with little or no detriment to the surrounding areas.

2.2 Optical Coherence Tomography

Ultrashort pulsed lasers are among the light sources used in optical coherence tomography (OCT), which is a non-invasive, interferometry, cross-sectional imaging technique. OCT enables the capture of three-dimensional images of tissue structure on the micron scale using near-infrared light. The use of relatively long wavelength light allows a deeper penetration into the scattering medium than is the case in other optical techniques such as confocal microscopy. The use of femtosecond lasers makes available extremely broad bandwidths and has enabled major advances in ultrahigh-resolution OCT imaging [3-4].

2.3 Two-Photon Excitation Microscopy (TPEM)

Smaller tissue regions at depths of up to about 1 mm may be investigated by two-photon excitation microscopy (TPEM), another and complimentary imaging method based on ultrashort pulses. The ultrashort pulse duration of femtosecond lasers allows for strong nonlinear excitation without the degree of damage caused by high average power lasers. As a result of nonlinear absorption, only the region of the laser focus has sufficient intensity to give rise to fluorescence. By scanning the laser focus over a three-dimensional grid in the sample, this fluorescence can be used to map the tissue [5] (see Figure 2-1).

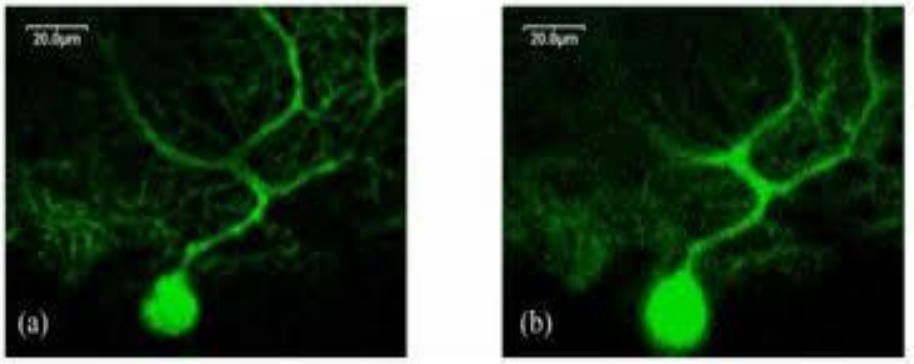

Figure 2-1 Two-photon (a) and single-photon (b) excitation fluorescence images of the same branch in a mouse brain expressing green-fluorescent protein (GFP). The two-photon image was taken using 0.4 kW optical pulses, and the single-photon image with a 488 nm argon-ion laser [6].

TPEM originated with a theoretical proposal by Sheppard et al [7] . followed by a seminal demonstration by Denk et al. in 1990 [8].

The two-photon fluorescence intensity (I) is proportional to the square of the peak power (P_{peak}). Taking into account the relationship between the peak power, the average power (P_{av}), the pulse duration (t), and the optical pulse period (T), the following equation is obtained,

$$I = k \left(\frac{T}{t}\right) P_{av}^2 \qquad 2.1$$

where k is a factor that depends on the photon absorption cross section of the fluorophore at the laser wavelength and on the spatial energy distribution in the focus.

The average output power needs to be high enough for excitation of the fluorophore to occur but not so high (except in the case of nonsurgical applications) as to damage biological samples. One particular danger is if the temperature of the tissues under investigation rises significantly due the absorption of infrared by water molecules; beyond a certain thermal threshold, cells and tissues will degrade due to protein denaturation. For such imaging through biological tissue, a wavelength region between

600 nm and 1300 nm is desirable because of the transmission window in the absorption profile as shown in Figure 2. For wavelengths higher than 1300 nm, light absorption by water molecules becomes substantial, although its effect also depends on the pulse energy (See Figure 2-2).

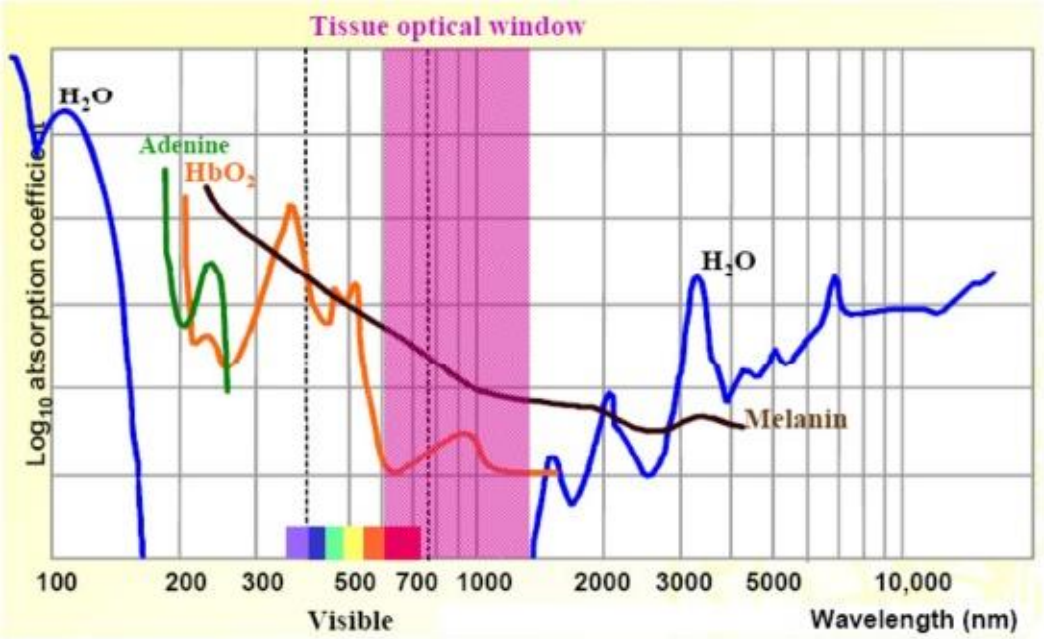

Figure 2-2 Absorption in tissue is dominated by protein and DNA in the UV, by water in the IR, and by haemoglobin and melanin in the visible light [9].

The enormous potential of TPEM as a biological research tool encouraged its rapid technological development. The availability of turnkey, tunable femtosecond lasers covering the 800 nm – 1600 nm wavelength range has vastly expanded the options for studying cellular and sub cellular functions with minimal damage to living tissue.

Two-photon microscopy using longer wavelengths has received special attention in recent years because of its ability to image deep tissue structures. This is of particular interest in studying, for example, blood flow and neuronal activity at depths greater than 0.6 mm. Kobat et al. compared the maximum imaging depth of blood vessels in a mouse brain attainable using excitations at 775 nm and 1280 nm, and reported a depth of 1 mm for the latter [10].

Ti:sapphire lasers have been the workhorse of imaging systems based on TPEM but have the disadvantages of being bulky, expensive, and requiring considerable maintenance. For these reasons, much effort has gone into developing pulsed light sources based on all-semiconductor lasers, such as the diode laser [11] (See Figure 2-3).

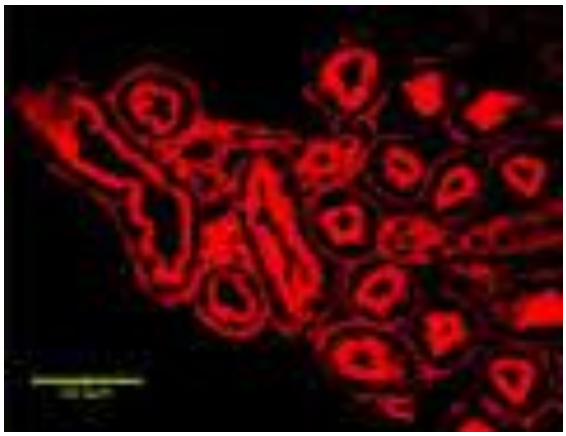

Figure 2-3 Two-photon excited fluorescence image of glomeruli and convoluted tubules in mouse kidney tissue, using an all-LD picosecond light source at average optical power 98 mW (32 W peak power) [11].

2.4 Possible Sources for Biomedical Applications

For biomedical applications, effective alternatives to Ti:sapphire lasers have been sought, not only for the reasons mentioned above, but also in order to minimize wavelength-dependent photo-bleaching and cell damage that might be caused by on-focus high-intensity near-infrared pulses. Cheng et al [12] reported on the implications of high illumination intensity, nonlinear photochemical processes on plant cell physiology and viability. The use of a Cr:forsterite laser [13] with its longer output wavelength, was found to significantly reduce multi-photon absorption by living tissue. Lengthy irradiation by a Cr:forsterite beam at more than 100 mW average power induced less damage than bursts of just a few seconds by a 10 mW Ti:Sapphire beam.

Effort has also been directed at developing other fs sources that are more compact and cost effective than Ti:sapphire technology. These include fibre lasers, Cr:LiSAF lasers and semiconductor lasers, although each of these, in turn, pose challenges if they are to reach their full potential.

Another approach to the use of ultrafast lasers for biomedical applications involves extreme chirped pulse amplification (X-CPA). This employs a colliding pulse external cavity mode-locked semiconductor laser, considerable pulse stretching, multiple amplification stages, and significant compression. In 2008, Kim et al [14] demonstrated a system based on X-CPA that could generate optical pulses of 590 fs at a wavelength of 975 nm and a peak power of 1.4 kW. At the time, this was a world record but it has since been superceded by Schlauch et al [15] through use of a passively mode-locked external cavity diode laser operating at around 830 nm and generating 622 fs pulses with average output power of 513 mW. The peak power achieved in this system was 2.5 kW.

Diode lasers, which form the subject of this work, are especially attractive because they can be pumped directly with an electrical current instead of an intrinsically more complex optical pump. However, for biomedical applications they have traditionally been hampered by two difficulties: first, their average power is typically only in the low mW range, so they need further amplification, for example by semiconductor tapered amplifiers, and, second, they cannot easily generate sub-picosecond pulse widths. The latter problem is ameliorated in mode-locked edge emitting diode lasers that are based on quantum dots [16]. In QD-based lasers the direct generation of weakly chirped sub-picosecond pulses becomes possible. With standard diode lasers, sub-picosecond pulse widths could in most cases only be realized by external pulse compression to reduce the chirp. Using this strategy, all semiconductor laser systems could be realized that provide

peak powers of 1.4 kW [14] in the case of colliding pulse mode-locked lasers or 2.5 kW in the case of passively mode-locked lasers [17].

2.5 Nanosurgery

Pulse energy is a key factor in giving rise to nonlinear effects, which are essential in order to observe biological structures down to the sub-cellular level. If the purpose is to image then the pulse energy must be kept low enough to avoid significant photodamage. However, in some applications, such as nanosurgery, the goal is to structurally modify or ablate tissue in very restricted, highly-targeted regions. This is achieved by using pulse intensities that give rise to tiny, rapidly expanding clouds of plasma in the focal volume [18]. It has been shown that ultrashort pulses, on the order of 100 fs, with modest pulse energies, can deposit sufficient energy (a few nJ) to cause tissue dissection when focused at high numerical aperture [19].

2.6 Second-and Third-Harmonic Generation

Other nonlinear imaging techniques based on ultrafast lasers have also been developed over the past two decades. Second harmonic generation (SHG), for example, is now employed as a contrast mechanism for some applications. This technique involves two photons simultaneously interacting with molecules in a sample and producing light at exactly half the excitation wavelength; it is especially applicable to imaging interfaces, such as cell membranes. Yokoyama et al [20] used SHG to generate 5 ps pulses at 770 nm with 1 kW peak power to image actin filaments in PtK2 cells. Third harmonic generation (THG) has also become a significant nonlinear imaging modality, especially

for mapping the distribution and orientation of different materials within a biogenic sample.

2.7 Three-Photon Fluorescence

Although the potential of using three photons in multiphoton fluorescence microscopy was realised in the 1990s, it is only very recently that the first practical instruments have been built to exploit it. Three-photon fluorescence offers the advantage of being able to image at greater depth, up to 3.5 mm, yet without harming the tissue under study. This makes it particularly useful in neurobiology where, for example, it is desirable to see cells under the white matter without having to remove or damage this uppermost layer of brain tissue. Horton et al. describe how they overcame some of the limitations of two-photon fluorescence microscopy through a combination of using long excitation wavelength (1700 nm) and higher-order nonlinear excitation [21].

Optically pumped vertical external-cavity surface-emitting lasers (VECSELs) have also been shown to be attractive compact sources of picosecond pulses with average power above 2 W or even of femtosecond pulses with pulse widths down to 60 fs and peak powers up to 315 W.

2.8 The Future

The great strides in biomedical imaging and the manipulation of biological systems on a submicron scale made possible by ultrafast laser technology ensure that rapid further development of this technology will take place. Progress can be expected in areas such as optimizing pulse phase and amplitude to reduce photodamage and bleaching; signal generation efficiency and spatial resolution; the introduction of new fluorescent labels;

and, especially in the case of clinical applications, the evolution of smaller and less costly ultrafast devices such as multiphoton endoscopes [22].

Ultrafast pulsed lasers can be used to achieve remarkable precision during surgical ablation. Through nonlinear interactions with tissue, they furnish a mostly non-thermal mean of ablation and a unique ability to create targeted damage within bulk tissue. These advantages have made ultrafast lasers the ideal surgical tool for various novel applications in ophthalmology. Clinical adoption of ultrafast lasers in other surgical applications will expand as the technology evolves to deliver ultrafast pulses by flexible fibres.

From the perspective of biomedical imaging, the central advantage of nonlinear microscopy based on ultrafast pulsed lasers is its ability to image deeply while at the same time causing minimal perturbation to the sample. This enables the researcher to look at subcellular structures and functioning in vivo over extended periods of time. Challenges to the future of this technology include pulse dispersion, beam delivery, and sample-induced aberrations.

Major efforts are also being made to improve imaging at greater tissue depths, through the development of new modalities, such as three-photon microscopy, and further development of two-photon microscopy at longer wavelengths, at 1300 nm and beyond, the latter being the subject of the present work [23] (See Figure 2-4)

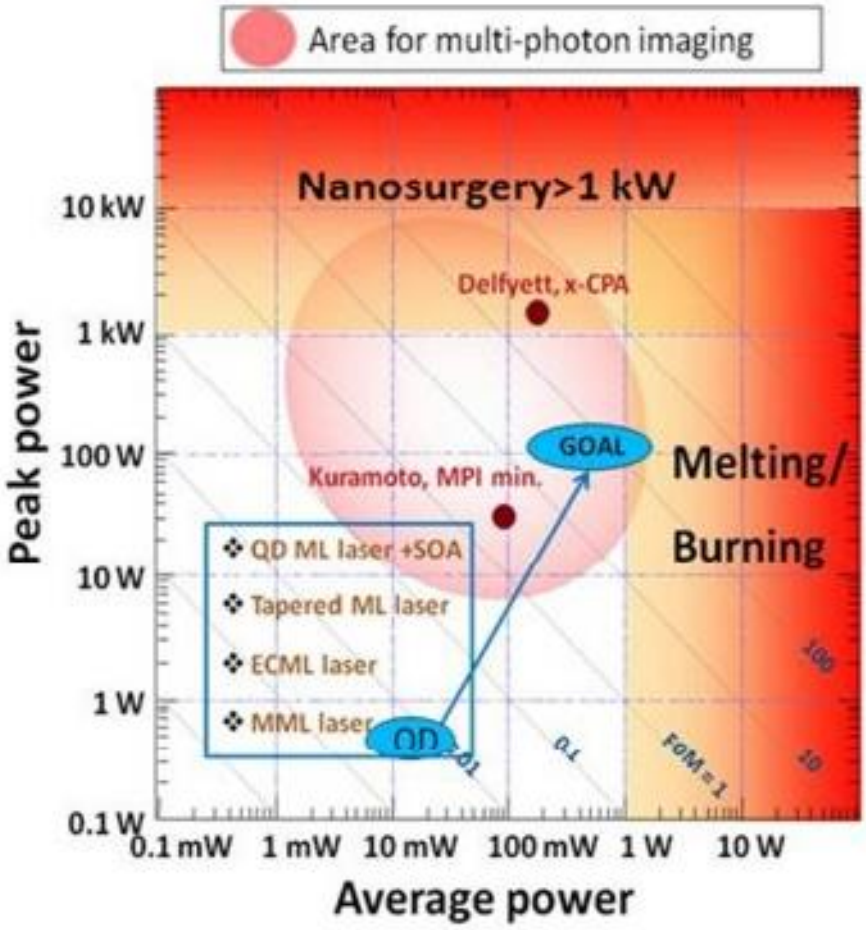

Figure 2-4 Mapping of the initial state of art at the beginning of this work and goal for the QD based mode-locked lasers.

.

2.9 References

[1] K. E. Sheetz and J. Squier, "Ultrafast optics: Imaging and manipulating biological systems," *Journal of Applied Physics,* vol. 105, p. 051101, 2009.

[2] W. Sibbett, A. Lagatsky, and C. Brown, "The development and application of femtosecond laser systems," *Optics express,* vol. 20, pp. 6989-7001, 2012.

[3] J. Fujimoto, A. Aguirre, Y. Chen, P. Herz, P.-L. Hsiung, T. Ko, N. Nishizawa, and F. Kärtner, "Ultrahigh-Resolution Optical Coherence Tomography Using Femtosecond Lasers," in *Ultrashort Laser Pulses in Biology and Medicine*, ed: Springer, 2008, pp. 3-27.

[4] J. G. Fujimoto, C. Pitris, S. A. Boppart, and M. E. Brezinski, "Optical coherence tomography: an emerging technology for biomedical imaging and optical biopsy," *Neoplasia (New York, NY),* vol. 2, p. 9, 2000.

[5] P. T. So, C. Y. Dong, B. R. Masters, and K. M. Berland, "Two-photon excitation fluorescence microscopy," *Annual Review of Biomedical Engineering,* vol. 2, pp. 399-429, 2000.

[6] H. Yokoyama, A. Sato, H.-C. Guo, K. Sato, M. Mure, and H. Tsubokawa, "Nonlinear-microscopy optical-pulse sources based on mode-locked semiconductor lasers," *Optics Express,* vol. 16, pp. 17752-17758, 2008.

[7] C. Sheppard and R. Kompfner, "Resonant scanning optical microscope," *Applied Optics,* vol. 17, pp. 2879-2882, 1978.

[8] W. Denk, J. H. Strickler, and W. W. Webb, "Two-photon laser scanning fluorescence microscopy," *Science,* vol. 248, pp. 73-76, 1990.

[9] V. Serebryakov, "Lectures notes," *St. Petersburg State University of information Technologies, Mechanics and Optics; Department of Laser Technologies and Applied Ecology*, 2007.

[10] D. Kobat, M. E. Durst, N. Nishimura, A. W. Wong, C. B. Schaffer, and C. Xu, "Deep tissue multiphoton microscopy using longer wavelength excitation," *Optics Express,* vol. 17, pp. 13354-13364, 2009.

[11] M. Kuramoto, N. Kitajima, H. Guo, Y. Furushima, M. Ikeda, and H. Yokoyama, "Two-photon fluorescence bioimaging with an all-semiconductor laser picosecond pulse source," *Optics Letters,* vol. 32, pp. 2726-2728, 2007.

[12] P.-c. Cheng, B.-L. Lin, F.-J. Kao, M. Gu, M.-G. Xu, X. Gan, M.-K. Huang, and Y.-S. Wang, "Multi-photon fluorescence microscopy—the response of plant cells to high intensity illumination," *Micron,* vol. 32, pp. 661-669, 2001.

[13] I.-H. Chen, S.-W. Chu, C.-K. Sun, P.-C. Cheng, and B.-L. Lin, "Wavelength dependent damage in biological multi-photon confocal microscopy: A micro-spectroscopic comparison between femtosecond Ti: sapphire and Cr: forsterite laser sources," *Optical and quantum electronics,* vol. 34, pp. 1251-1266, 2002.

[14] K. Kim, S. Lee, and P. Delfyett, "1.4 kW high peak power generation from an all semiconductor mode-locked master oscillator power amplifier system based on eXtreme Chirped Pulse Amplification (X-CPA)," *Optics express,* vol. 13, pp. 4600-4606, 2005.

[15] T. Schlauch, J. Balzer, M. Hofmann, A. Klehr, G. Erbert, and G. Tränkle, "Passively mode-locked two section laser diode with intracavity dispersion control," in *SPIE OPTO*, 2011, pp. 79370S-79370S-7.

[16] E. Rafailov, M. Cataluna, and W. Sibbett, "Mode-locked quantum-dot lasers," *Nature Photonics,* vol. 1, pp. 395-401, 2007.

[17] T. Schlauch, M. Li, M. Hofmann, A. Klehr, G. Erbert, and G. Trankle, "High pak power femtosecond pulses from modelocked semiconductor laser in external cavity," *Electronics Letters,* vol. 44, pp. 678-679, 2008.

[18] A. Vogel and V. Venugopalan, "Mechanisms of pulsed laser ablation of biological tissues," *Chemical Reviews,* vol. 103, pp. 577-644, 2003.

[19] N. Shen, D. Datta, C. B. Schaffer, P. LeDuc, D. E. Ingber, and E. Mazur, "Ablation of cytoskeletal filaments and mitochondria in live cells using a femtosecond laser nanoscissor," *Mech. Chem. Biosyst,* vol. 2, pp. 17-25, 2005.

[20] H. Yokoyama, H. Guo, T. Yoda, K. Takashima, K.-i. Sato, H. Taniguchi, and H. Ito, "Two-photon bioimaging with picosecond optical pulses from a semiconductor laser," *Optics Express,* vol. 14, pp. 3467-3471, 2006.

[21] N. G. Horton, K. Wang, D. Kobat, C. G. Clark, F. W. Wise, C. B. Schaffer, and C. Xu, "In vivo three-photon microscopy of subcortical structures within an intact mouse brain," *Nature Photonics,* vol. 7, pp. 205-209, 2013.

[22] J. M. Eichenholz, M. Li, I. Read, S. Marzenell, P. Féru, R. Boggy, and J. Kafka, "Future trends and applications of ultrafast laser technology," in *Lasers and Applications in Science and Engineering*, 2006, pp. 61000H-61000H-13.

[23] G. Norris, R. Amor, J. Dempster, W. B. Amos, and G. McCONNELL, "A promising new wavelength region for three-photon fluorescence microscopy of live cells," *Journal of Mcroscopy,* vol. 246, pp. 266-273, 2012.

Chapter 3. **Mode locked lasers: Physics**

3.1 Quantum Dot-Based Mode-Locked Lasers

Recently, quantum dot-based mode-locked lasers have been developed which offer the next generation of compact ultrashort pulse sources thanks to the discrete nature of the density of states [1]. The contemporary technologies of quantum-dot (QD) growth offer a significant degree of control over the emission spectrum of QD devices, which can then be tailored for different applications: for example, a broadly-tunable laser (1073.9 nm - 1173.9 nm, 1141.6 nm - 1251.7 nm, and 1198.2 nm - 1253.1 nm) [2-8] such as a monolithic multi-section laser incorporating five QD layers. These have demonstrated a wavelength tunability ranging from 1004.3 nm to 1029.1 nm which is controlled by different injection currents in the multiple sections [3]. The electronically-controlled 45 nm wavelength sweep range is the result of chirped multiple QD-based mode-locked monolithic lasers [6]. Alternatively, external cavity diode lasers incorporating multiple chirped QD layers and bent waveguide have also demonstrated impressive tunability ranges (up to 202 nm) with nearly 500 mW maximum output power under continuous-wave operation [2].

3.2 Semiconductor Optical Amplifiers (SOAs)

Semiconductor optical amplifiers (SOAs) are optoelectronic devices that use a combination of semiconductors, such as InP/GaAs or InAs/GaAs, as the gain medium. They work in a similar way to semiconductor lasers, that is, by amplifying the incident light through stimulated emission. A double heterostructure is normally employed in which a thin active semiconductor of ~0.1 μm thickness is sandwiched between p-type

and n-type cladding layers of another semiconductor with a larger bandgap, resulting in a heterostructure that is forward-biased through metallic contacts [9].

The schematic operation of an SOA with both input and output fibres is shown in Figure 3-1. An optical signal is injected into the waveguide of an SOA and, during propagation, is amplified, the optical gain being achieved through the injection of an electric current into the active region.

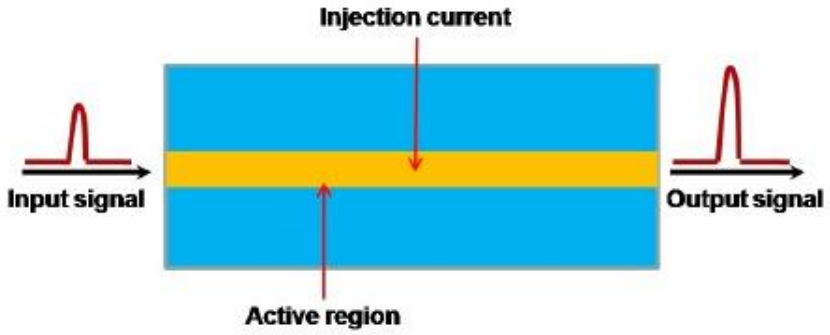

Figure 3-1 Schematic of an SOA [10].

SOAs are classified into two main types depending on the material in the active region: bulk SOAs, consisting simply of a bandgap material, and quantum well SOAs, in which the active region is normally based on a separate confinement material, consisting of quantum wells and barriers.

SOAs can also be classified according to their residual reflectivity. Fabry-Perot (FP) amplifiers have significant reflectivities at their input and output facets, resulting in the light being reflected back into the active region, which thus acts as a resonant cavity. In contrast, the travelling wave (TW) amplifier has a small-facet reflectivity and the incident light is amplified in a single pass through the amplifier.

Quantum-dot semiconductor optical amplifiers (QD-SOAs), such as the one used in the present work, are particularly useful in ultrafast laser systems for biomedical applications because of their ability to produce high peak-power pulses, which, in turn,

give rise to strong nonlinear effects that are desirable in bio-imaging. Properties that make QD-SOAs well suited for amplifying ultrashort pulses include their high gain saturation characteristics, broad gain bandwidth, fast gain recovery time, and low noise [11].

The laser system used here is a master-oscillator power amplifier (MOPA) based on a QD external-cavity passively mode-locked laser (QD-ECMLL), amplified by a tapered QD-SOA, in which the width of the waveguide increases along its length. The SOA and oscillator have a similar epitaxial structure in order to achieve excellent mode matching.

3.3 Electrically Pumped Vertical External-Cavity Surface- Emitting Lasers

By means of optically pumped vertical external-cavity surface-emitting lasers (OP-VECSELs), also known as semiconductor disk lasers (SDLs), the concept of an external-cavity surface-emitting semiconductor laser was successfully employed to achieve significant power-scaling in both continuous wave and mode-locked regimes [12-13]. The lowest repetition rate demonstrated in mode-locked OP-VECSELs was 86 MHz at 980 nm waveband was demonstrated in pulsed SESAM-free configurations [14-15]. OP-VECSELs are used for a number of applications, including nonlinear imaging techniques in biophotonics [16]. Electrically pumped vertical external-cavity surface- emitting lasers (EP-VECSELs) were envisioned to further reduce size footprint size and increase efficiency whilst keeping the flexibility of their optically pumped counterparts for lower power applications [17]. The output power from mode-locked EP-VECSELs was mainly controlled by limited contact aperture size and achievable beam quality. Pulse duration was defined by narrow optical bandwidth because of the semiconductor micro-cavity formed by two Bragg reflectors [18].

VECSELs are generally recognised as an extremely flexible device with a unique set of advantages [19-21]. The first advantage is high output power up to tens of watts in CW with optically pumped mode, and a second is outstanding beam quality with true TEM_{oo} emission. Both of these features are the result of building an extended cavity outside a semiconductor gain chip because of more design flexibility [22]. In this chapter the development of electrically pumped VECSELs and related issues are discussed. The experimental results of the testing of these devices in both continuous wave and mode-locking regimes are presented.

3.4 Structure of EP-VECSELs and Fabrication

Generally speaking, the design of optically pumped SDLs includes calculation of the correct distributed Bragg reflector (DBR) with the required reflectivity and an active region with the desired number of QW or QD layers and their position. Changing the area of the external pump spot on the device offers the possibility of a separate modification because of parameters such as power-scaling. The growth and fabrication processes are made simpler by avoiding the need for doping and electrical contacts. In the case of EP-VECSELs, however, the design is more complex because of the need for a trade-off between optical and electrical parameters [23-24]. Typically an EP-VECSEL consists of a p-doped highly reflective bottom DBR in which a number of QWs are inserted above and positioned at the antinodes of the optical standing wave, thus achieving the maximum gain. A partially reflective n-doped DBR of around 80 % is deposited above the QWs. Figure 3-2 shows a schematic cross-section of the semiconductor part of the EP-VECSEL with a quantum-well active region and n-type current spreading layer [25].

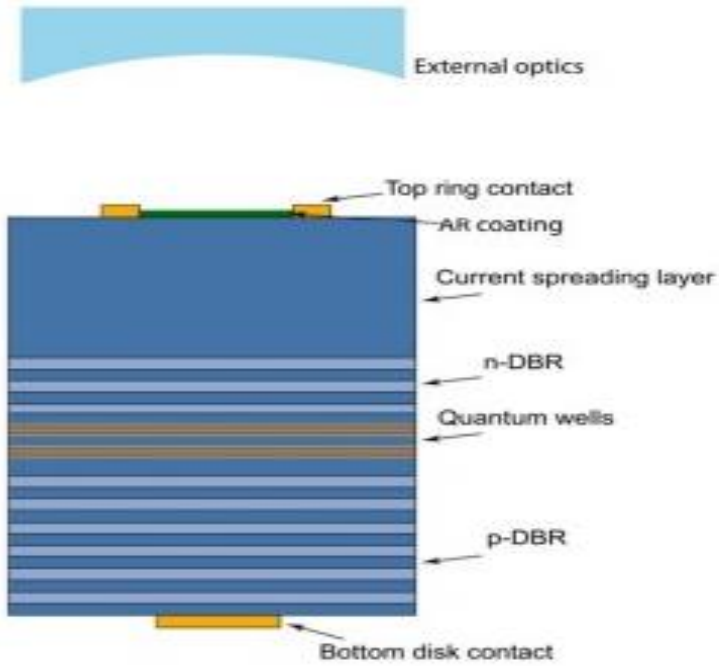

Figure 3-2 A schematic-cross section view of EP-VECSEL [25].

Additionally the overall design of the EP-VECSEL as discussed above involves trade-offs between many competing parameters. In the example of the p-doped DBR the hole mobility leads to high resistivity of the layers, hence increasing Joule heating and degradation of the device performance. For example, if the number of quarter-wave thick layers is reduced the high reflectivity value is sacrificed. Furthermore, in such a case heavier doping must be used which in turn increases the losses owing to free carrier absorption, especially when doping levels exceed 10^{18} cm^{-3}. The optimal solution to this problem is mole fraction grading at the layer interfaces [24]. Alternatively, n-doped DBR is slightly less demanding as it features lower resistivity and layers with or without doping grading can be grown. Typically, doping concentrations for both are of the order of 10^{18} cm^{-3}, and of the order of 10^{17} cm^{-3} - 10^{18} cm^{-3} for the current spreading layer [18]. A sample near-field electroluminescence profile measurement is shown in Figure 3-3 as well as data for differing bottom contact diameters. The measured profiles reflect the carriers' distribution across the emitter. At sizes above 100 μm the intensity

at the edges of the profile is increased, revealing lower carrier concentration in the centre of the device.

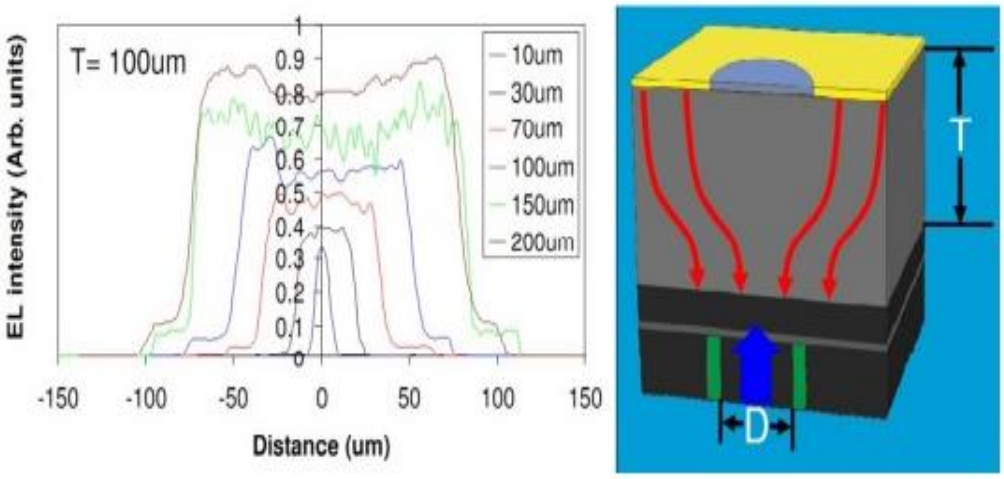

Figure 3-3 Near-field electroluminescence profile measurements of EP-VECSEL with different bottom contact diameters [23].

Research aimed at improving the performance of EP-VECSELs continues [26]. The advantages of incorporating QDs to allow the extension of wavelength coverage to 1.1 µm to 1.3 µm and potentially lowering the threshold of such devices to improve the overall efficiency are clear. The main remaining problem is that QDs exhibit relatively low gain compared with QW structures but this issue is generally overcome by growing a number of layers of QD to increase the gain [27]. If, however, the multilayered approach is used the active region becomes unsuitably thick for the EP-VECSEL, resulting in problems with carrier transport uniformity.

3.5 Semiconductor Saturable Absorber Mirror (SESAM)

Any general introduction to SESAM must acknowledge that this component in the compact mode-locking solid state laser is an extremely important one offering the

possibility of passive pulsed solid laser systems [28]. These extend from Q-switched pulses in the nanosecond and picosecond regime to mode-locked pulses from tens of picoseconds to sub 10 fs. This section reviews the theory and design of SESAMs and focuses on certain specific topics such as their structural design and fabrication [29].

A saturable absorber is a material in which the light intensity increases precisely because the absorption decreases. The three key parameters are the wavelength range in which it absorbs its dynamic response, how fast it recovers and lastly its saturation intensity and fluence, i.e. at what intensity or pulse energy density it saturates. Semiconductors, however, can absorb radiation over a broad range of wavelengths (from visible to mid-infrared). By altering the growth parameters and device designs, their absorption recovery time and saturation fluence can be controlled. The SESAM is a saturable absorber that operates in reflection, the reflectivity increasing with higher incoming pulse intensity [30].

Over the last few years there have been significant improvements in device design, fabrication process and long-term device reliability, resulting in designs that cover wavelengths from 800 nm to 1600 nm, pulse widths from femtoseconds to nanoseconds and power level from milliwatts to 100 watts. A semiconductor absorbs light when the photon energy is sufficient to excite carriers from the valence band to the conduction band. Under conditions of strong excitation the absorption is saturated because possible initial states of the pump transition are depleted while the final states are partially occupied. A partial recovery of the absorption stems from the carriers in each band thermalising in 60 fs to 300 fs. On a longer timescale, however, such as between a few ps and ns by recombination and trapping the carrier will be removed. The differing timescales are useful for mode-locking when the longer time constant results in a reduced saturation intensity for part of the absorption, facilitating self-starting mode-locking; the faster time constant is more effective in shaping sub-ps pulses. These

factors produce a significant system where SESAM allows for easy achievement of self-starting mode-locking [31].

With the low intensity of part of the pulse being absorbed and the high intensity passing through the material with little loss, the result is a compression of the pulse. Figure 3-4 shows the three fundamental passive mode-locking models, i.e., both fast and slow are used in this context. In conclusion, the above three models demonstrate results of differing pulses where a combination of different gain medium and absorbers is used [28].

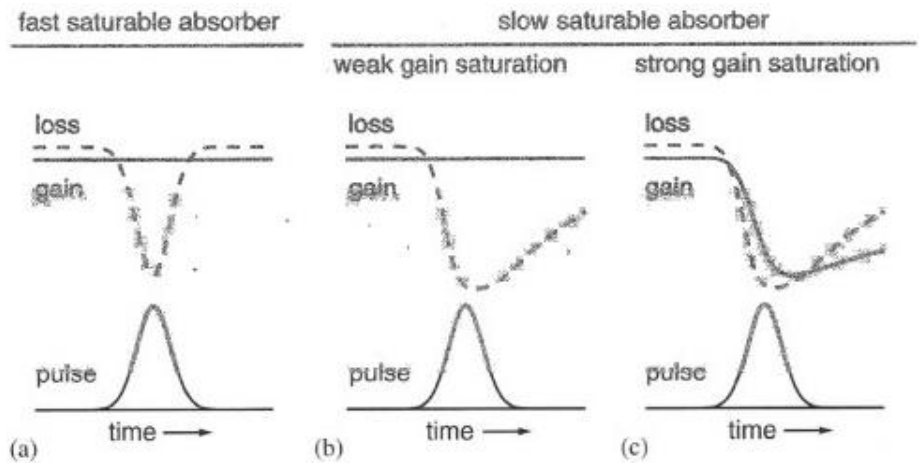

Figure 3-4 Pulse formation mechanisms using fast and slow saturable absorbers [32].

3.6 Design and Fabrication of SESAMs

The DBR for the design wavelength is first deposited on the semiconductor substrate with the absorber region of the SESAM deposited on top. Light reflection from the DBR and semiconductor air interface creates a standing wave effect in the absorber region. The creation of a resonant period structure using spacer layers is the result of QD and QW layers being positioned at the antinodes of such a standing wave [33]. SESAMs do not usually use a blocking layer, which allows faster carrier recombination and the top of the SESAM to be covered by a GaAs layer. Adjustments can be made to

the thickness of the absorber section to allow it to be in resonance or antiresonance with the design wavelength. This results in significant flexibility and allows for the different properties of the SESAM which affect the enhancement factor in the subcavity, field intensity at the semiconductor air interface and operational bandwidth and dispersion value [34].

Figure 3-5 shows two sample structures of a SESAM. The left part of the structure shows part of the DBR followed by absorber sections containing a single QW. Part (a) is the case of an antiresonant structure and part (b) shows a resonant type of SESAM [35]. Whereas a resonant SESAM structure has lower threshold damage value, conversely the antiresonant structure is less sensitive to spectral shifts in the laser and thus has larger tolerances in the growth process.

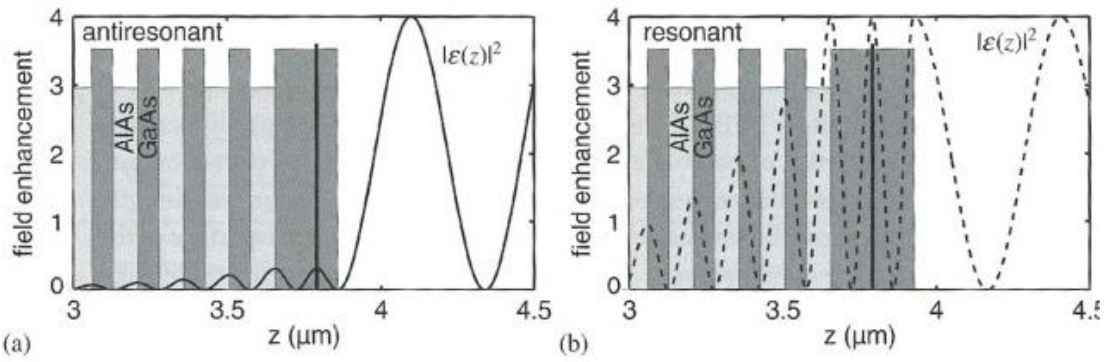

Figure 3-5 Sample structures of (a) antiresonant and (b) resonant type SESAMs [35].

Dispersion control also plays an important role when the pulse duration is in the order of a few ps or less. Group delay dispersion (GDD) in the cavity stemming from light matter interaction again differs for different types of SESAMs reveals GDD as a function of operating wavelength for resonant and antiresonant SESAMs designed for 1040 nm. GDD shows much less fluctuation around the design wavelength in the antiresonance compared with the resonant SESAM [36-37].

3.7 Pulse Generation in Semiconductor Lasers

The introduction of short periods of net gain or loss is the basis for the idea of pulse generation from semiconductor lasers. Gain switching, Q-switching and mode-locking are the three methods applied to semiconductor lasers to generate optical pulses [38]. Of these three techniques, this thesis focuses on mode-locking and a general description of which is offered below.

3.7.1 Mode-Locking

Mode-locking is a widely used method for producing short pulses and the highest repetition rates available from ultrafast lasers. It involves the locking of the phases of the longitudinal modes of the laser which results in the generation of a sequence of pulses with a repetition rate corresponding to the cavity round trip time. This is the case whether the laser systems is semiconductor or crystal-based laser systems, in principle a standing wave resonator, the pulse repetition rate f_R is approximately given by:

$$f_R = \frac{c}{2nL} \tag{3.1}$$

where c is the speed of light in a vacuum, n is the refractive index and L is the length of the laser cavity.

A further property of mode locked lasers is that the energy dispersed in several modes in continuous wave (CW) operation is now concentrated in short pulses of light. Clearly another significant property of such lasers is that even though the average power can be modest, the peak power can be high which is important, for example, for nonlinear applications [39].

$$P_{peak} = \frac{E_p}{\Delta\tau} \Rightarrow P_{peak} = \frac{1}{\Delta\tau} \cdot \frac{P_{av}}{f_R} \quad 3.2$$

where E_p is the pulse energy.

3.8 Types of Mode-Locking

In the quest for ultrafast transform-limited and high repetition rate lasers, mode-locked lasers have been central. A variety of mode-locking techniques and semiconductor device structures have been demonstrated and optimised. This research involves three techniques, i.e. active mode-locking, passive mode-locking, and hybrid mode-locking [10].

3.8.1 Active Mode-Locking

By modulating the loss or gain of the laser at a frequency corresponding to the repetition rates of the pulse, we can achieve active mode-locking in semiconductor lasers can be achieved. When there is lower loss or higher gain in short periods of time the output energy of the laser at the same time is concentrated [40]. To modulate the losses and thus establish a constant phase relationship between the longitudinal modes of the cavity, electric optic or acoustic optic modulators can be used as shutters. Optical transmission and signal processing applications make use of these features, however, high repetition frequencies are not easily obtained through directly driven modulation of lasers because the fast RF modulation of the drive current becomes more and more difficult with increasing frequency [39]. This results in short optical pulses with a constant phase relationship, as shown in Figure 3-6; the period of modulation should be approximately equal to the cavity round trip time, i.e. where the frequency of the output optical pulses is equal to the frequency of the driving current [38].

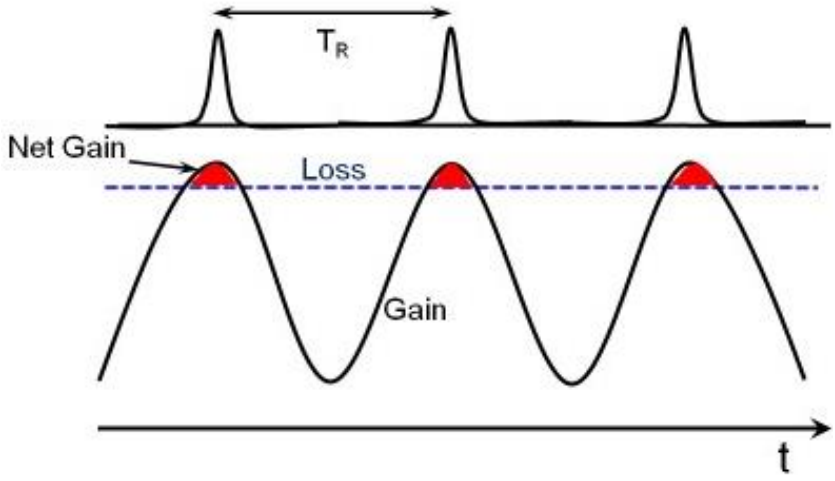

Figure 3-6 Schematic of pulse formation in time domain in active mode-locked lasers. The time window indicated in red colour represents the time duration when the device is in net gain.

3.8.2 Passive Mode-Locking

Passive mode-locking has no requirement for any external signal for modulating the gain or the loss of the laser because it incorporates an intra-cavity intensity-dependent loss element. For example, in quantum well (QW) lasers a saturable absorber (SA) is typically placed in the cavity close to one of the facets and acts as an intensity-dependent loss element. The SA section and the gain section are made of the same semiconductor material, resulting in the same bandgap.

However the SA absorbs the generated photons in the active region of the lasers which in turn causes transition of electrons from the valence band (VB) to the conduction band (CB). Where the excited electrons fill the CB and the holes fill the VB further transitions of electrons from the VB to CB are prevented leading to a point, where the SA is fully saturated and the absorber band edge is forced towards the short wavelength end of the spectrum. Figure 3-7 shows the absorption versus incident light irradiance of a typical saturable absorber.

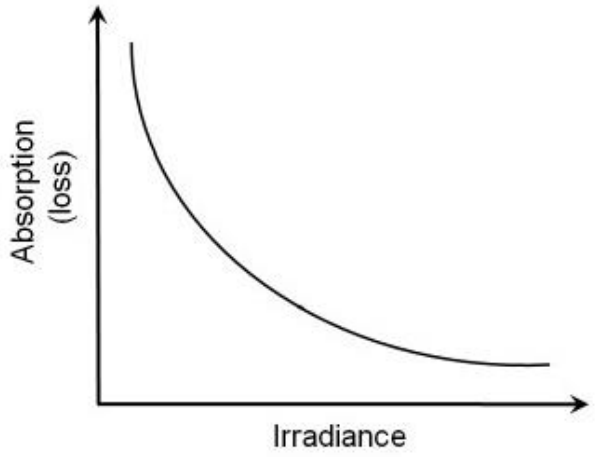

Figure 3-7 Schematic showing Absorption versus incident light Irradiance behaviour of a saturable absorber [41].

In QW lasers that are monolithically integrated passively mode locked the mechanism of growth of mode locked pulses is initially where the active medium of the laser provides spontaneous emission characterised in coherent fluctuations of intensity in the laser cavity. These fluctuations with higher intensity will then experience less absorption in the SA and will be partially transmitted by the SA, due to its intensity dependent transmission properties as shown in Figure 3-7. On the other hand, the low intensity portions of the high intensity spikes are strongly attenuated. As the light in the cavity oscillates this process is repeated and narrower and higher intensity optical pulse are formed in the cavity [41-42].

A crucial role is played by the dynamics of absorption and gain play in pulse shaping. A net gain window is achieved when the leading edge of the pulse reaches the absorber; the loss saturates more quickly than the gain, as depicted in Figure 3-8.

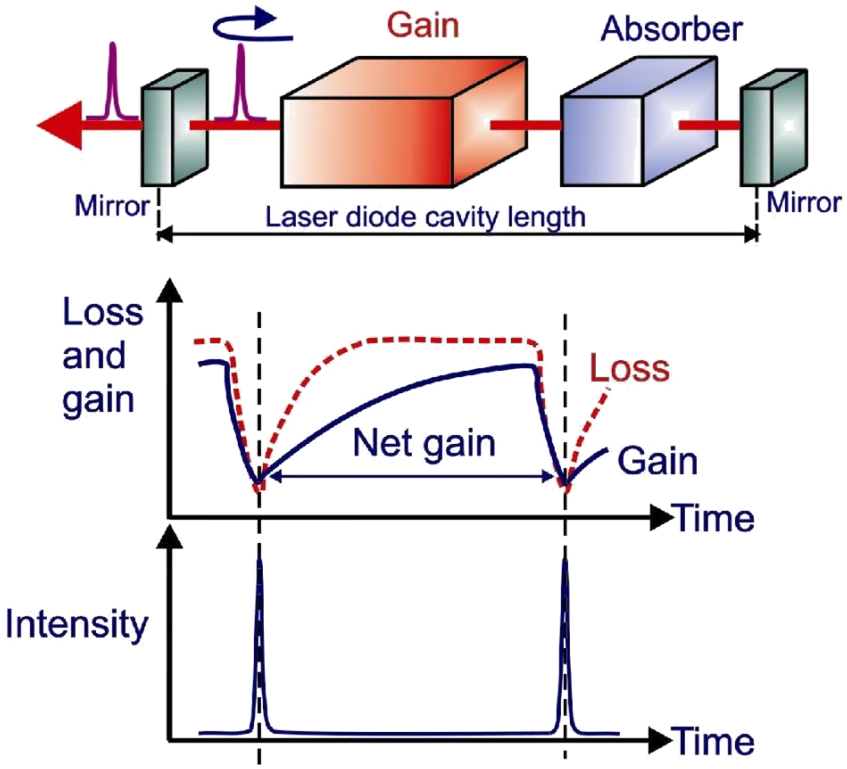

Figure 3-8 A schematic diagram of the main components that form a two-section laser diode (top). Loss and gain dynamics which lead to pulse generation (bottom) [1].

The absorber, returning from the state of saturation to the initial state of high loss, attenuates the trailing edge of the pulse. It is clear why the saturation fluence and the recovery time of the absorber are of primary importance in the formation of mode-locking pulses.

Because of higher losses from the attenuation of the trailing edge of the pulse the leading edge of the pulse experiences losses and saturates the SA. In such conditions the central part of the pulse (i.e. high intensity) is transmitted whereas the trailing edge of the pulse again experiences loss because of the recovery of the SA. Spontaneous emission cannot be built up between the emitted pulses when the value of the loss remains greater than the gain everywhere else except near the peak of the pulse [38].

3.8.2.1 Instabilities in Passive Mode-Locking

In the steady state, the various effects that influence the pulse circulating in the laser resonator balance out so that after each round trip the pulse parameters are constant, or nearly so. Consequently, when the pulse hits the output coupler mirror, a usable pulse is emitted, so that a regular pulse train leaves the laser.

However, a variety of instabilities are able to disrupt the performance of a passive mode-locked system if it moves away from steady state. In their theoretical study, Vladimirov and Turaev [43], find that two mechanisms, in particular, play a leading role in causing the onset and breakup of the fundamental and multiple mode-locked operation. The first of these mechanisms is the low-frequency Q-switching instability, in which there is a window of positive net gain (gain greater than loss) at the leading edge of the pulse, leading to a low-frequency pulsating envelope of the mode-locking pulse train. The other one is the chaotic behaviour, in which there is a window of positive net gain at the trailing edge. The mode-locking train then acquires a chaotic envelope, and the laser may consequently generate multiple pulses per round-trip with unstable spacing and/or energy.

3.8.2.2 Q-switching Instabilities

Stability of Q-switched mode locking is typically good when the pulses do not attenuate too much between bunches. However, Q-switching instabilities may come about when the pulses in each bunch are formed essentially from noise and the pulse energy within the optical cavity rises significantly above its steady-state value. The saturable absorber responds to this rise with reduced resonator losses, so that the damping of relaxation oscillations is lowered; consequently, there is a net positive gain and the pulse energy

can increase further. If the gain saturation is not sufficient to offset the destabilizing effect of the absorber then Q-switching instability occurs. This may involve wild swings in peak pulse energy, width of pulse, and phase.

Judicious design helps avoid this type of instability. Among the strategies available are: selecting a gain medium with large laser cross sections, using a resonator with small mode areas or using a long resonator with low losses and high intracavity power, and optimizing the saturable absorber. However, in certain operating regimes, for example high pulse repetition rates in conjunction with short pulses or high output powers, suppressing Q-switching instabilities may demand compromises on the duration of pulse, efficiency of the laser, or thermal load of the saturable absorber [44].

3.8.2.3 Chaotic Envelope Instability

There is also a range of other types of instability, which can come into play as a passive mode locked system moves out of steady state. These instabilities can be related, for example to excessive nonlinearities, to an inappropriate degree of absorber saturation, to absorber recovery that is too slow, to higher-order dispersion, or to inhomogeneous gain saturation, and it is not always clear which of these is at work.

Chief among the leading edge instabilities is chaotic envelope. A higher gain current may lead to a shorter gain recovery time, which in combination with a relatively long pulse roundtrip time in a long cavity, especially in an external cavity (e.g. with a repetition rate of ~200 MHz), could lead to the appearance of multiple pulses in a wider net gain window, i.e., harmonic mode-locking, which sets a limit to the lowest repetition rate and the highest operating current.

3.8.2.4 Conditions for Passive Mode-Locking

The classification of absorbers stems from the recovery time, whether it is longer or shorter, depending on the recovery time being longer or shorter than the pulse duration. Short pulse generation in semiconductor use is the combination of slow saturable absorption and gain saturation. Another crucial aspect for successful mode-locking is the use of saturation dynamics which can be translated in terms of saturation fluence, F_{sat}, or saturation energy,

$$E_{sat} = AF_{sat} \tag{3.3}$$

Where A is the optical mode cross sectional area E_{sat} is a measure of how much energy is necessary to saturate the absorption or the gain. The achievement of robust mode-locking depends on whether the saturation energy of the absorber, E_{sat}^{a}, is as small as possible and smaller than the saturation energy of the gain, E_{sat}^{g} [45],

$$E_{sat}^{a} = \frac{hvA}{\frac{\partial a}{\partial N}} < E_{sat}^{g} = \frac{hvA}{\frac{\partial g}{\partial N}} \tag{3.4}$$

Where h is Planck's constant, v is the optical frequency, A is the optical mode cross-sectional area, $\frac{\partial g}{\partial N}$is the differential loss, $\frac{\partial a}{\partial N}$is the differential gain, a is the absorber, and g is the gain.

Differential loss should be higher than differential gain, see Figure 3-9.

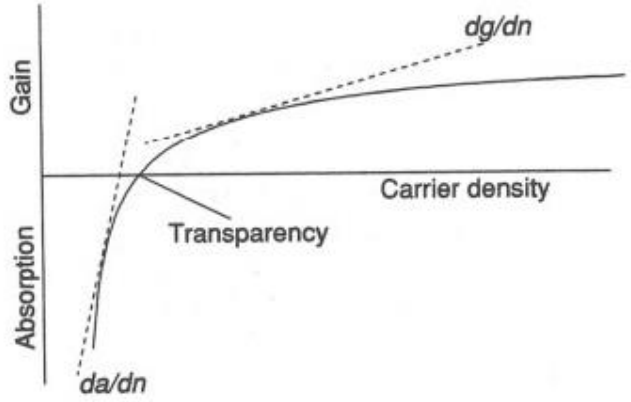

Figure 3-9 Gain/loss dynamics versus carrier concentration for successful mode-locking in laser diodes [46].

A crucial role is played by the absorbers recovery time in terms of ultra short pulse generation in high repetition rate lasers. This is critical in the formation of narrow net gain and if this requirement is met then the gain overcomes the loss only near the peak of the power and the spontaneous emission is not amplified between the pulses. The bust of noise is the result of an instantaneous phase locking occurring amongst a number of modes in regard to the frequency domain description of mode locking. The self saturation at the saturable absorber then helps to sustain and strengthen self starting mode-locking.

The QD saturable absorber's recovery is associated primarily with thermionic emission and tunnelling mechanisms. When a low reverse bias was applied to the absorber a recovery time of 62 ps was observed. This was not governed by the recombination process but by the thermal activation of the electrons from the QD ground state into an excited state with subsequent emission into the GaAs matrix. When a higher reverse bias was applied, the decrease in the absorption recovery time was observed down to 700 fs. The tunnelling electron escape mechanism from the QD ground state into the GaAs barrier becomes dominant as the barrier height is lowered by the electric field and a triangular barrier is formed [47-49].

3.8.2.5 Saturable Absorber for Passive Mode-Locking

Playing a fundamental role in the proper investigation of both mode-locking regimes and short pulse generation in MLLs, is the interaction between the recovery times of SA and nonlinear saturation in both gain and absorber sections comes into play [50-51]. The relationship between pulse duration and SA lifetime is shown in Figure 3-10 it is evident that both pulse generation and the carrier lifetime in the SA section decrease. The result of the combination of both pulse shortening and broadening mechanisms in the gain and absorber sections of the laser causes the pulse circulation in the laser cavity to be continuously reshaped. As pointed out in the previous section, the pulse shortening is due the dependent gain and loss and the net gain window contributes to the pulse shortening in the laser cavity. In the mode- locking performance and pulse properties of the mode-locked lasers fast nonlinearities such as spectral hole burning and dynamic carrier heating also play a significant role [51-52]. Such fast and efficient linearities of gain and absorption accompanied by fast refractive index nonlinearities add a fast component to the slow self-phase modulation which in turn is caused by changes in carrier density [52].

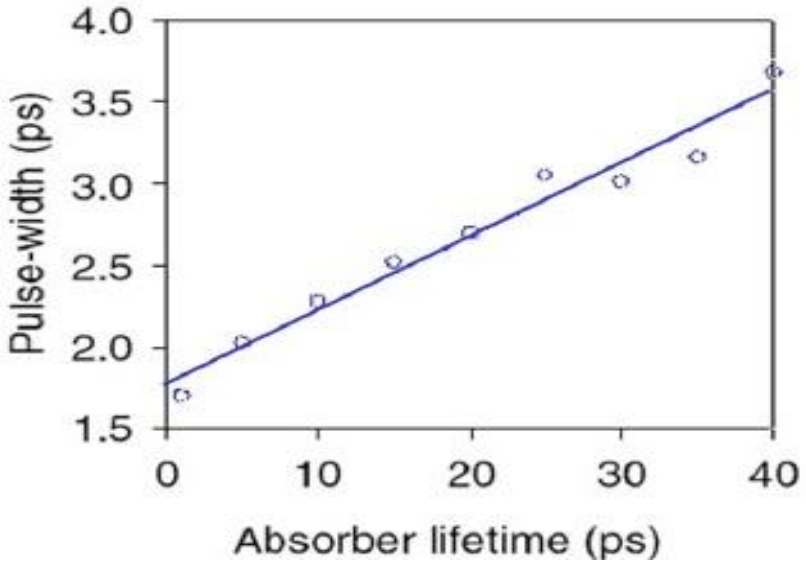

Figure 3-10 Plot showing the dependence of pulse duration on the SA lifetime [51].

3.8.3 Hybrid Mode-Locking

A combination of both passive and active mode-locking results in hybrid mode-locking. In which short optical pulses are produced in the same way as in the passive mode-locked laser and then synchronised optically or electrically to control the pulse timing [53]. To aid in the stability of the pulse and reduction of the jitter, the injection of a stable external signal to the hybrid mode-locked laser is required [54]. Hybrid mode-locking combines the best of active and passive mode-locking: in other words, the short pulse generation properties of passively mode-locked lasers are combined with the small timing jitter and stable operation properties of actively mode-locked lasers [55]. An obvious practical use of this system would be in telecommunications and data communication systems.

3.9 Advantages of QD materials.

3.9.1 Broad gain Bandwidth

Quantum dot semiconductor structures are innovative materials for the generation and amplification of femtosecond pulses. The reason for this is that one of the key parameters influencing the emission spectrum and the optical gain in such devices is the spectral broadening associated with the distribution of dot sizes. Provided all of the bandwidth can be engaged coherently and dispersion effects appropriately minimised, the very broad bandwidth available in QD mode-locked lasers is potentially useful for generating sub-100 fs pulses [56].

A comparison between QDs and QWs demonstrates that each has advantages over the other. For example, QW mode locked lasers provide some gain narrowing or filtering effects [56] whereas QD mode-locked lasers gain broad bandwidth and are inhomogeneous. Moreover due to the particular nature of QD lasers many possibilities open up in respect of the exploitation of the ground state GS and excited state ES bands, This enables multi -wavelength band switchable mode locking. On the other hand the interplay between GS and ES can be used in novel mode locking regimes. It is possible to set up tunable mode locked sources using an external cavity that can operate in the wavelength range that extends from the GS to the ES transition bands [3]. The inhomogeneous nature of the gain can also bring some advantages regarding the generation of low jitter pulses, however. A further benefit of QDs is that they offer the possibility of lower mode partition noise, enabling the generation of individual comb components with reduced relative intensity noise. [57].

3.9.2 Ultrafast Carrier Dynamics

In early studies of QD materials it was thought that their carrier dynamics would be significantly slower than those in QW materials, due to the reason being the existence of a phonon bottleneck effect [58]. Subsequently experiments actually proved the opposite when access to some recombination paths for the QD carrier structure demonstrated ultrafast recovery both under absorption and under gain conditions [59]. The absorber dynamics of surface and wave-guided QD structures were investigated by using a pump probe technique [60-61].

These investigations demonstrated that there were at least two distinct time constants (one corresponding to the rapid first stage, determined by intrados relaxation, and the other to the slower recovery phase at the trailing edge of the pulse) [62-63] for the recovery of the absorption as shown in Figure 3-11 where a fast recovery of 1 ps is followed by a slower recovery process that extends over 100 ps [61]. Recently, sub-picosecond carrier recovery was measured directly in a QD absorption modulator when a reverse bias was applied [61]. The range of the absorption recovery times was from 62 ps pulse duration to 700 fs repetition rate and demonstrated a decrease by nearly two orders of magnitude when the reverse bias applied to the structure was changed from 0 V to 6 V. Clearly there is significant promise for ultrafast modulators operating above 1 THz along with the optimisation of saturable absorbers used for the passive mode locking of semi conductor lasers where an integrated saturable absorber should be fast enough to accommodate the high repetition rate pulses generated by QD lasers.

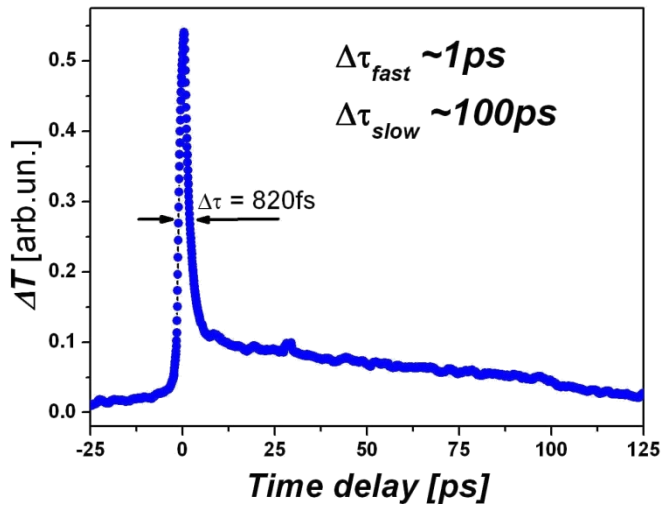

Figure 3-11 Pump-probe measurement of carrier lifetime in a QD waveguided device [61].

3.9.3 Low Threshold Current

Although QD diode lasers have the advantage of a low threshold current to initiate lasing [64] most QD lasers also exhibit mode-locked operation from the threshold of laser emission. For example, using a 1.23 μm by 5.1 mm QD laser, formed by atomic layer epitaxy due to low transparency current, low threshold current densities of 11.5 A/cm^2 are typically seen. Two stable states between the no-lasing state and the onset of lasing mode-locking may be present, as shown experimentally [65-66] and numerically [67]. A low threshold current can represent a device that is compatible as an efficient and compact source of ultrashort pulses where the demand for electrical power is low. Additionally, a low threshold avoids the need for higher carrier densities for the pumping of the laser, suggesting that less amplified spontaneous emission and reduced noise are generated by pulse sequences.

3.9.4 Low Temperature Sensitivity

QD lasers are excellent candidates for application in optical communications because the discrete nature of density of states exhibits low temperature sensitivity [68]. More importantly, QD lasers also demonstrate resilience to temperature effects while in a mode-locked operation. Furthermore, stable mode-locked operation by a QD laser has been shown at temperatures up to 80 °C [69]. A later experiment showed that the duration of the pulse generation actually decreases with temperature [70]. This can be attributed to a faster absorber recovery time with increasing temperature [71].

3.9.5 Linewidth Enhancement Factors

Ultrashort laser pulses may exhibit chirp, which is a temporal broadening of the pulse, or a rise or fall in its instantaneous frequency. Chirp is a result of dispersion in the propagating medium and of self phase modulation. It is usually quantified by the linewidth enhancement factor (LEF) – a constant of proportionality that relates changes of phase to changes in gain. If α is the LEF, then,

$$\Delta\varphi = \frac{1}{2}\alpha\Delta g \qquad 3.5$$

where $\Delta\varphi$ is the phase change and Δg the change of power gain.

Advantages follow from keeping LEF to a minimum. These include weaker self-modulation effects, lowered sensitivity to optical feedback, and reduced chirp. Of key concern is whether the optical pulses are Fourier transform-limited or chirped. This is determined by the time bandwidth product, which is the product of the temporal and spectral width of a pulse. The time bandwidth product indicates how close a pulse is to the transform limit; that is to say, how close the pulse duration is to the limit set by its

spectral width. It is thus an aspect of pulse quality: bandwidth-limited pulses have the least possible time bandwidth product, whereas chirped pulses have larger values.

The time bandwidth product is given by,

$$\Delta v \cdot \Delta \tau = \frac{c \cdot \Delta\lambda \cdot \Delta\tau}{\lambda^2} \qquad 3.6$$

where c is the speed of light, λ is the central emission wavelength, $\Delta\lambda$ is the FWHM, and $\Delta\tau$ is the pulse width (information about λ and $\Delta\lambda$, to enable calculation of the time bandwidth product, is obtained through use of an optical spectrum analyser). When spectral components fall within the bandwidth of the laser pulse there is time coincidence and the pulse is at its transform limit.

In 1999, the first measurement of LEF in an InAs QD laser diode gave a value of 0.1 below threshold [72], hinting at a bright future for transform-limited pulse generation by mode-locked QD lasers. However, since then a number of experimental studies have been published with varying outcomes, some reporting LEF values in QD devices close to zero, others finding higher values than in the case of QW [72-74].

Low LEF tends to occur within a narrow range of bias conditions, notably very close to threshold. In practical devices, LEF is found to increase significantly as the operating current is increased.

The spectral dependence of LEF above threshold in QD lasers has recently been described by Kim and Delfyett [75] along with the investigation of the spectral dependence of pulse duration and linear chirp. This work has shown that LEF is reduced when the laser is operated at about 10 nm offset from its gain peak at around 1264 nm. Even more dramatic is the effect on the anti-Stoke side, where LEF is ~1 as compared to 6 close to the gain peak. On the Stokes side, LEF is reduced only to ~4, which has a direct impact on the pulse duration and linear chirp in a tunable mode-locked QD laser.

While maintaining constant conditions, the laser was tuned in the spectral range around the gain peak from 1260 nm to 1285 nm. The spectral bandwidth on the anti-Stoke side was found to be broader around 8 nm than the band on the Stokes side. The linear chirp, on the other hand, was found to double from 3 to 6 ps nm when the wavelength was tuned from 1260 nm to 1285 nm. Such results suggest that the carrier-induced refractive index change is similar on the anti-Stokes side, although it was pointed out that there were also several other additional factors contributing to this behaviour, such as excited state effects and inhomogeneous broadening [76-77].

3.10 Mode-locked QD Lasers: the State of the Art

In 2001, Hung et al. built the first demonstration of a QD mode-locked laser which reported 17 ps pulse duration at 1.3 μm and a repetition rate of 7.4 GHz produced by a two-layer QD with a 1278 nm wavelength [65]. The highest repetition rate of 238 GHz was achieved by a GaAs-based QD laser in colliding pulse mode-locking regime [78]. The report stated that transform limited pulses of 1.3 ps duration were generated with 1.4 nm full width half-maximum of optical spectrum at 1280 nm wavelength. A further level was reached, however, when three-watt peak power was achieved by a five-layer QD-based 1.26 μm laser with 390 fs optical pulses [1, 79]. In 2006, Thomson and co-workers demonstrated the generation of pulses as short as 790 fs at 1276 nm wavelength with a peak power of 500 mW by using a flared waveguide configuration in a two-section QD laser [80-81]. Further developments followed in terms of power and ultrashort pulse generation with tapered geometry QD lasers. GaAs-based 10-layer QD lasers working in passive mode-locked regime generated pulse duration at 360 fs at 17 GHz frequency. The emission wavelength was centred at 1280 nm with optical spectra of 5.56 nm resulting in TBWP of 0.36 and a peak power up to 2.25 W [80-81].

Recently, a high peak power up to 17.7 W was attained by this group [82]. In Table 3-1 an overview summary is presented of mode-locked lasers based on InAs QD grown on a GaAs substrate.

Table 3-1 Overview of mode-locked InGaAsP quantum well lasers with the following characteristics: τ_p-pulse duration, λ_o-emission wavelength, $\Delta\lambda$- full width half maximum, frep- pulse repetition rate, P_{peak}–peak power, TBWP- time bandwidth product, N/A- not applicable. The best performances are in bold. Abbreviations used: M (monolithic), ESC (external plus SOA compression), MTW (monolithic tapered waveguide), H (hybrid), CPH (colliding pulse/harmonic), M-SOA (monolithic + SOA), P (passive) and EXT (external) [39, 83].

Number QD layers	Setup	ML Regime	τ_p (ps)	λ_o (nm)	$\Delta\lambda$ (nm)	freq (GHz)	P_{peak} (mW)	TBWP	Ref
2	M	P	17.00	1278	1	7.4	7	3.1	[65]
3	M	H/P	<14.20	1107	0.8	10	4	2.8	[84]
5	M	P	1.70	1277	.86	9.7	60	.27	[85]
5	M	H	11.00	1286	.22	20	N/A	.44	[86]
10	M	P	10	1291	.2	18	2.5	.36	[87]
5	M	P	.39	1260	14	21	3000	1	[1, 79]
10	ESC	P	1.2	1268	3.1	4.95	1220	.69	[88]
5	M	CPH	1.3	1280	1.4	238	10	.33	[78]
5	M	P	7	1190	5.5	21	156	8.1	[69]
5	MTW	P	.79	1276	3.6	24	500	.5	[66]
15	H	M-SOA	.7	1300	8.5	20	130	1.1	[89]
15	H	M-SOA	1.8	1300	2.2	40	140	.7	[89]
15	M	P	1.9	1300	4.2	80	110	1.5	[89]
6	M	P	6.4	1216	2.6	7.2	224	3.4	[90]
5	EXT	P	.93	1300	2.3	.31	410	.385	[91-92]
10	MTW	P	.36	1280	5.56	17	2250	.36	[80-81]
6	M	P	10	1209	2.8	10.2	110	5.7	[93]
8	M	P	5	1240	4.3	4.97	N/A	4.2	[94]

Number QD layers	Setup	ML Regime	τ_p (ps)	λ_o (nm)	$\Delta\lambda$ (nm)	freq (GHz)	P_{peak} (mW)	TBWP	Ref
10	EXT	P	13.6	1274	1.2	1.14	1500	3.02	[95]
10	EXT	P	12	1268	4	.281	500	8.9	[96-97]
5	EXT	P	2.2	1300	5.3	1.1	160	2.1	[92]
8	M	P	2.7	N/A	N/A	5	N/A	N/A	[98]
15	M	P	1.2	1300	N/A	40	N/A	N/A	[99]
10	M	P	1.26	1260	5.6	10	17700	1.33	[82]

3.11 References

[1] E. Rafailov, M. Cataluna, and W. Sibbett, "Mode-locked quantum-dot lasers," *Nature photonics*, vol. 1, pp. 395-401, 2007.

[2] K. A. Fedorova, M. A. Cataluna, I. Krestnikov, D. Livshits, and E. U. Rafailov, "Broadly tunable high-power InAs/GaAs quantum-dot external cavity diode lasers," *Optics Express*, vol. 18, pp. 19438-19443, 2010.

[3] J. Y.Kim, M.-T. Choi, W. Lee, and P. J. Delfyett, "Wavelength tunable mode-locked quantum-dot laser," *Proc. SPIE*,vol. 6243, pp. 1-8, 2006.

[4] X. Q. Lv, P. Jin, W. Wang, and Z. Wang, "Broadband external cavity tunable quantum dot lasers with low injection current density," *Optical Express*, 18(9), 8916-8922,2010.

[5] X. Q.Lv, P. Jin, and Z. Wang, "Broadly tunable grating-coupled external cavity laser with quantum-dot active region," *Photonics Technology Letters, IEEE*, vol. 22, pp. 1799-1801, 2010.

[6] D. I. Nikitichev, M. A. Cataluna, Y. Ding, K. Fedorova, I. Krestnikov, D. Livshits, and E. U. Rafailov, "High-power spectral bistability in a multi-section quantum-dot laser under continuous-wave or mode-locked operation," in *Lasers and Electro-Optics (CLEO), 2011 Conference on*, 2011, pp. 1-2.

[7] G. Ortner, C. N. Ortner, C. Allen, P. Dion, D. Barrios, D. Poitras, G. Dalacu, J. Pakulski, P. J. Lapointe, W. Poole, S. Render, and Raymond, "External cavity InAs⁄InP quantum dot laser with a tuning range of 166 nm," *Applied Physics Letters*, vol. 88, p. 121119, 2006.

[8] B. Stevens, D. Childs, K. Groom, M. Hopkinson, and R. Hogg, "All semiconductor swept laser source utilizing quantum dots," *Applied Physics Letters*, vol. 91, pp. 121119-121119-3, 2007.

[9] M. J. Connelly, *Semiconductor Optical amplifier*. *Heidelberg*: Springer, 2002.

[10] J. Akbar, "High power mode locked lasers monolithically integrated with semiconductor optical amplifiers," Ph.D. thesis,University of Glasgow, 2012.

[11] Y. Ding, R. Aviles-Espinosa, M. Cataluna, D. Nikitichev, M. Ruiz, M. Tran, Y. Robert, A. Kapsalis, H. Simos, C. Mesaritakis, T. Xu, P. Bardella, M. Rossetti, I. Krestnikov, D. Livshits, I. Krestnikov, D. Syvridis, M. Krakowski, P. Loza-Alvarez, and E. Rafailov, "High peak-power picosecond pulse generation at 1.26 μm using a quantum-dot-based external-cavity mode-locked laser and tapered optical amplifier," *Optics Express,* vol. 20, pp. 14308-14320, 2012.

[12] B. Heinen, T. L. Wang, M. Sparenberg, A. Weber, B. Kunert, J. Hader, S. W. Koch, J. V. Moloney, M. Koch, and W. Stolz, "106 W continuous-wave output power from vertical-external-cavity surface-emitting laser," *Electronics Letters,* vol. 48, pp. 516-U102, Apr 2012.

[13] M. Scheller, T. L. Wang, B. Kunert, W. Stolz, S. W. Koch, and J. V. Moloney, "Passively modelocked VECSEL emitting 682 fs pulses with 5.1W of average output power," *Electronics Letters,* vol. 48, pp. 588-U123, May 2012.

[14] M. Butkus, E. A. Viktorov, T. Erneux, C. J. Hamilton, G. Maker, G. P. A. Malcolm, and E. U. Rafailov, *Optics Express , to be published*.

[15] L. Kornaszewski, G. Maker, G. Malcolm, M. Butkus, E. U. Rafailov, and C. J. Hamilton, "SESAM-free mode-locked semiconductor disk laser," *Laser and Photonics Reviews,* vol. 6, pp. L20-L23, 2012.

[16] R. Aviles-Espinosa, G. Filippidis, C. Hamilton, G. Malcolm, K. J. Weingarten, T. Sudmeyer, Y. Barbarin, U. Keller, S. Santos, D. Artigas, and P. Loza-Alvarez, "Compact ultrafast semiconductor disk laser: targeting GFP based nonlinear applications in living organisms," *Biomedical Optics Express,* vol. 2, pp. 739-747, Apr 2011.

[17] J. G. McInerney, A. Mooradian, A. Lewis, A. Shchegrov, E. M. Strzelecka, D. Lee, J. P. Watson, A. Liebman, G. P. Carey, B. D. Cantos, W. R. Hitchens, and D. Heald, "High-power surface emitting semiconductor laser with extended vertical compound cavity," *Electronics Letters*, vol. 39, pp. 523-525, Mar 2003.

[18] J. R. Orchard, D. T. D. Childs, L. C. Lin, B. J. Stevens, D. M. Williams, and R. A. Hogg, "Design Rules and Characterisation of Electrically Pumped Vertical External Cavity Surface Emitting Lasers," *Japanese Journal of Applied Physics*, vol. 50, Apr 2011.

[19] J. E. Hastie, J. M. Hopkins, C. W. Jeon, S. Calvez, D. Burns, M. D. Dawson, R. Abram, E. Riis, A. I. Ferguson, and W. J. Alford, "Microchip vertical external cavity surface emitting lasers," *Electronics Letters*, vol. 39, pp. 1324-1326, 2003.

[20] M. Kuznetsov, F. Hakimi, R. Sprague, and A. Mooradian, "Design and characteristics of high-power (> 0.5-W CW) diode-pumped vertical-external-cavity surface-emitting semiconductor lasers with circular TEM 00 beams," *IEEE Journal of Selected Topics in Quantum Electronics*, vol. 5, pp. 561-573, 1999.

[21] A. Tropper, H. Foreman, A. Garnache, K. Wilcox, and S. Hoogland, "Vertical-external-cavity semiconductor lasers," *Journal of Physics D: Applied Physics*, vol. 37, p. R75, 2004.

[22] T. D. Germann, "Design and realization of novel GaAs based laser concepts," Universitätsbibliothek, 2011.

[23] D. Childs, J. Orchard, D. Williams, L.-C. Lin, B. Stevens, J. Roberts, and R. Hogg, "Trade-offs in the realization of electrically pumped vertical external cavity surface emitting lasers," in *2010 22nd IEEE International Semiconductor Laser Conf (ISLC)*, 2010, pp. 87-88.

[24] P. Kreuter, B. Witzigmann, D. Maas, Y. Barbarin, T. Südmeyer, and U. Keller, "On the design of electrically pumped vertical-external-cavity surface-emitting lasers," *Applied Physics B,* vol. 91, pp. 257-264, 2008.

[25] M. Butkus, "Quantum dot based semiconductor disk lasers," Ph.D. thesis,University of Dundee, 2012.

[26] Novalux. Inc, "Manufacturable high-power, single-mode surface emitting lasers," *III-Vs Review, vol. 14,* 2001.

[27] M. Butkus, K. Wilcox, J. Rautiainen, O. Okhotnikov, S. Mikhrin, I. Krestnikov, A. Kovsh, M. Hoffmann, T. Südmeyer, U. Keller, and E. Rafailov, "High-power quantum-dot-based semiconductor disk laser," *Optics Letters,* vol. 34, pp. 1672-1674, 2009.

[28] U. Keller, K. J. Weingarten, F. X. Kartner, D. Kopf, B. Braun, I. D. Jung, R. Fluck, C. Honninger, N. Matuschek, and J. Aus der Au, "Semiconductor saturable absorber mirrors (SESAM's) for femtosecond to nanosecond pulse generation in solid-state lasers," *IEEE Journal of Selected Topics in Quantum Electronics*, vol. 2, pp. 435-453, 1996.

[29] Y. Zhang and Y. Zhao, "Semiconductor Saturable Absorber Mirror (SESAM)," *New Mexico, Spring,* 2005.

[30] C. Hönninger, R. Paschotta, F. Morier-Genoud, M. Moser, and U. Keller, "Q-switching stability limits of continuous-wave passive mode locking," *JOSA B,* vol. 16, pp. 46-56, 1999.

[31] U. Keller, "Recent developments in compact ultrafast lasers," *Nature,* vol. 424, pp. 831-838, 2003.

[32] R. Ell, U. Morgner, F. KÃÂrtner, J. G. Fujimoto, E. P. Ippen, V. Scheuer, G. Angelow, T. Tschudi, M. J. Lederer, and A. Boiko, "Generation of 5-fs pulses

and octave-spanning spectra directly from a Ti: sapphire laser," *Optics Letters,* vol. 26, pp. 373-375, 2001.

[33] M. Y. A. Raja, S. R. Brueck, M. Osinski, C. F. Schaus, J. G. McInerney, T. Brennan, and B. Hammons, "Resonant periodic gain surface-emitting semiconductor lasers," *IEEE Journal ofQuantum Electronics,* vol. 25, pp. 1500-1512, 1989.

[34] U. Keller, "Semiconductor nonlinearities for solid-state laser modelocking and Q-switching," *Semiconductors and Semimetals,* vol. 59, pp. 211-286, 1998.

[35] T. Südmeyer, D. J. Maas, and U. Keller, "Mode-Locked Semiconductor Disk Lasers," *Semiconductor Disk Lasers: Physics and Technology,* pp. 213-261, 2010.

[36] M. Hoffmann, O. D. Sieber, V. J. Wittwer, I. L. Krestnikov, D. A. Livshits, Y. Barbarin, T. Südmeyer, and U. Keller, "Femtosecond high-power quantum dot vertical external cavity surface emitting laser," *Optics express,* vol. 19, pp. 8108-8116, 2011.

[37] G. Spühler, K. Weingarten, R. Grange, L. Krainer, M. Haiml, V. Liverini, M. Golling, S. Schön, and U. Keller, "Semiconductor saturable absorber mirror structures with low saturation fluence," *Applied Physics B,* vol. 81, pp. 27-32, 2005.

[38] P. Vasil'Ev, "Ultrashort pulse generation in diode lasers," *Optical and Quantum Electronics,* vol. 24, pp. 801-824, 1992.

[39] M. A. Cataluna, "Ultrashort-pulse generation from quantum-dot semiconductor diode lasers," Ph.D. thesis, University of St Andrews, 2008.

[40] J. Wilson and J. Hawkes, *Optoelectronics-an introduction*: Englewood Cliffs, NJ: Prentice Hall, 1989.

[41] J. Wilson and J. F. Hawkes, "Optoelectronics-an introduction," *Optoelectronics-An introduction (2nd edition), by J. Wilson and JFB Hawkes. Englewood Cliffs, NJ, Prentice Hall, 1989, 483 p.*, vol. 1, 1989.

[42] S. McMaster, "Monolithically integrated mode-locked ring lasers and Mach-Zehnder interferometers in AlGaInAs," Ph.D. thesis, University of Glasgow, 2010.

[43] A. G. Vladimirov and D. Turaev, "Model for passive mode locking in semiconductor lasers," *Physical Review A*, vol. 72, p. 033808, 2005.

[44] T. Kolokolnikov, M. Nizette, T. Erneux, N. Joly, and S. Bielawski, "The Q-switching instability in passively mode-locked lasers," *Physica D: Nonlinear Phenomena*, vol. 219, pp. 13-21, 2006.

[45] R. D. Dupuis, P. D. Dapkus, R. M. Kolbas, N. Holonyak, and H. J. Shichijo, "Photopumped laser operation of MO-CVD AlxGa1−xAs near a GaAs quantum well (λ=6200Å, 77°K)," *Appl. Phys.* Lett. vol 33, p. 596 1978.

[46] P. Vasil'ev, "Ultrafast Laser Diodes: Fundamentals and Applications," *Artech House, London*, 1995.

[47] P. Fry, J. Finley, L. Wilson, A. Lemaitre, D. Mowbray, M. Skolnick, M. Hopkinson, G. Hill, and J. Clark, "Electric-field-dependent carrier capture and escape in self-assembled InAs/GaAs quantum dots," *Applied Physics Letters*, vol. 77, pp. 4344-4346, 2000.

[48] C. Kapteyn, F. Heinrichsdorff, O. Stier, R. Heitz, M. Grundmann, N. Zakharov, D. Bimberg, and P. Werner, "Electron escape from InAs quantum dots," *Physical Review B*, vol. 60, p. 14265, 1999.

[49] D. Malins, A. Gomez-Iglesias, S. White, W. Sibbett, A. Miller, and E. Rafailov, "Ultrafast electroabsorption dynamics in an InAs quantum dot saturable absorber at 1.3 μm," *Applied Physics Letters*, vol. 89, pp. 171111-171111-3, 2006.

[50] J. Javaloyes and S. Balle, "Mode-locking in semiconductor Fabry-Pérot lasers," *IEEE Journal of Quantum Electronics,* vol. 46, pp. 1023-1030, 2010.

[51] K. Williams, M. Thompson, and I. White, "Long-wavelength monolithic mode-locked diode lasers," *New Journal of Physics,* vol. 6, p. 179, 2004.

[52] E. Avrutin, J. Marsh, and E. Portnoi, "Monolithic and multi-GigaHertz mode-locked semiconductor lasers: Constructions, experiments, models and applications," in *Optoel, IEE Proc*, 2000, pp. 251-278.

[53] G. Fiol, M. Kleinert, D. Arsenijević, and D. Bimberg, "1.3 μm range 40 GHz quantum-dot mode-locked laser under external continuous wave light injection or optical feedback," *Semiconductor Science and Technology,* vol. 26, p. 014006, 2011.

[54] B. A. Khawaja and M. J. Cryan, "Wireless hybrid mode locked lasers for next generation radio-over-fiber systems," *Journal of Lightwave Technology,* vol. 28, pp. 2268-2276, 2010.

[55] T. Hoshida, H.-F. Liu, M. Tsuchiya, Y. Ogawa, and T. Kamiya, "Subharmonic hybrid mode-locking of a monolithic semiconductor laser," *IEEE Journal of Selected Topics in Quantum Electronics,* vol. 2, pp. 514-522, 1996.

[56] P. J. Delfyett, H. Shi, S. Gee, C. P. Barty, G. Alphonse, and J. Connolly, "Intracavity spectral shaping in external cavity mode-locked semiconductor diode lasers," *IEEE Journal of Selected Topics in Quantum Electronics,* vol. 4, pp. 216-223, 1998.

[57] P. J. Delfyett, S. Gee, M.-T. Choi, H. Izadpanah, W. Lee, S. Ozharar, F. Quinlan, and T. Yilmaz, "Optical frequency combs from semiconductor lasers and applications in ultrawideband signal processing and communications," *Journal of Lightwave Technology,* vol. 24, p. 2701, 2006.

[58] K. Mukai, N. Ohtsuka, H. Shoji, and M. Sugawara, "Phonon bottleneck in self-formed In_ {x} Ga_ {1-x} As/GaAs quantum dots by electroluminescence and time-resolved photoluminescence," *Physical Review B,* vol. 54, p. R5243, 1996.

[59] P. Borri, S. Schneider, W. Langbein, and D. Bimberg, "Ultrafast carrier dynamics in InGaAs quantum dot materials and devices," *Journal of Optics A: Pure and Applied Optics,* vol. 8, p. S33-S46, 2006.

[60] P. Borri, W. Langbein, J. M. Hvam, F. Heinrichsdorff, M.-H. Mao, and D. Bimberg, "Spectral hole-burning and carrier-heating dynamics in InGaAs quantum-dot amplifiers," *IEEE Journal of Selected Topics in Quantum Electronics,* vol. 6, pp. 544-551, 2000.

[61] E. Rafailov, S. White, A. Lagatsky, A. Miller, W. Sibbett, D. Livshits, A. Zhukov, and V. Ustinov, "Fast quantum-dot saturable absorber for passive mode-locking of solid-state lasers," *Photonics Technology Letters, IEEE,* vol. 16, pp. 2439-2441, 2004.

[62] E. A. Viktorov, T. Erneux, P. Mandel, T. Piwonski, G. Madden, J. Pulka, G. Huyet, and J. Houlihan, "Recovery time scales in a reversed-biased quantum dot absorber," *Applied Physics Letters,* vol. 94, p. 3, 2009.

[63] E. A. Viktorov, T. Erneux, T. Piwonski, J. Pulka, G. Huyet, and J. Houlihan, "Pump dependence of the dynamics of quantum dot based waveguide absorbers," *Applied Physics Letters,* vol. 100, p. 241108, 2012.

[64] V. M. Ustinov, *Quantum Dot Lasers* vol. 11: Oxford University Press, 2003.

[65] X. Huang, A. Stintz, H. Li, L. Lester, J. Cheng, and K. Malloy, "Passive mode-locking in 1.3 μm two-section InAs quantum dot lasers," *Applied Physics Letters,* vol. 78, pp. 2825-2827, 2001.

[66] M. Thompson, A. Rae, R. Sellin, C. Marinelli, R. Penty, I. White, A. Kovsh, S. Mikhrin, D. Livshits, and I. Krestnikov, "Subpicosecond high-power mode

locking using flared waveguide monolithic quantum-dot lasers," *Applied Physics Letters*, vol. 88, pp. 133119-133119-3, 2006.

[67] E. A. Viktorov, P. Mandel, A. G. Vladimirov, and U. Bandelow, "Model for mode locking in quantum dot lasers," *Applied Physics Letters*, vol. 88, pp. 201102-201102-3, 2006.

[68] S. Mikhrin, A. Kovsh, I. Krestnikov, A. Kozhukhov, D. Livshits, N. Ledentsov, Y. M. Shernyakov, I. Novikov, M. Maximov, and V. Ustinov, "High power temperature-insensitive 1.3 μm InAs/InGaAs/GaAs quantum dot lasers," *Semiconductor Science and Technology*, vol. 20, p. 340, 2005.

[69] M. Cataluna, E. Rafailov, A. McRobbie, W. Sibbett, D. Livshits, and A. Kovsh, "Stable mode-locked operation up to 80 C from an InGaAs quantum-dot laser," *Photonics Technology Letters, IEEE*, vol. 18, pp. 1500-1502, 2006.

[70] M. Cataluna, E. A. Viktorov, P. Mandel, W. Sibbett, D. Livshits, J. Weimert, A. Kovsh, and E. Rafailov, "Temperature dependence of pulse duration in a mode-locked quantum-dot laser," *Applied Physics Letters*, vol. 90, pp. 101102-101102-3, 2007.

[71] M. Cataluna, D. Malins, A. Gomez-Iglesias, W. Sibbett, A. Miller, and E. Rafailov, "Temperature dependence of electroabsorption dynamics in an InAs quantum-dot saturable absorber at 1.3 μm and its impact on mode-locked quantum-dot lasers," *Applied Physics Letters*, vol. 97, pp. 121110-121110-3, 2010.

[72] T. Newell, D. Bossert, A. Stintz, B. Fuchs, K. Malloy, and L. Lester, "Gain and linewidth enhancement factor in InAs quantum-dot laser diodes," *Photonics Technology Letters, IEEE*, vol. 11, pp. 1527-1529, 1999.

[73] B. Dagens, A. Markus, J. Chen, J.-G. Provost, D. Make, O. Le Gouezigou, J. Landreau, A. Fiore, and B. Thedrez, "Giant linewidth enhancement factor and

purely frequency modulated emission from quantum dot laser," *Electronics Letters*, vol. 41, pp. 323-324, 2005.

[74] A. Ukhanov, A. Stintz, P. Eliseev, and K. Malloy, "Comparison of the carrier induced refractive index, gain, and linewidth enhancement factor in quantum dot and quantum well lasers," *Applied Physics Letters*, vol. 84, pp. 1058-1060, 2004.

[75] J. Kim and P. J. Delfyett, "Above threshold spectral dependence of linewidth enhancement factor, optical duration and linear chirp of quantum dot lasers," *Optics express*, vol. 17, pp. 22566-22570, 2009.

[76] S. Schneider, P. Borri, W. Langbein, U. Woggon, R. L. Sellin, D. Ouyang, and D. Bimberg, "Linewidth enhancement factor in InGaAs quantum-dot amplifiers," *Quantum Electronics, IEEE Journal of*, vol. 40, pp. 1423-1429, 2004.

[77] J. M. Vázquez, H. Nilsson, J.-Z. Zhang, and I. Galbraith, "Linewidth enhancement factor of quantum-dot optical amplifiers," *Quantum Electronics, IEEE Journal of*, vol. 42, pp. 986-993, 2006.

[78] A. Rae, M. Thompson, R. Penty, I. White, A. Kovsh, S. Mikhrin, D. Livshits, and I. Krestnikov, "Harmonic mode-locking of a quantum-dot laser diode," in *Lasers and Electro-Optics Society, 2006. LEOS 2006. 19th Annual Meeting of the IEEE*, 2006, pp. 874-875.

[79] E. Rafailov, M. Cataluna, W. Sibbett, N. Ilinskaya, Y. M. Zadiranov, A. Zhukov, V. Ustinov, D. Livshits, A. Kovsh, and N. Ledentsov, "High-power picosecond and femtosecond pulse generation from a two-section mode-locked quantum-dot laser," *Applied Physics Letters*, vol. 87, pp. 081107-081107-3, 2005.

[80] M. Thompson, R. Penty, and I. White, "Regimes of mode-locking in tapered quantum dot laser diodes," in *Semiconductor Laser Conference, 2008. ISLC 2008. IEEE 21st International*, 2008, pp. 27-28.

[81] M. G. Thompson, A. R. Rae, M. Xia, R. V. Penty, and I. H. White, "InGaAs quantum-dot mode-locked laser diodes," *IEEE Journal of Selected Topics in Quantum Electronics,* vol. 15, pp. 661-672, 2009.

[82] D. Nikitichev, Y. Ding, M. Cataluna, E. Rafailov, L. Drzewietzki, S. Breuer, W. Elsaesser, M. Rossetti, P. Bardella, and T. Xu, "High peak power and sub-picosecond Fourier-limited pulse generation from passively mode-locked monolithic two-section gain-guided tapered InGaAs quantum-dot lasers," *Laser Physics,* vol. 22, pp. 715-724, 2012.

[83] D. I. Nikitichev, "High power ultra-short pulse Quantum-dot lasers," Ph. D.thesis, University of Dundee, 2012.

[84] M. Thompson, C. Marinelli, K. Tan, K. Williams, R. Penty, I. White, I. Kaiander, R. Sellin, D. Bimberg, and D.-J. Kang, "10 GHz hybrid modelocking of monolithic InGaAs quantum dot lasers," *Electronics Letters,* vol. 39, pp. 1121-1122, 2003.

[85] A. Gubenko, L. Gadjiev, N. Il'Inskaya, Y. M. Zadiranov, A. Zhukov, V. Ustinov, Z. I. Alferov, E. Portnoi, A. Kovsh, and D. Livshits, "Mode-locking at 9.7 GHz repetition rate with 1.7 ps pulse duration in two-section QD lasers," in *Semiconductor Laser Conference, 2004. Conference Digest. 2004 IEEE 19th International*, 2004, pp. 51-52.

[86] M. Kuntz, G. Fiol, M. Lämmlin, D. Bimberg, M. Thompson, K. Tan, C. Marinelli, A. Wonfor, R. Sellin, and R. Penty, "Direct modulation and mode locking of 1.3 μm quantum dot lasers," *New Journal of Physics,* vol. 6, p. 181, 2004.

[87] M. Thompson, K. Tan, C. Marinelli, K. Williams, R. Penty, I. White, M. Kuntz, D. Ouyang, D. Bimberg, and V. Ustinov, "Transform-limited optical pulses from 18 GHz monolithic modelocked quantum dot lasers operating at~ 1.3 μm," *Electronics Letters*, vol. 40, pp. 346-347, 2004.

[88] M.-T. Choi, "Ultrashort, high power, and ultralow noise mode-locked optical pulse generation using quantum-dot semiconductor lasers," Ph. D.thesis, University of Central Florida Orlando, Florida, 2006.

[89] M. Laemmlin, G. Fiol, C. Meuer, M. Kuntz, F. Hopfer, A. Kovsh, N. Ledentsov, and D. Bimberg, "Distortion-free optical amplification of 20-80 GHz modelocked laser pulses at 1.3 μm using quantum dots," *Electronics Letters*, vol. 42, pp. 697-699, 2006.

[90] Y.-C. Xin, L. Lester, and D. Kane, "Frequency-resolved optical gating characterisation of passively modelocked quantum-dot laser," *Electronics Letters*, vol. 44, pp. 1255-1257, 2008.

[91] M. Xia, M. G. Thompson, R. V. Penty, and I. H. White, "External-cavity mode-locked quantum-dot lasers for low repetition rate, sub-picosecond pulse generation," in *Lasers and Electro-Optics Conference*, 2008.

[92] M. Xia, M. G. Thompson, R. V. Penty, and I. H. White, "External-cavity mode-locked quantum-dot laser diodes for low repetition rate, sub-picosecond pulse generation," *IEEE Journal of Selected Topics in Quantum Electronics*, vol. 17, pp. 1264-1271, 2011.

[93] C.-Y. Lin, Y.-C. Xin, J. Kim, C. Christodoulou, and L. Lester, "Compact optical generation of microwave signals using a monolithic quantum dot passively mode-locked laser," *Photonics Journal, IEEE*, vol. 1, pp. 236-244, 2009.

[94] L. Lester, D. Kane, N. Usechak, C.-Y. Lin, Y. Li, Y.-C. Xin, and V. Kovanis, "Pulse characteristics of passively mode-locked quantum dot lasers," in *OPTO*, 2010, pp. 761607-761607-9.

[95] Y. Ding, D. Nikitichev, I. Krestnikov, D. Livshits, M. Cataluna, and E. Rafailov, "Quantum-dot external-cavity passively modelocked laser with high peak power and pulse energy," *Electronics Letters*, vol. 46, pp. 1516-1518, 2010.

[96] M. A. Cataluna, Y. Ding, D. I. Nikitichev, K. A. Fedorova, and E. U. Rafailov, "High-Power Versatile Picosecond Pulse Generation from Mode-Locked Quantum-Dot Laser Diodes," *LEEE Journal of Selected Topics in Quantum Electronics*, vol. 17, pp. 1302-1310, Sep-Oct 2011.

[97] Y. Ding, M. A. Cataluna, D. Nikitichev, I. Krestnikov, D. Livshits, and E. Rafailov, "Broad repetition-rate tunable quantum-dot external-cavity passively mode-locked laser with extremely narrow radio frequency linewidth," *Applied Physics Express*, vol. 4, p. 2703, 2011.

[98] Y. Li, C.-Y. Lin, D. Chang, C. Langrock, M. M. Fejer, D. Kane, and L. F. Lester, "Pulse characterization of a passively mode-locked quantum dot semiconductor laser using FROG and autocorrelation," in *Lasers and Electro-Optics (CLEO), 2011 Conf*, 2011, pp. 1-2.

[99] M. Radziunas, A. G. Vladimirov, E. A. Viktorov, G. Fiol, H. Schmeckebier, and D. Bimberg, "Pulse Broadening in Quantum-Dot Mode-Locked Semiconductor Lasers: Simulation, Analysis, and Experiments," *IEEE Journal of Quantum Electronics*, vol. 47, pp. 935-943, 2011.

Chapter 4. **Characterisation of Mode locked Operation in QD-lasers**

4.1 Characterization Techniques

4.1.1 Measurement of Ultrafast pulses

Three commonly used techniques for determining the pulse duration of ultrafast laser systems are streak camera measurements, optical correlation, and frequency-resolved optical gating (FROG).

A streak camera works by transforming the time variation of the intensity of a pulse into a spatial profile across the width of a detector [1]. The pulse enters the instrument through a narrow slit along one direction and is then deflected in the perpendicular direction so that photons that arrive first impinge on the detector in a different location from photons that arrive later. The resulting image forms a "streak" of light, from which the duration of the pulse can be inferred. Even the best optoelectronic streak cameras cannot resolve below about 100 fs, and such capability is only possible for wavelengths in the range 280nm to 850 nm; the time resolution of this technique drops to a few ps in the infrared range. Measurement of pulses as short as a few fs in the infrared requires other methods, such as autocorrelation or FROG.

Optical autocorrelator can be used to measure the duration of pulses in the picosecond or femtosecond range [2]. The basic principle is to superimpose a pulse with a time-delayed copy of itself. The resulting interaction within a nonlinear crystal is used to obtain a signal that depends on the pulse overlap; the duration of the pulse can be obtained from this signal.

In order to extract a pulse duration, a decision must first be made regarding the shape of the pulse after a best fit to the required correlation is carried out. The most commonly encountered shapes are Gaussian, hyperbolic secant (sech), and Lorentzian. Depending on the particular type of pulse, the full width at half maximum (FWHM) of the correlation trace is multiplied by a given factor to obtain the pulse duration. Furthermore, the time bandwidth product (TBWP) differs for each function type. As a result of this work, it was found that a Gaussian pulse shape, best fitted all lasers, pulses, and optical spectra. The FWHM of the correlation should be multiplied by 0.707; for hyperbolic $sech^2$ it is 0.6482 and for Lorentzian 0.5. In order to obtain the pulse duration the TBWP is 0.4413 and 0.2206 for Gaussian and Lorentzian plus shapes, respectively (see Table 4-1).

An analysis of the shape of the autocorrelation function reveals whether it is an actual pulse or simply noise. There is a degree uncertainty in fitting a pulse shape to the autocorrelation trace because information on the phase of the pulse is lacking. With this technique there can also be difficulty in discriminating between weak background noise and an optical pulse. However, despite such disadvantages, intensity autocorrelation is a very effective and cost-efficient solution for estimating the duration of optical pulses of less than 100 ps and a short as a few fs [3].

Table 4-1 Second-order autocorrelation functions and bandwidth products for Gaussian, Hyperbolic Secant squared (where c = 2.71) and Lorentzian pulse shapes. TBWP- time bandwidth product [4].

Pulse Shape	$I_{AC}(\tau)$ =	I(t)	$\Delta t/\Delta\tau$	Pulsewidth (FWHM) Δt	TBWP ($\Delta t\Delta\nu$)
Gaussian	$e^{\left(-\ln(2)\left(\frac{2\tau}{\Delta\tau}\right)^2\right)}$	$e^{\left(-\ln(2)\left(\frac{2\tau}{\Delta\tau}\right)^2\right)}$	0.7071	1.665	0.4413
Hyperbolic sech^2	$\frac{3\left(\frac{c\tau}{\Delta\tau}\coth\left(\frac{c\tau}{\Delta\tau}\right)-1\right)}{\sinh^2\left(\frac{c\tau}{\Delta\tau}\right)}$	$\operatorname{sech}^2\left(\frac{1.7625t}{\Delta\tau}\right)$	0.6482	1.763	0.3148
Lorentzian	$\frac{1}{1+\left(\frac{2\tau}{\Delta\tau}\right)^2}$	$\frac{1}{1+\left(\frac{2\tau}{\Delta\tau}\right)^2}$	0.5	2	0.2206

FROG is a technique that uses a similar set-up to an autocorrelator except that in place of a photodetector, the detector used is a spectrometer. It has the advantage of being able to completely characterize a pulse, supplying not only the duration but also the phase. In FROG, a pulse gates itself in a nonlinear medium and the resulting gated piece of the pulse is then spectrally resolved as a function of the delay between the two pulses. A measurement involves recording tens or hundreds of spectra for different settings of the arrival time difference of the two pulses [5].

In the present investigation, because phase was not required, an optical autocorrelator – a Femtochrome FR-103XL/IR – was used for establishing the pulse duration. Details of this instrument are given in Section 4.2.1.

4.1.2 RF Spectra and Mode-Locking Stability

After conversion of the optical signal into an RF signal by a photo diode with a suitable bandwidth the pulse repetition frequency can be accurately measured by an electrical

spectrum analyser. This deduces from the RF signal-to-noise ratio of the fundamental and harmonics along with the -3 dB bandwidth whether there is stability of mode-locking or not. For example, the quality of the pulse frequency oscillation depends on the linewidth of the RF signal and if broadened, jitter is high resulting in noise around the carrier. Consequently mode-locking is considered to be stable when the linewidth is narrow and RF signal-to-noise ratio is higher than 20 dB. Clearly the identification of the best parameters of stable mode-locking suggests that a broad RF linewidth corresponds to unstable mode-locking whilst a narrow one signifies the opposite.

In order to convert the optical signal into an electrical RF signal, a fast 29 GHz photodiode (model D-15 Newport) was used. The photodetector element is an interdigitated metal-semiconductor-metal (MSM) structure fabricator in an InGaAs semiconductor structure. Light absorbed between the MSM fingers generates electron-hole pairs that are swept through the active region to their respective electrodes in picoseconds [4].

4.1.3 Power Characteristics

In the experiment conducted for this study, a power meter was used to find an average power (P_{av}) to measure peak power (P_p). Clearly it is important to understand the difference, and the relationship between average power and peak power. The energy content of the pulse is equal to the peak power of the pulse multiplied by the pulse width. However power meters measure the power over a longer period of time, giving an average power. The duty cycle of a system is the ratio between the pulse width ($\Delta\tau_p$) and pulse period (T) and the proportion of time during which a component, device or system is operated. The peak power can be calculated from the following equation:

$$P_p = \frac{P_{av}T}{\Delta\tau_p} \tag{4.1}$$

where P_p is the peak power, P_{av} is the average power, T is the pulse period, and $\Delta\tau_p$ is the pulse width.

The equation can be used for defining the peak power of the laser when the amplified spontaneous emission is negligible. Such an emission should be subtracted from the average power for correct pulse energy estimation.

4.2 Experimental Setup

In the present research, three experiments were carried out with similar characterisation techniques; however each included a different element than the others Figure 4-1 shows the experimental setup used in two of the three experiments; in the third there was a slight modification for the external cavity configuration. During the output of the tapered lasers, several cylindrical lenses were also used to collimate the beam due to astigmatism.

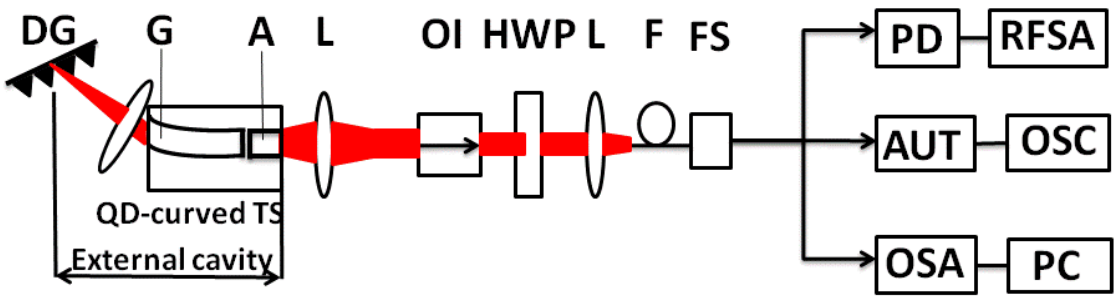

Figure 4-1 Experimental set-up for a passive mode-locked external cavity quantum dot (QD) curved two-section (TS) diode laser: DG: diffractive grating, A- absorber section, G- gain section, L: lens, OI: optical isolator, HWP: haft wave plate, F: fibre, FS: fibre splitter, PD: photo diode, RFSA: RF spectrum analyser, AUT: autocorrelator, OSC: oscilloscope, OSA: Optical spectrum analyser, PC-personal computer.

In order to control the temperature of the laser, it was mounted on a Peltier cooler. The laser diode is an electrically pumped device of two parts: the gain section and the absorber section. A Thurlby PL 320(30V-2A) power supply was used to obtain a forward bias and a reverse bias. In order to collimate the light to the testing equipment, aspheric lenses were used. To protect the laser from feedback an optical isolator was used and a half-wave plate aided the achievement of correct polarisation. To split the beam into three different characterisation techniques, a fibre optical coupler was used. The output average power, determined by the power meter, produced three results, one being the autocorrelator with oscilloscope which allows the measurement of ultra short pulses, another being an RF spectrum analyser combined with a fast photodiode showing the operating frequency and quality of mode locking, and finally one being an optical spectrum that displays the central emission wavelengths.

4.2.1 Autocorrelator

The optical autocorrelator used in the present work is a Femtochrome FR-103XL/IR with a resolution of 1 fs, and dispersion-free scan range of greater than 185 ps. It employs a second-harmonic generation crystal, a photomultiplier tube, and a system of noncollinear geometry that results in a background-free autocorrelation measurement. The operation is based on a Michelson interferometer (see the Figure 4-2) [2].

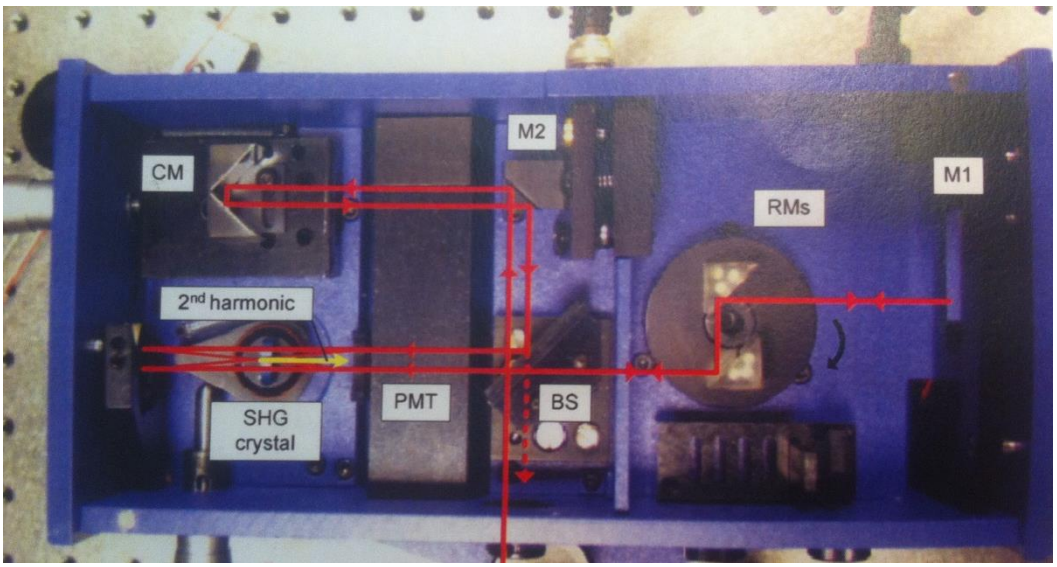

Figure 4-2 Top view of a Femtochrome FR103XL/IR autocorrelator with the optical path traced in red. Shown are the beam splitter (BS), rotating mirrors (RM), mirrors (M1 and M2), corner mirror (CM), photomultiplier tube (PMT) and the second-harmonic generation crystal (SHG).

Periodic delays are introduced by means of a rotating parallel mirror assembly as shown in Figure 4-3 [3]. The delay generated by the assembly is an exact sinusoidal function of time and the whole scan range occurs for small angles, for which the linear approximation is excellent. The error in the measured autocorrelation at full width half maximum is less than 0.5%, even for pulses as long as 100 ps.

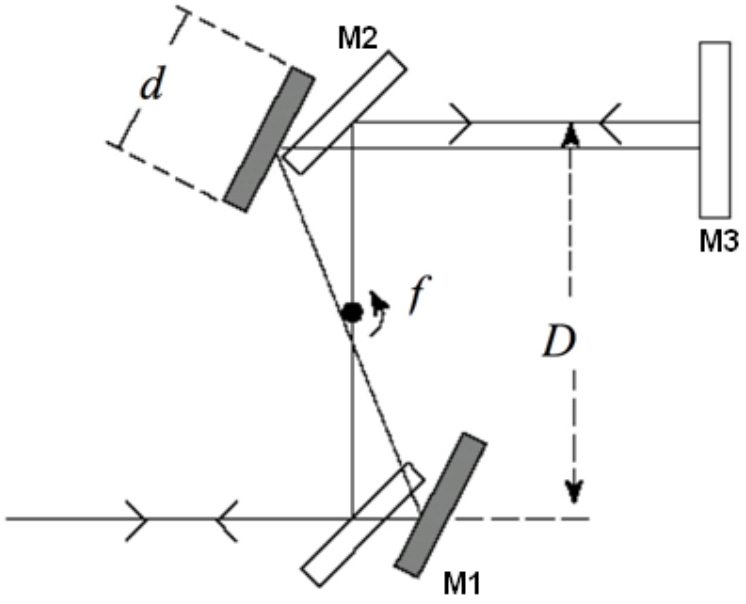

Figure 4-3 Rotating parallel mirrors in the autocorrelator.

A nonlinear lithium iodate ($LiIO_3$) crystal (1mm/24°) provides second-harmonic generation in the spectral range 700 nm – 1800 nm, and a fundamental filter operating in the range 1100 nm – 1300 nm is used. A curved mirror (upper left in Figure 4-3) provides the focus in the NL crystal.

The repeated linear generation of ultrashort pulses takes place in one arm of the interferometer through the use of a pair of parallel mirrors centred on a rotating axis. These mirrors change the optical path of the beam such that the transmitted pulse is delayed (or advanced) about the neutral position. If the angular change is small, the delay *T* is given by [2],

$$T = \frac{4\pi f D t}{c} \tag{4.2}$$

where *D* is the separation of the parallel mirrors, *f* is the frequency of rotation, and *c* is the speed of light.

A Textronix TDS2022B 200 MHz 2-channel digital storage oscilloscope, operating at 2GS/s real time, was synchronized to the rotation and used to continuously display the autocorrelation of the pulses.

The total scan range T_t is given by [3],

$$T_t = \frac{\sqrt{2}d}{c} \tag{4.3}$$

where *d* is the length of the scanning mirror and *c* is the speed of light.

A figure of nonlinearity (NL) over the full scan range is [2].

$$NL = \frac{d}{4D} \tag{4.4}$$

In the standard configuration of the FR-103XL/IR, d = 1.70", D = 3", f = 10 Hz (although 5 Hz and 2.5 Hz are also selectable). Hence the following values are obtained from the equations above:

T/t = 31 ps/ms;

T_t = 200 ps;

NL = 7%/100 ps.

When the autocorrelation has been obtained, the product of the FWHM of the trace, the delay calibration factors T/t, and a factor associated with the pulse shape gives the true value of the pulse width. Resolution is limited only by the thickness of the nonlinear crystal, which is typically 0.3 mm, giving a resolution of about 15 fs. The sensitivity of the autocorrelator depends on the operational wavelength and the characteristics of the NL crystal: an average input power of a few mW is generally enough. The lowest detectable signal level can be as little as $P_p P_{av}$ mW^2.

4.2.2 Different Grating and Diffraction Orders

It is well known that if a plane wave is incident at an angle θ_i, the grating equation is given by,

$$d(\sin\theta_m + \sin\theta_i) = m\lambda \qquad 4.5$$

The light that corresponds to direct transmission (or specular reflection in the case of a reflection grating) is called the zero order, and is denoted as m = 0. The other maxima occur at angles that are represented by the non-zero integer m. Note that m can be positive or negative, resulting in diffracted orders on both sides of the zero-order beams.

The blazed diffraction grating (DG) has a wavelength of 1.25 µm and groove of 600 grooves/mm Figure 4-4.

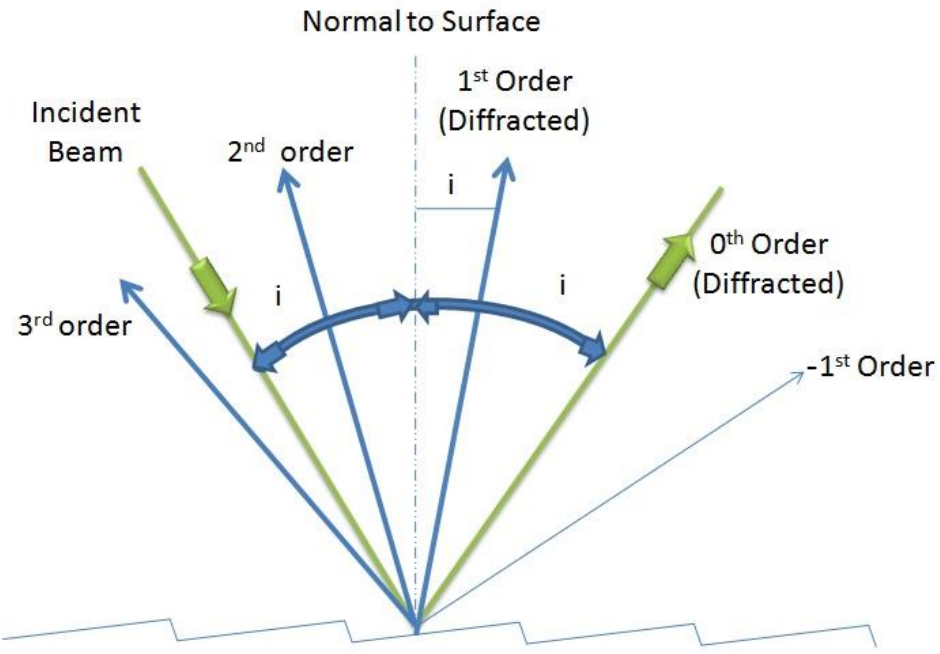

Figure 4-4 Specular reflection in the case of a reflection grating.

An idealised grating is considered here which is made up of a set of long and infinitely narrow slits of spacing *d*. When a plane wave of wavelength λ is incident normally on the grating, each slit in the grating acts as a point source propagating in all directions.

4.2.3 Peltier Cooler

In this research in order to control the temperature/ power supply , a Peltier cooler (Model SE 5010 Marlow Industries) was mounted p-side up on the mount which was covered with thin layers of heat sink compound for better heat transfer from the laser. The temperature controller and [power supply is designed for the precision for the temperature controller (between -99.9 °C to 150 °C) of all types of thermoelectric cooling devices. A Peltier cooler or a thermoelectric heat pump is a solid state active heat pump which) with the consumption of electrical energy.

4.2.4 Optical Isolator and Half Plate

Faraday optical isolators consist of three elements- entrance and exit polarisers and a Faraday rotator. A terbium gallium garnet crystal acts as a permanent magnet within the rotator allowing for the magnetic field and the length of the crystal to be adjusted in order that the input light's polarisation rotates by 45° on exiting the crystal. In the reverse direction the Faraday rotator repeats the same direction as before so that the polarisation of the light is now rotated 90°with respect to the input signal so that the light travels in only one direction. Furthermore it protects the laser from optical elements feedback causing instabilities in the operation of lasers.

Used in the present experiment, a mounted achromatic half-wave plate (1100 nm – 2000 nm AHWP05M-1600 Thorlab) was used for rotating the plane of plane polarised light. It is crucial for the autocorrelator that the polarisation has to be in the right direction in order to generate any second harmonic signal.

4.2.5 Optical Spectrometer

The laser spectrometer WaveScan APE (Angevandte Physic und Elektronik GmbH) RS232 was used in the experiments to measure the spectrum of continuous wave or high pulse repletion rate laser systems. The optics unit is controlled by a personal computer (PC) via the RS232 serial port using the control software LasScan. This software allows data transfer between the spectrometer and the PC and offers quasi real-time graphical monitoring of the spectra as well as data storage and processing. The WaveScan is a grating spectrometer in the Littrow conformation with a focal length of 200 mm. The diffraction grating rotates with a rate at a rate of approximately 6 rounds per second and separates the several spectral components of the spectrum from the incident beam.

4.2.6 Power Meter

In this research a power meter (model no 2936C Newport) was used for measuring average power with a high power thermopile detector 818P-001-12 with filter. Such a detector has become a popular choice for power measurements primarily due to the high power measurement capability as well as the broadband nature of the detectors. It can measure between 1 μWand 1 W of average power.

4.2.7 Beam Quality (M^2)

The quantity M^2, known as the beam quality factor or beam parameter product, is a dimensionless, measurable quantity that indicates the degree of imperfection of a laser beam. The closer the value of M^2 is to 1.0, the closer the beam can be focused to its diffraction-limited spot size [6]. The value of M^2 is defined as the "ratio of the beam parameter product of the beam of interest to the beam parameter product of a M^2 can be defined as the ratio of the divergence of the actual beam to that of a theoretical, diffraction-limited beam with the same waist diameter [7]. That is,

$$M^2 = \frac{\Theta}{\theta} \tag{4.6}$$

where Θ is the measured, far-field, full-angle divergence of the actual beam and θ is the theoretical far-field divergence of a 'perfect' Gaussian beam which has the same waist diameter as the measured beam. The perfect Gaussian beam can be defined as,

$$\theta = \frac{2\lambda}{\pi W_O} \tag{4.7}$$

where λ is the wavelength of the actual beam and W_O is the waist radius.

4.3 References

[1] M. Ferianis and M. Danailov, "Streak Camera Characterization Using a Femtosecond Ti: Sapphire Laser," in *AIP Conference Proceedings*, 2002, pp. 203-211.

[2] Z. A. Yasa and N. M. Amer, "A rapid-scanning autocorrelation scheme for continuous monitoring of picosecond laser pulses," *Optics Communications*, vol. 36, pp. 406-408, 1981.

[3] E. P. Ippen and C. V. Shank, "Techniques for Measurements, in Ultrashort Light Pulses," in *Ultrashort Light Pulses,S.L. Shapiro, Ed* Springer: New York, 1977.

[4] D. I. Nikitichev, "High power ultra-short pulse Quantum-dot lasers," Ph. D. thesis, University of Dundee, 2012.

[5] G. Taft, A. Rundquist, M. M. Murnane, I. P. Christov, H. C. Kapteyn, K. W. DeLong, D. N. Fittinghoff, M. Krumbugel, J. N. Sweetser, and R. Trebino, "Measurement of 10-fs laser pulses," *Selected Topics in Quantum Electronics, IEEE Journal of*, vol. 2, pp. 575-585, 1996.

[6] I. Standard, "11146,“," *Lasers and laser-related equipment–Test methods for laser beam widths, divergence angles and beam propagation ratios*, 2005.

[7] T. F. Johnston Jr, "Beam propagation M 2 measurement made as easy as it gets: the four-cuts method," *Applied Optics*, vol. 37, 1998.

Chapter 5. **Mode-locked QD lasers - External Cavity**

5.1.1 Experimental Set-up and Device

The two-section laser investigated was made up of a ridge-waveguide structure from a QD wafer the active region of which consisted of 10 non-identical InAs QD layers grown on GaAs substrate by molecular beam epitaxy. They were covered by non-identical InGaAs capping layers and then incorporated into $AI_{0.35}Ga_{0.65}As$ cladding layers as demonstrated in [1]. Three groups of QDs with different photoluminescence peak positions at 1211 nm, 1243 nm and 1285 nm were made into 10 layers, resulting in this QD structure design where continuous wavelength tuning between the ground and excited-state optical transitions of different QD groups was demonstrated.

The waveguide in the gain section was bent and terminated at an angle of 7° from the regular direction of the cleaved facet, in combination with antireflection (AR) coating (R ~10^{-5}), and the back facet was high-reflection (HR) coated (R ~95 %). The total length of the QD device was 4 mm, with a ridge waveguide width of 6 µm. A reverse bias was applied to the section placed nearer to the back facet, thus forming a distributed saturable absorber with a total length of 800 µm whereas the gain section was forward-biased. By means of a thermoelectric Peliter cooler the temperature of the chip was kept at 20°C. The fundamental mode-locking at 740 MHz was found when the external length was 18.9 cm and a diffraction grating with 1200 grooves/mm. Such a configuration in combination with the chirped QD structure grown on a GaAs substrate by molecular beam epitaxy facilitated a broad wavelength tuning range. A simplified schematic of the experimental set-up is presented in Figure 5-1.

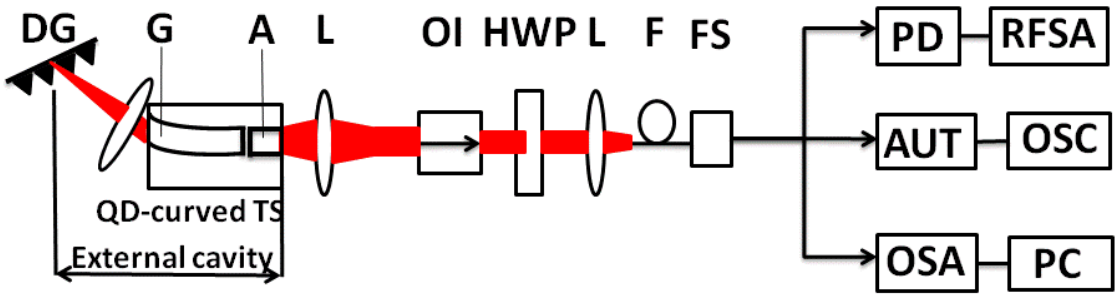

Figure 5-1 Experimental set-up for a passive mode-locked external cavity quantum dot (QD) curved two-section (TS) diode laser: DG: diffractive grating, A- absorber section, G- gain section, L: lens, OI: optical isolator, HWP: haft wave plate, F: fibre, FS: fibre splitter, PD: photo diode, RFSA: RF spectrum analyser, AUT: autocorrelator, OSC: oscilloscope, OSA: Optical spectrum analyser, PC-personal computer.

A non-collinear autocorrelator based on second-harmonic generation (Femtochrome FR103XL/IR) was used to find pulse duration in combination with a high-speed 29 GHz photodiode. Spectral characteristics were measured with an optical spectrum analyser (Advantest Q8383).

5.1.2 Results

Electroluminescence (EL) measurements have been conducted on a QD gain chip as used in the present work for a variety of bias and temperature conditions [1]. For a given temperature, the width of the EL spectra increases with increasing current and the peak intensity shifts to shorter wavelengths. (See Figure 5-2) At a fixed injected current, the peak of the spectra moves to longer wavelengths as the temperature rises, and the spectra broaden.

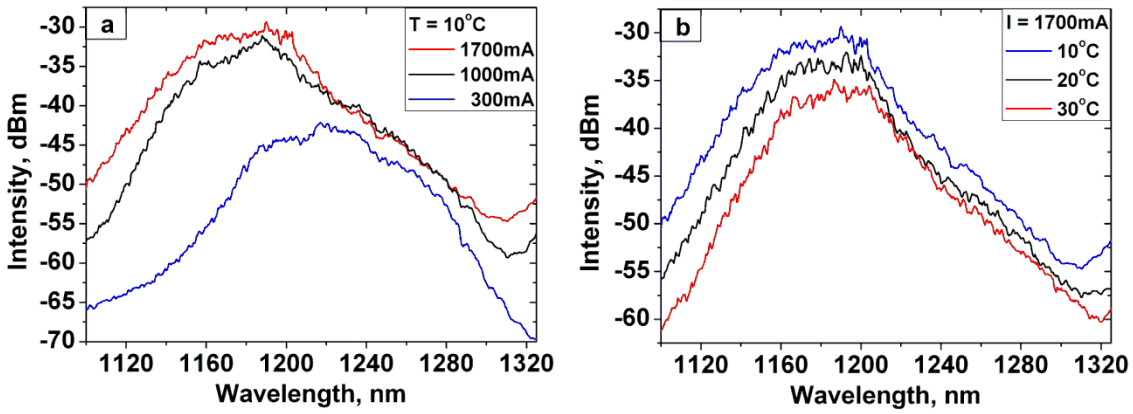

Figure 5-2 Electroluminescence spectra of the QD gain chip for different bias and temperature conditions [1].

Under various bias conditions, broad wavelength tunability in mode-locked regime is achieved when the gain section current starts in the range of 500 mA to 1 A, and the reverse bias from 1 V to 5 V. A maximum tuning range of 136.5 nm with dynamic contrast higher than 50 dB in the spectral range from 1182.5 nm to 1319 nm was found possible for gain current of 1 A and reverse bias of 3 V at an operating temperature of 20 °C, as shown in Figure 5-3.

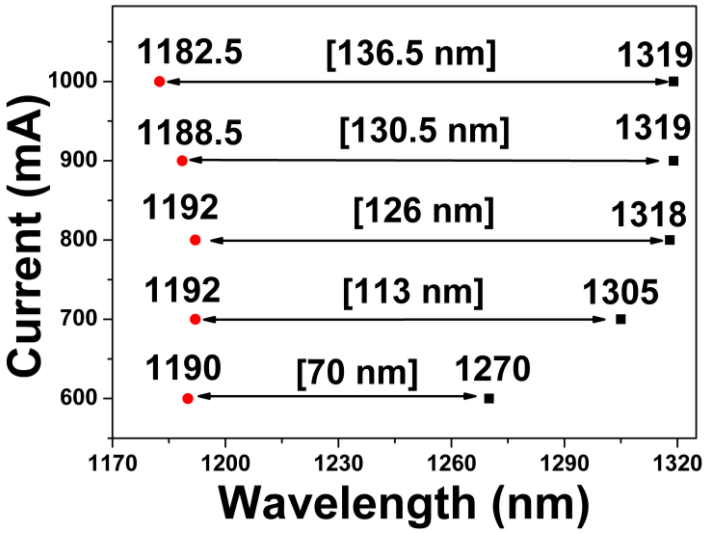

Figure 5-3 Wavelength tuning range in mode-locked regime is presented for different applied gain current and 3 V reverse bias. The highest tuning range of 136.5 nm is achieved for gain current of 1A.

It is crucial to stress that the lasing wavelength of 1319 nm is the longest lasing wavelength reported until now from a tunable mode-locked GaAs-based QD laser.

Moreover, it should be emphasised that we observed a continuous wavelength tuning of over 136 nm owed to non-identical QD layer structure set in comparison with an earlier finding where optical spectra tuning was achieved for ground state from ~1265 nm to ~1295 nm and for excited state from ~1170 nm to ~1220 nm [2]. As can be seen in Figure 5-3, the tunability range in mode-locked operation can be extended from 70 nm to 136.5 nm by increasing the gain current from 600 mA to 1 A under constant 3 V reverse bias.

Optical spectra for the broadest tuning regime for gain current of 1 A and reverse bias of 3 V are presented in Figure 5-4.

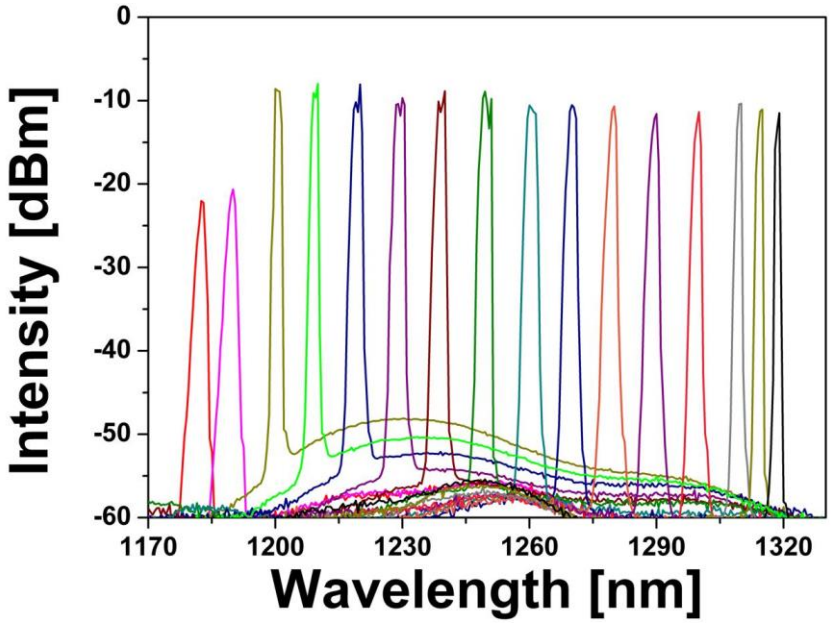

Figure 5-4 Wavelength tunability in mode-locked regime from 1182.5 nm to 1319 nm at 3 V reverse bias and 1 A gain current.

Peak power and pulse duration dynamics for 3 V and 900 mA are shown in Figure 5-5 where the pulse duration changes from 12.8 ps to 39 ps along with peak power up to 532 mW (at 1226 nm wavelength) in the similar bias conditions (Figure 5-5a). The power and duration behaviour observed in (Figure 5-5a) is due to the properties the QD medium. The autocorrelation trace presented in the inset of (Figure 5-5b) a Gaussian curve fit to the data results in an FWHM of the autocorrelation trace (Δt) of 21.7 ps and

a deconvolved pulse duration ($\Delta\tau$) of 15.3 ps. from the corresponding optical spectra an effective spectral width of ~1 nm is determined. This demonstrates a resulting time bandwidth product of three, suggesting that the pulses remain highly chirped.

The observed behaviour of the peak power and pulse duration can be explained largely in terms of the properties of the diffraction grating (DG). The peak power does not change much with increasing current applied to the gain chip because the increase in pulse duration with increasing current offsets the rising average output power. The power falls as the voltage falls, while the pulse duration shortens with voltage up to some point and then lengthens again (see Figure 5-5a).

The pulse duration from a set-up with a first-order DG would be expected to be significantly narrower than one with a second-order DG and, indeed, this is what was found in practice. The FWHM of the spectra in the case of the second-order DG was narrower than that produced by the first-order DG across the whole tuning range. On the other hand, the pulse durations in both cases were similar, with just a slightly broader pulse duration resulting from the second-order grating. The narrowest pulse of ~14 ps was obtained in the first-order set-up. The dynamic contrast of RF spectra from the first-order DG is higher than from the second-order one, indicating that mode-locking is superior in the former case. The point in the red rectangle (see Figure 5-5b) was chosen at the highest power, with a good duration.

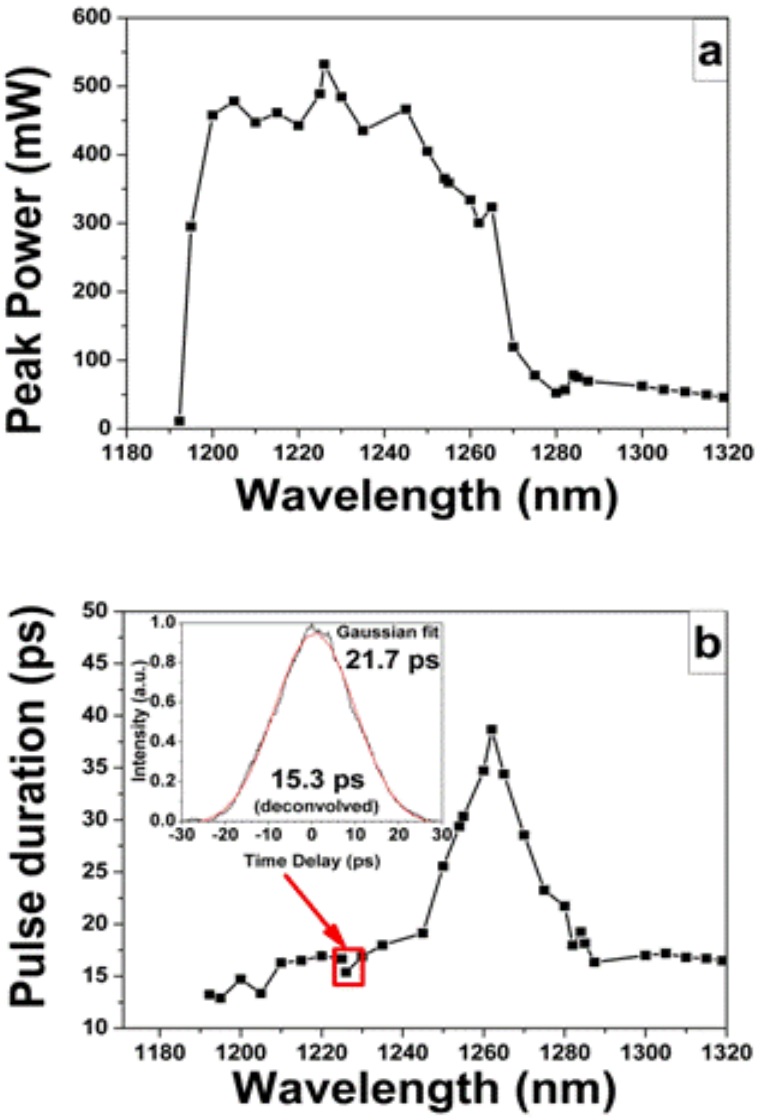

Figure 5-5 a) Peak power and (b) pulse duration dynamics with the emission wavelength in mode-locked regime for gain current of 900 mA and reverse bias of 3V, inset: autocorrelation trace for 1226 nm.

Furthermore, the pulse duration and peak power dynamics at a constant wavelength of 1226 nm were investigated, with the results shown in Figure 5-6. A reverse bias of between 3 V and 5 V was applied across the absorber section, and the gain current was varied between 500 mA and 1 A. It can be seen that, in general, peak power depends strongly on current, increasing as the current increases across the experimental range. The peak power was observed to reach a maximum of 870 mW for a reverse bias of 4 V and driving current 1 A. The pulse duration shortened as the reverse bias applied to the absorber section was increased: a well-known effect due to a decrease in the relaxation

time with increasing reverse bias. The shortest pulse duration obtained for the spectral band was 18.4 ps at a reverse bias of 4 V, 1 A gain current, and 9.7 mW average powers.

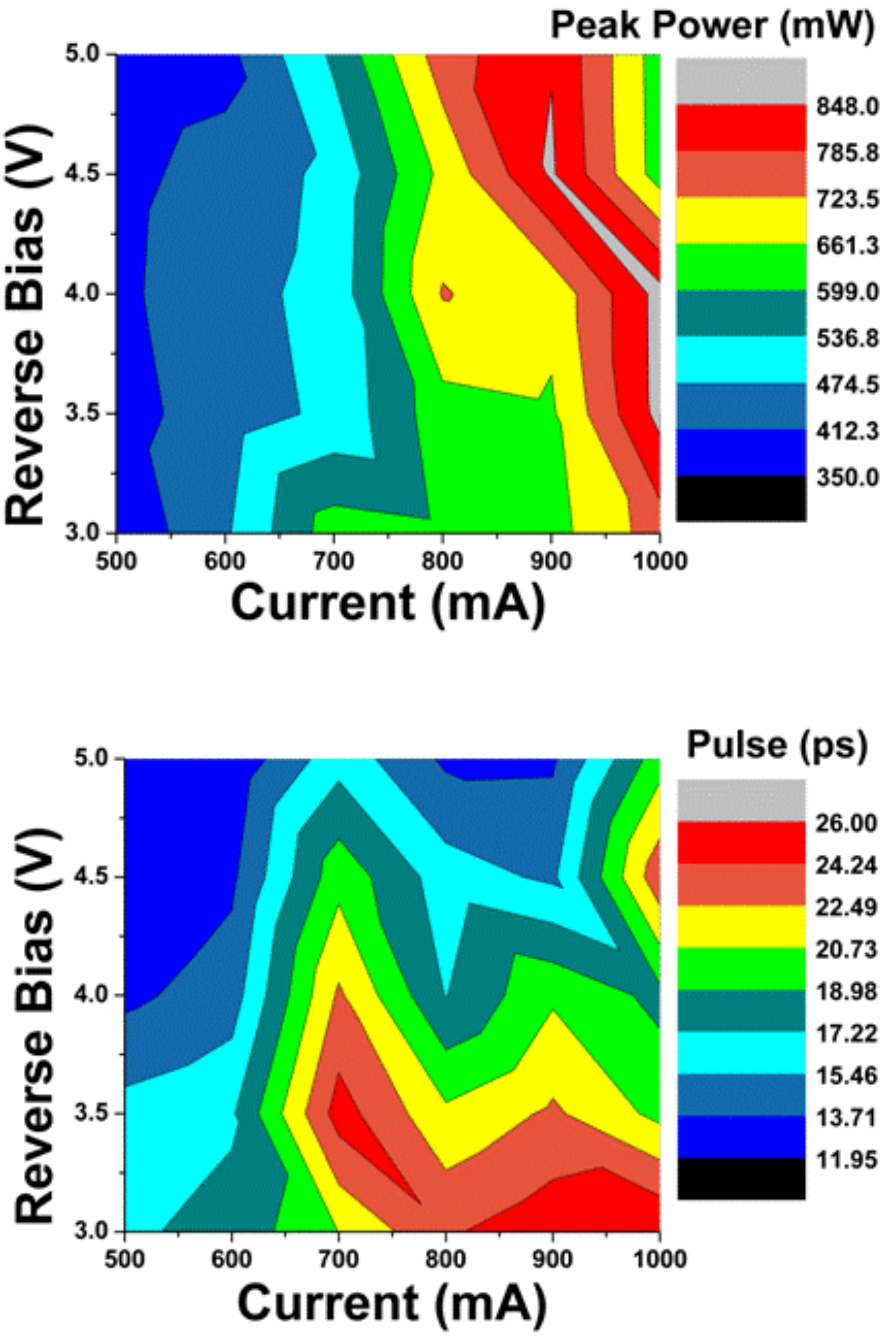

Figure 5-6 (top) Peak power and (bottom) pulse duration dynamics with different bias conditions for 1226 nm wavelength. The highest peak power of 870 mW was achieved for current of 1 A and reverse bias of 4 V.

Autocorrelation trace and RF spectrum for this regime are presented in Figure 5-7. A Gaussian curve fitted to the data results in an FWHM of the autocorrelation trace (Δt) of 26.1 ps and a deconvolved pulse duration (Δτ) of 18.4 ps, (top) Autocorrelation, (bottom) RF spectrum for highest peak power regime at -4.5 V reverse bias and 1 A gain current for fundamental mode-locking regime at a fundamental frequency of 740 MHz were recorded. The large number of harmonics in the RF spectrum indicates the high quality of mode-locking, as shown in Figure 3-7b. A time-bandwidth product of 4.4 for this regime was estimated with a 1.2 nm spectral width.

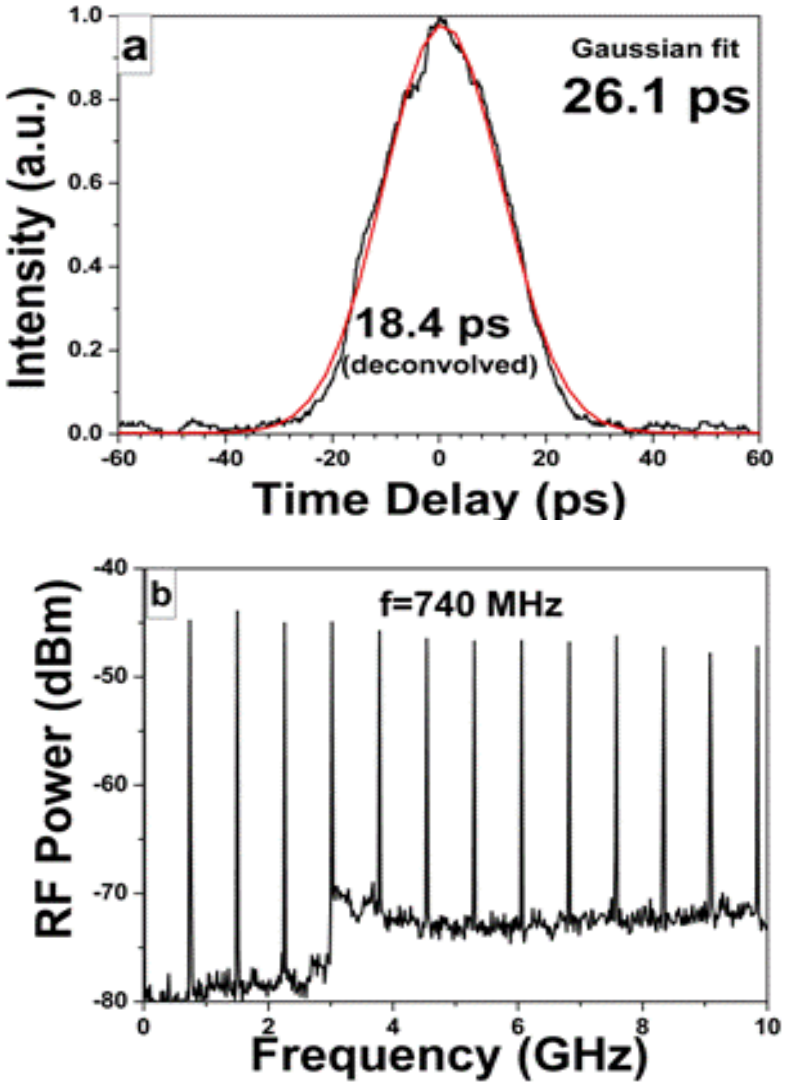

Figure 5-7 (a)Autocorrelation, (b) RF spectrum for highest peak power regime at -4.5V reverse bias and 1A gain current for fundamental mode-locking regime of ~740 MHz.

We observed stable fundamental mode-locking and harmonic mode-locking depending on the optical feedback. To sustain stable fundamental mode-locking, high-order harmonic mode-locking should be suppressed by low net gain achieved by optimising the optical feedback. The photocurrent in the absorber should be kept at between 10 mA and 20 mA as previously [3]. The higher forward bias in the gain section leads to an earlier and more complete gain recovery time, which in combination with the relatively long pulse roundtrip time in the long cavity, could lead to the appearance of multiple pulse in a wider net gain window [4]. Otherwise harmonic mode-locking can be dominant with the increasing photocurrent.

Various potential applications stemming from tunable lasers generating picosecond pulses might be used for bio-medical and a generation of tunable visible light by second-harmonic generation [5].

5.2 Conclusion

In this chapter, we have demonstrated broad (136.5 nm) wavelength tunability in a passive mode-locked regime from a multi-section QD laser in external cavity configuration, operating in the spectral range of 1182.5 nm to 1319 nm. The pulse duration varied from 12.8 ps to 39 ps and maximum peak power up to 870 mW was observed at 1226 nm wavelengths.

Clearly this is a significant finding, i.e. a broad spectral range combined with a small pulse duration resulting in considerable peak power.

5.3 References

[1] K. A. Fedorova, M. A. Cataluna, I. Krestnikov, D. Livshits, and E. U. Rafailov, "Broadly tunable high-power InAs/GaAs quantum-dot external cavity diode lasers," *Optics Express,* vol. 18, pp. 19438-19443, 2010.

[2] J. Kim, et al, "Wavelength tunable mode-locked quantum-dot laser," *Orlando (Kissimmee), FL, USA: SPIE.,* 2006.

[3] Y. Ding, M. A. Cataluna, D. Nikitichev, I. Krestnikov, D. Livshits, and E. Rafailov, "Broad repetition-rate tunable quantum-dot external-cavity passively mode-locked laser with extremely narrow radio frequency linewidth," *Applied Physics Express,* vol. 4, p. 2703, 2011.

[4] Y. Ding, D. Nikitichev, I. Krestnikov, D. Livshits, M. Cataluna, and E. Rafailov, "Quantum-dot external-cavity passively modelocked laser with high peak power and pulse energy," *Electronics Letters,* vol. 46, pp. 1516-1518, 2010.

[5] K. A. Fedorova, "Novel semiconductor based broadly tunable light sources," Ph.D. thesis, University of Dundee, 2011.

Chapter 6. **Quantum Dot Based Pulsed Laser System**

6.1 Introduction

Ultrafast high-power semiconductor laser systems (i.e., a few tens Watts peak power) with wide wavelength tuning range and broad tunability of the pulse repetition rate are very useful for nonlinear imaging techniques [1], especially in the biomedical field [2]. An external cavity has many advantages, such as wavelength (using diffraction grating) and repetition rate tunability (by changing the cavity length). In this chapter, a range of diode lasers with two waveguide (gain chip and semiconductor optical amplifier) configuration is presented [3].

6.2 Master Oscillator Power Amplifier

A master oscillator power amplifier (MOPA) is a configuration consisting of a master laser (or seed laser, here a quantum-dot external-cavity passively mode-locked lasers (QD-ECMLLs) with diffraction grating (DG) and a quantum-dot semiconductor optical amplifier (a QD-SOA is used in this study) to boost the out-put power. The diagram below illustrates a MOPA setup, where the master laser is a QD-ECMLL and the optical amplifier is a QD-SOA (see Figure 6-1).

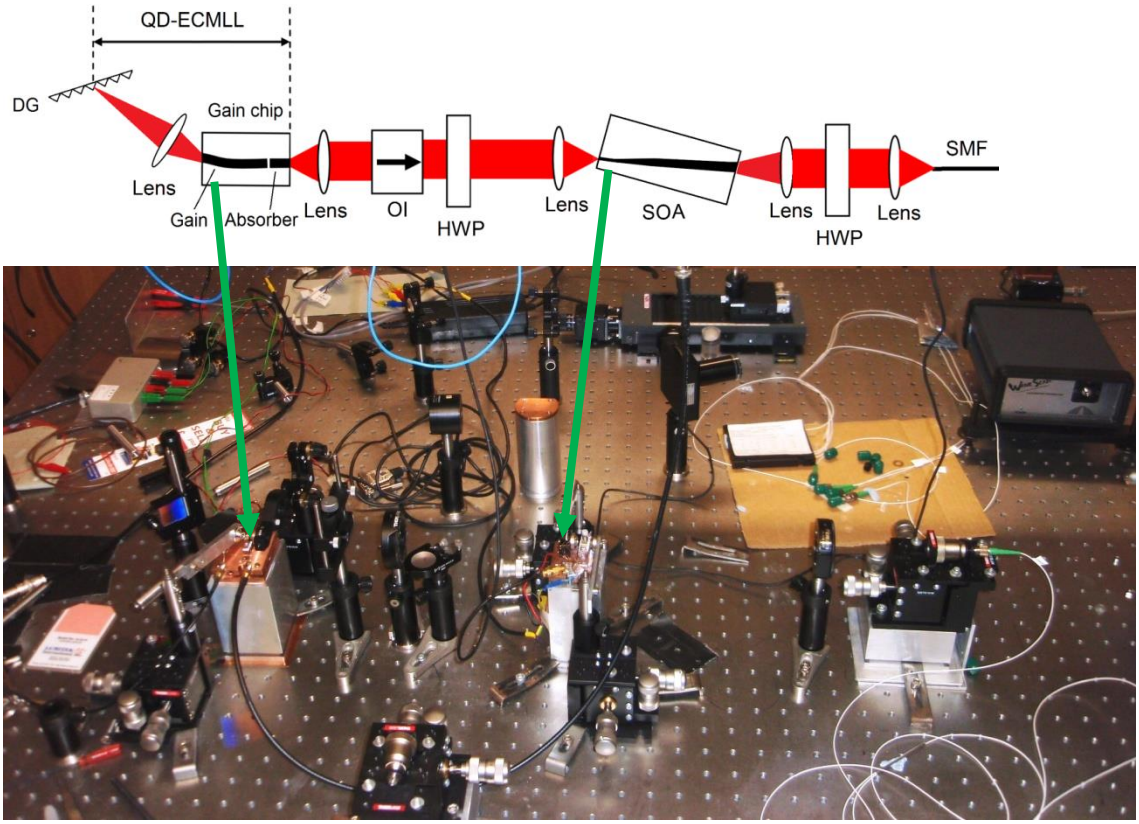

Figure 6-1 Configuration of a tunable MOPA system and measurement setup. OI: optical isolator; HWP: half wave plate; SMF: single-mode fiber; FS: fiber splitter; OSA: optical spectrum analyzer; Autoco: autocorrelator; Osc: oscilloscope; PD: photo detector; RFSA: RF spectrum analyzer.

With a MOPA instead of a laser, it can be easier to reach the required performance, i.e., in terms of linewidth, wavelength tuning range, repetition rate tunability, beam quality, pulse duration or output power. This is because various performance aspects are decoupled from the generation of high powers. This gives extra flexibility, e.g. when a mode-locked laser diode is used as a seed laser.

6.3 Structure and Device Design of InAs/GaAs (QD-ECMLLs) and (QD-SOA)

The semiconductor optical amplifier SOA and gain chip were fabricated by Innolume on a n+ GaAs (100) substrate by molecular beam epitaxy (MBE). The active region contained 10 layers of chirped InAs/GaAs QDs in order to achieve broad gain spectrum using an epitaxy similar to that used in previous papers [4-5]. The sample gain chip is shown in Figure 6-2.

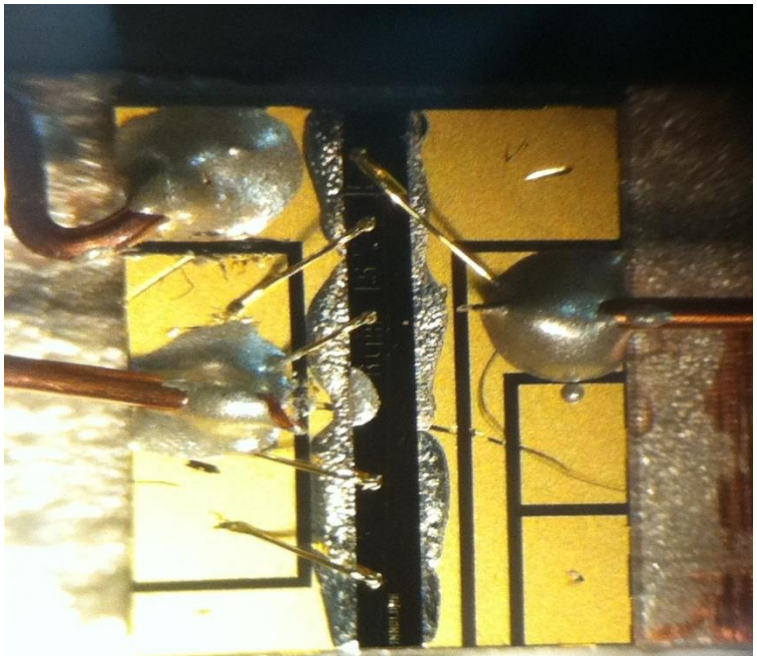

Figure 6-2 InGaAs strained multiple quantum dots gain chip.

The 10 QD layers in the active region were made up of three groups of quantum dots with different emission peak positions. These were arranged geometrically as follows: three QD layers with a central emission at 1211 nm, three QD layers at 1243 nm, and four QD layers at 1285 nm [6]. In order to achieve these various shifted spectral emissions, the InGaAs capping layer thickness differed slightly between the three groups, which resulted in an overall variation in the average size of the quantum dots

for each group of dots. As a result, there are two main contributions to the inhomogeneous broadening of size of the QDs within each group of QD layers and which is inherent to their self-assembled growth. The second contribution is the intentional variation in capping layer thickness which changes the average size of the dots among the three different groups of QD layers. Moreover, each group of QD layers allows access to their ground-state and excited-state optical transitions, which are then slightly shifted from group to group. This approach allows for a continuous wavelength tuning between the ground-state and excited-state optical transitions of the different QD groups [7].

6.4 Device Description (QD-ECMLLs)

The two-section gain chip used for the QD-ECMLL consisted of a gain section and a saturable absorber (SA section). The 6 μm wide ridge waveguide in the gain section was bent and terminated at an angle of 7° relative to the cleaved facet, in combination with an antireflection (AR) coating (R ~10^{-5}), while the front facet was coated with a R ~ 1% coating, which allowed for cavity feedback and a high output power. The total chip length was 4 mm, with an 800 μm long SA section placed near the front facet. The QD-ECMLLs was kept at 20 °C by Peltier coolers.

6.5 Device Description (SOA)

The SOA had a length of 6 mm and a gain guided waveguide width changing from 14 μm at the input facet to 80 μm at the output facet. The tapered SOA was fabricated from the wafer with the same epitaxial structure as the gain chip. The SOA was kept at 20 °C by Peltier coolers.

6.6 MOPA with 1st –order Diffraction Grating

6.6.1 Experimental set-up

The experimental set-up is shown in Figure 6-3. A gain chip with a cavity length of 4mm and a ridge width of 6 µm was mounted on a copper heat sink and its temperature was controlled by Peltier coolers. The ECMLL cavity consisted of a standard 600 grooves/mm (blaze wavelength of 1.25 µm) diffraction grating in quasi-Littrow configuration and 40X (NA~0.55) AR-coated aspheric lenses. The distance between the gain chip and the diffraction grating was 20 cm. Tuning was achieved by rotating the grating to select a certain wavelength emission to be reflected back to the laser. The output of the front facer was collimated with an aspheric lens, as shown in Figure 6-3.

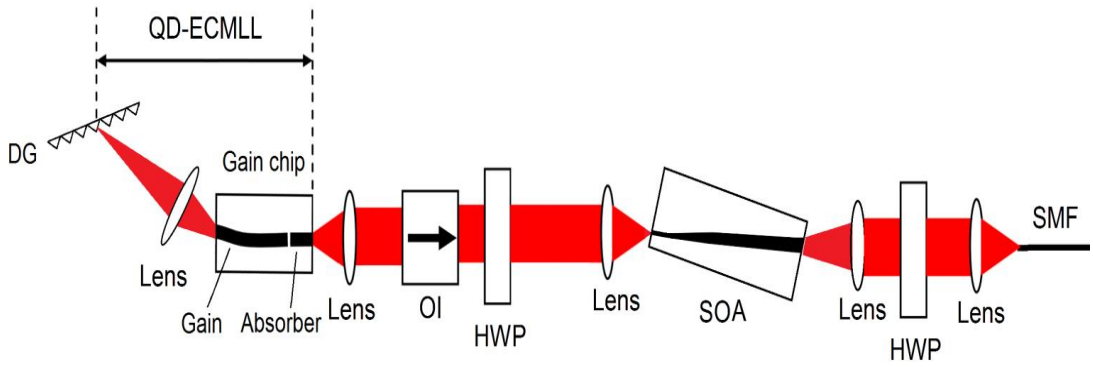

Figure 6-3 Configuration of a tunable MOPA system and measurement setup. OI: optical isolator; HWP: half wave plate; SMF: single-mode fibre; FS: fiber splitter; OSA: optical spectrum analyser; Autoco: autocorrelator; Osc: oscilloscope; PD: photo detector; RFSA: RF spectrum analyser.

The SOA had a length of 6 mm and a gain guided waveguide width changing from 14 µm at the input facet to 80µm at the output facet. The tapered SOA was fabricated from the wafer with the same epitaxial structure as the gain chip. Both the gain chip and the SOA were kept at 20 ^{o}C by Peltier coolers.

6.6.2 Results 1st –order Diffraction Grating

Utilising the tunable MOPA set-up in mode-locked operation, with a 600 mA bias current applied to the gain chip (corresponding to 3.1 KA/cm^2) and SOA current of 2180 mA (710 A/cm^3), it was possible to achieve a tuning range of 42 nm for the InAs/GaAs QD-ECMLLs in the SOA configuration at 20 °C. The optical spectra for the 1st order diffraction grating are shown in Figure 6-4.

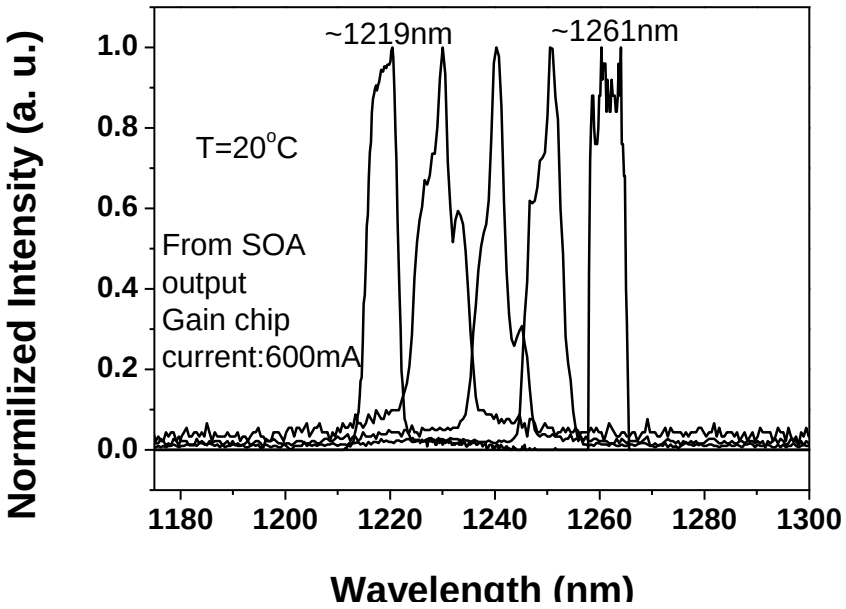

Figure 6-4 Optical spectra of tunable MOPA in mode-locked operation with chip gain current of 600 mA, reverse bias of 0 V to 5 V, and SOA current of 2180 mA.

In order to determine the pulse characteristics for the laser, the output light was passed into an autocorrelator and a trace obtained for a number of peaks, as shown in Figure 6-4. The results for two such peaks (1219 nm and 1230 nm) are shown in Figure 6-5 and Figure 6-6 respectively.

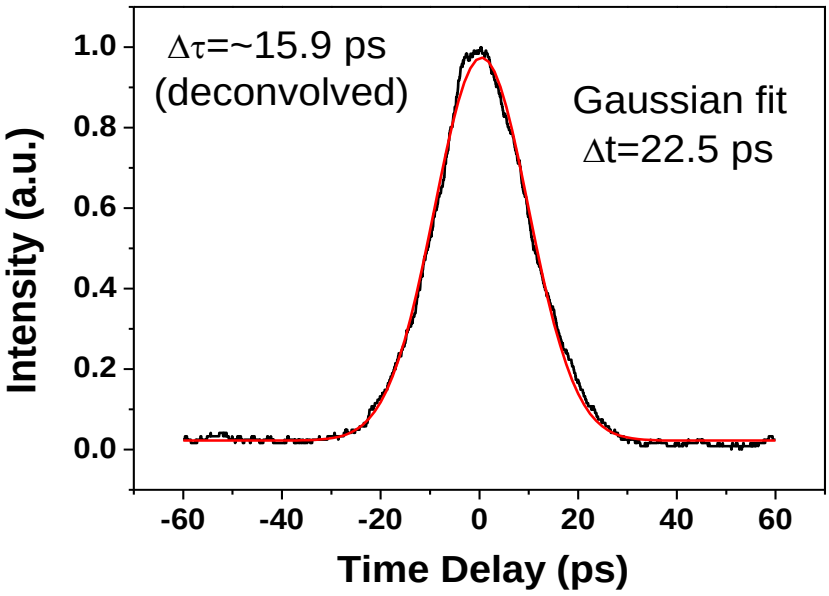

Figure 6-5 Autocorrelation trace at reverse bias of 1 V and forward current of 600 mA on the gain chip and SOA current of 2180 mA at 20 °C at the operation wavelength of 1219 nm.

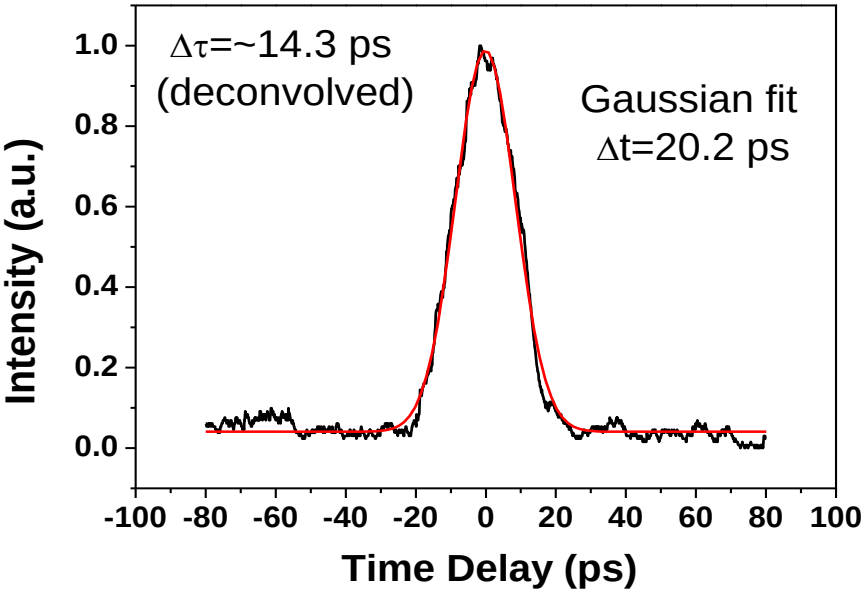

Figure 6-6 Autocorrelation trace at reverse bias of 5 V and forward current of 600 mA on the gain chip and SOA current of 2180 mA at 20 °C at the operation wavelength of 1230 nm.

For the operation wavelength of 1219 nm (Figure 6-5) a Gaussian curve fitted to the data resulted in an FWHM of the autocorrelation trace (Δt) of 22.5 ps and a deconvolved pulse duration (Δτ) of 15.9 ps. Under the same conditions (temperature

and current), the pulse characteristics for the 1230 nm wavelength resulted in an FWHM of the autocorrelation trace (Δt) of 20.2 ps and a deconvolved pulse duration (Δτ) of 14.3 ps (Figure 6-6).

RF characteristics for the operation wavelength of 1230 nm are presented in Figure 6-7 from which it can be seen that at this wavelength there is a high signal to noise ratio and that the fundamental repetition rate was 1.336 GHz which exhibits a dynamic range of 45 dB. Furthermore it can be seen from the inset that mode-locking is indeed occurs at the operating wavelength of 1230 nm.

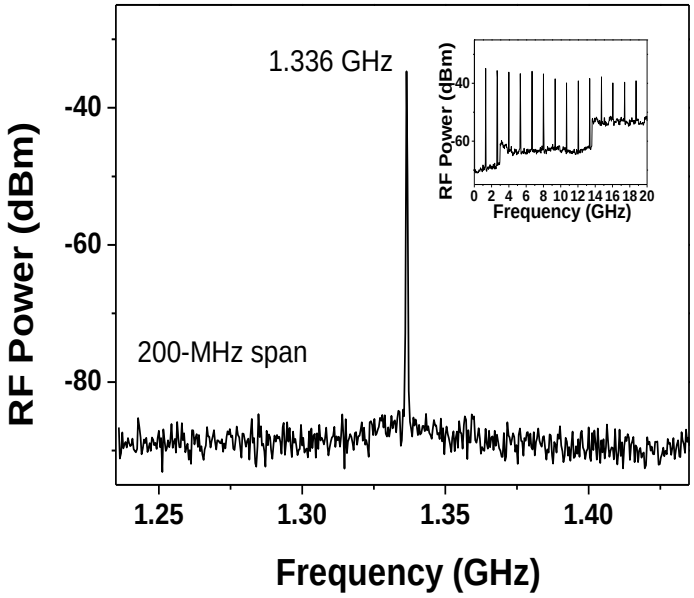

Figure 6-7 Spectra with different spans at reverse bias of 5 V and forward current of 600 mA on the gain chip and SOA current of 2180 mA at 20 °C at the operation wavelength of 1230 nm.

The effect of the pulse duration with reverse bias voltage was also investigated and the results are shown in Figure 6-8. The initial conditions (gain chip forward current, SOA current, temperature and laser output wavelength) were kept constant whilst the reverse bias varied in the range of 0 V to 5 V. It was found that as the reverse bias was increased the pulse duration decreased in a linear fashion. which can be attributed to a decrease in the absorber lifetime [8].

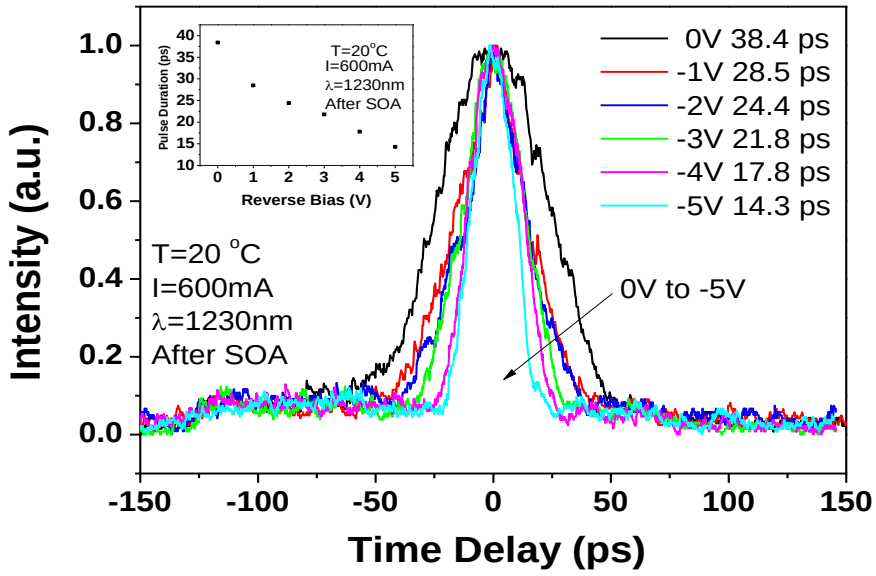

Figure 6-8 Autocorrelation trace at reverse bias from 0 V to 5 V and forward current of 600 mA on the gain chip and SOA current of 2180 mA at 20 °C at the operation wavelength of 1230 nm, assuming a Gaussian shaped pulse with a loots resolution.

The peak power was found to vary as a function of wavelength (Figure 6-9) and maximum peak power of 4W occurred for wavelength of 1230nm with corresponding pulse duration of 14.3 ps.

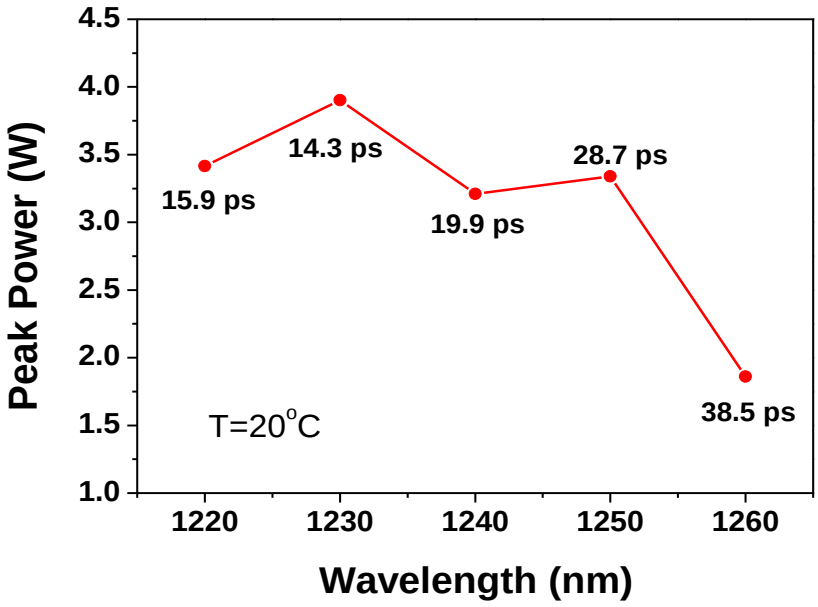

Figure 6-9 Output peak power from SOA under different wavelengths at 20 °C. Gain chip current and SOA current are 600 mA and 2180 mA, respectively. The highest peak power is around 4 W.

The tunability range can be increased by increasing the forward current, as shown in Figure 6-10. It can be seen that this widening of the tunability range occurs preferentially on the blue side of the spectrum, which can be attributed to the increasingly stronger carrier filling of the higher-energy, higher-degeneracy ES levels, as previously observed in CW tunable QD lasers. In comparison, the carrier density and hence the spectral width of gain are pinned above threshold and do not increase with current in other type of lasers [4]. Under the gain chip current of 600 mA, a 42 nm tuning range was therefore achieved with stable fundamental mode-locked operation.

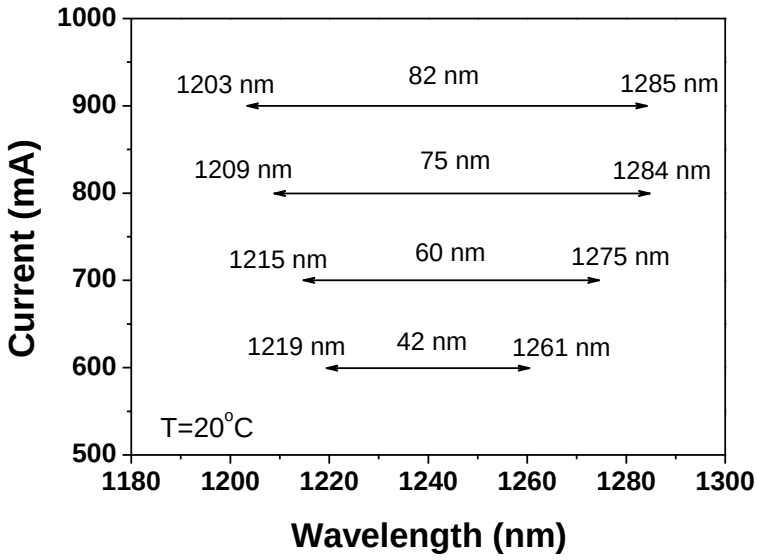

Figure 6-10 Mode-locked tuning range limits from the gain chip under different forward currents at 20 °C.

6.6.3 Results 2nd-order diffraction grating

Utilising the tunable MOPA setup in mode-locked operation, with a 600 mA bias current applied to the gain chip (corresponding to 3.1 KA/cm^2) and SOA current of 2180 mA (710 A/cm^3), it was possible to achieve a tuning range of 60 nm for the InAs/GaAs QD-ECMLLs in the SOA configuration at 20°C. The optical spectra for the 2nd order diffraction grating are shown in Figure 6-11.

.

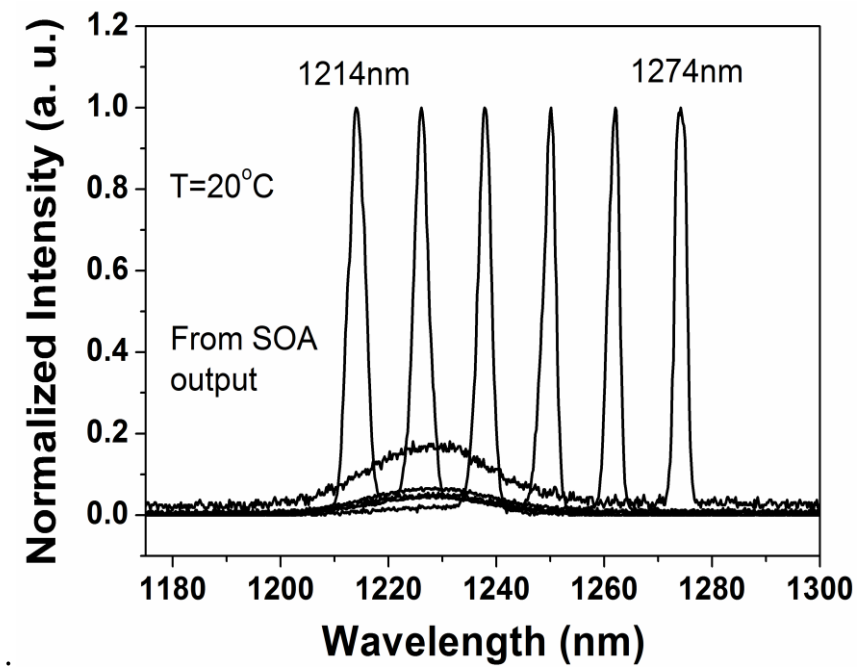

Figure 6-11 Pulse characteristics of two representative operation wavelengths of 1226 nm and 1214 nm.

In order to determine the pulse characteristics for the laser, the output light was passed into an autocorrelator and a trace obtained for a number of peaks, as shown in Figure 6-11. The results for two such peaks (1226 nm and 1214 nm) are shown in Figure 6-12 and Figure 6-13 respectively. For the operation wavelength of 1226 nm (Figure 6-12) a Gaussian curve fitted to the data resulted in an FWHM of the autocorrelation trace (Δt) of 21.1 ps and a deconvolved pulse duration ($\Delta \tau$) of 15 ps. Under the same conditions (temperature and current), the pulse characteristics for the 1214 nm wavelength resulted in an FWHM of the autocorrelation trace (Δt) of 23.3 ps and a deconvolved pulse duration ($\Delta \tau$) of 16.5 ps (Figure 6-13).

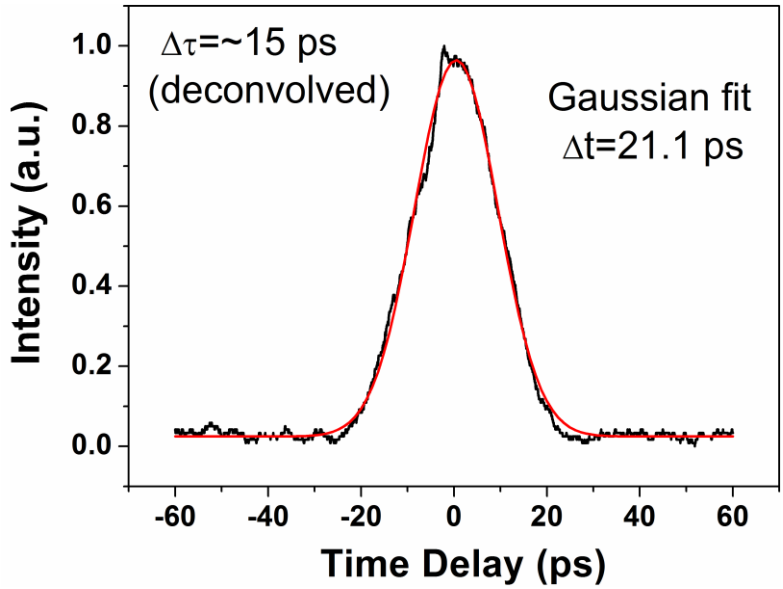

Figure 6-12 Autocorrelation trace at reverse bias of 1 V and forward current of 600 mA on the gain chip and SOA current of 2180 mA at 20 °C at the operation wavelength of 1226 nm.

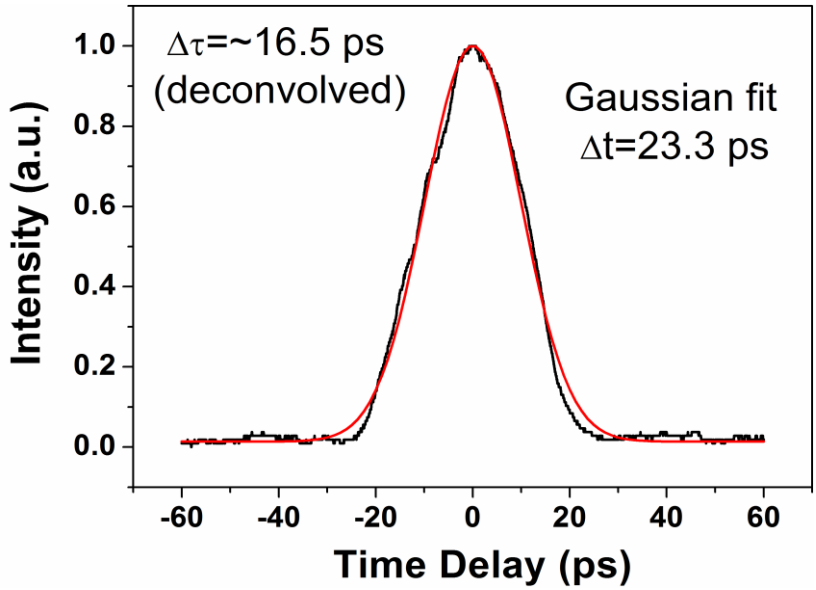

Figure 6-13 Autocorrelation trace at reverse bias of 5 V and forward current of 600 mA on the gain chip and SOA current of 2180 mA at 20 °C at the operation wavelength of 1214 nm.

In order to determine the RF characteristics for the laser, the output light was passed into a RFSA and a trace obtained for a number of peaks, The results for two such peaks (1226 nm and 1214 nm) are shown in Figure 6-14 and Figure 6-15 respectively.

At the operating wavelength of 1226 nm see Figure 6-14 from which it can be seen that at this wavelength there is a high signal-to-noise ratio and that the fundamental repetition rate was 1.316 GHz which exhibits a dynamic range (signal-to-noise ratio) of 45 dB. Furthermore it can be seen that mode-locking indeed occurs for the operating wavelength of 1226 nm. Under the same conditions (temperature and current), RF characteristics for the 1214 nm wavelength resulted, showing that at this wavelength there is a high signal-to-noise ratio and that the fundamental repetition rate of 1.324 GHz exhibits a dynamic range of 45 dB (Figure 6-15). Therefore it can be seen that mode-locking indeed occurs for the operating wavelength of 1214 nm.

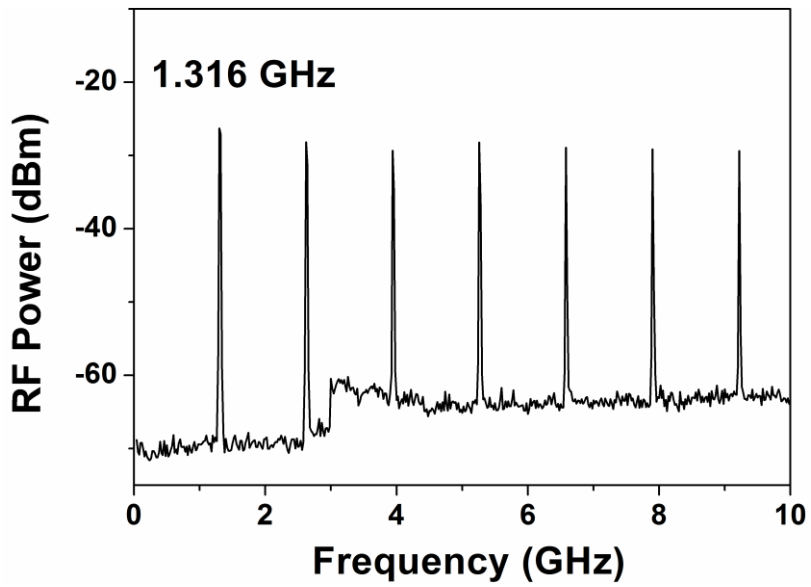

Figure 6-14 RF spectrum at reverse bias of 5 V and forward current of 600 mA on the gain chip and SOA current of 2185 mA at 20 °C at the operation wavelength of 1226 nm.

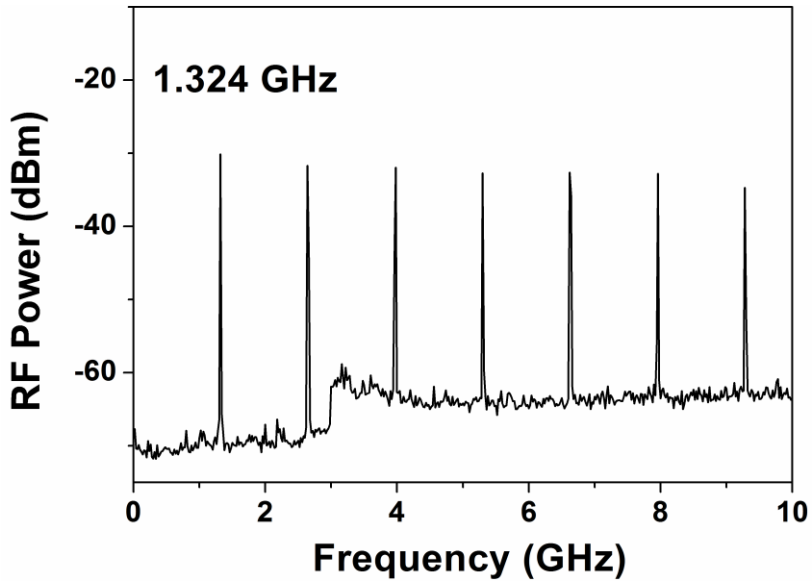

Figure 6-15 RF spectrum at reverse bias of 2 V and forward current of 600 mA on the gain chip and SOA current of 2185 mA at 20 °C at the operation wavelength of 1214 nm.

Output peak power and gain from SOA at different wave lengths are shown in Figure 6-16 and maximum peak power of 4.39 W occurs for wavelength of 1226 nm with corresponding pulse duration of 15 ps. The peak power spectral density of (max: 31.4 dBm/nm) can be seen.

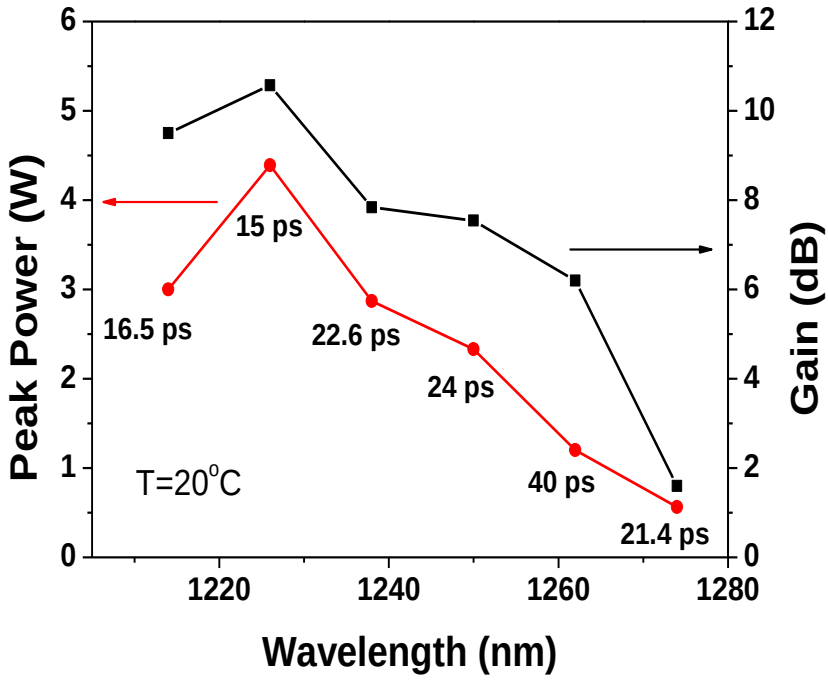

Figure 6-16 Output peak power and gain from SOA at different wavelengths. Gain chip current and SOA current are 600 mA and 2185 mA, respectively. The highest peak power is around 4.39 W.

The tunability range can be increased by increasing the forward current, as shown in Figure 6-17. The tuning range in from these cases can be increased by increasing the injection current of the gain chip. The maximum fundamental mode-locking (FML) wavelength tuning range of nearly 96 nm (from 1187 nm to 1283 nm) is presented in Figure 6-17. It can be seen that this widening of the tunability range occurs preferentially on the blue side of the spectrum, which can be attributed to the previous mentioned mechanism, i.e. increasingly stronger carrier filling of the higher-energy, higher-degeneracy ES levels, as previously observed in CW tunable QD lasers. Under the gain chip current of 600 mA, a 60 nm tuning range was therefore achieved with a stable fundamental mode-locked operation.

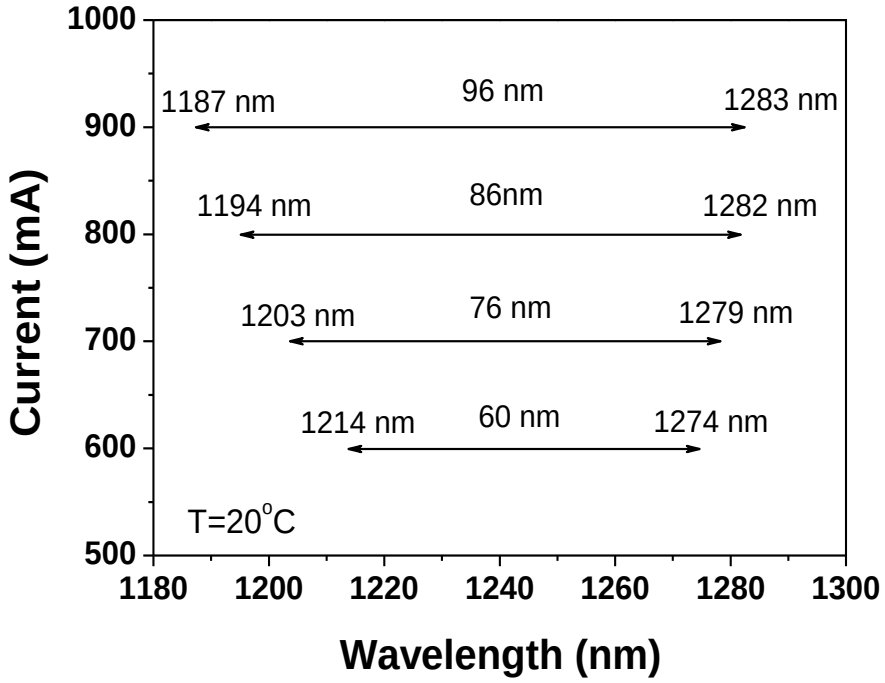

Figure 6-17 Mode-locked tuning range limits from the gain chip under different forward currents at 20 °C (for sub mount).

6.7 Comparison Between 1st-order and 2nd-order Diffraction Grating for Tuning Range

Broad wavelength tunability in the mode-locked regime was achieved under various bias conditions: gain chip current of 600 mA to 900 mA, reverse bias applied to the absorber section of the gain chip changing between 1 V and 5 V, and SOA current of 2180 mA.

As shown in Figure 6-18 the tuning range from both cases can be increased by increasing the injection current of the gain chip. The maximum fundamental mode-locking (FML) wavelength tuning range of nearly 100 nm (from 1187 nm to 1283 nm) has been achieved under 900 mA current applied to the gain chip with the 2nd-order diffraction grating. In comparison, the maximum FML wavelength tuning range with a 1st-order diffraction grating is only 82 nm under the similar operating conditions.

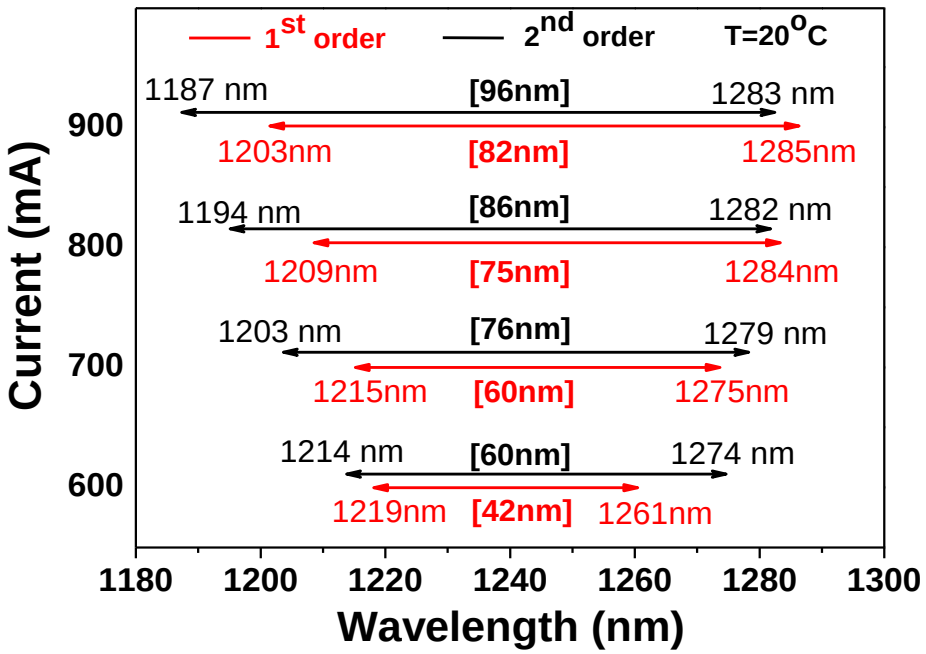

Figure 6-18 Tuning range limits for the MOPA system operating in the mode-locking regime for different pump currents applied to the gain chip and constant SOA current of 2180 mA for two configurations of the external cavity: using the 1st (red lines) and the 2nd (black lines) diffraction grating orders.

Applying a higher injection current, of 1A, to the gain chip, a 118-nm tuning range was achieved from the 2nd-order diffraction grating, Figure 6-19. FML stability (from the RF linewidth and signal-to-noise ratio) under such a high current is not, however, as good as that under a relatively low current because of a faster gain recovery [9]. Investigation is still in progress.

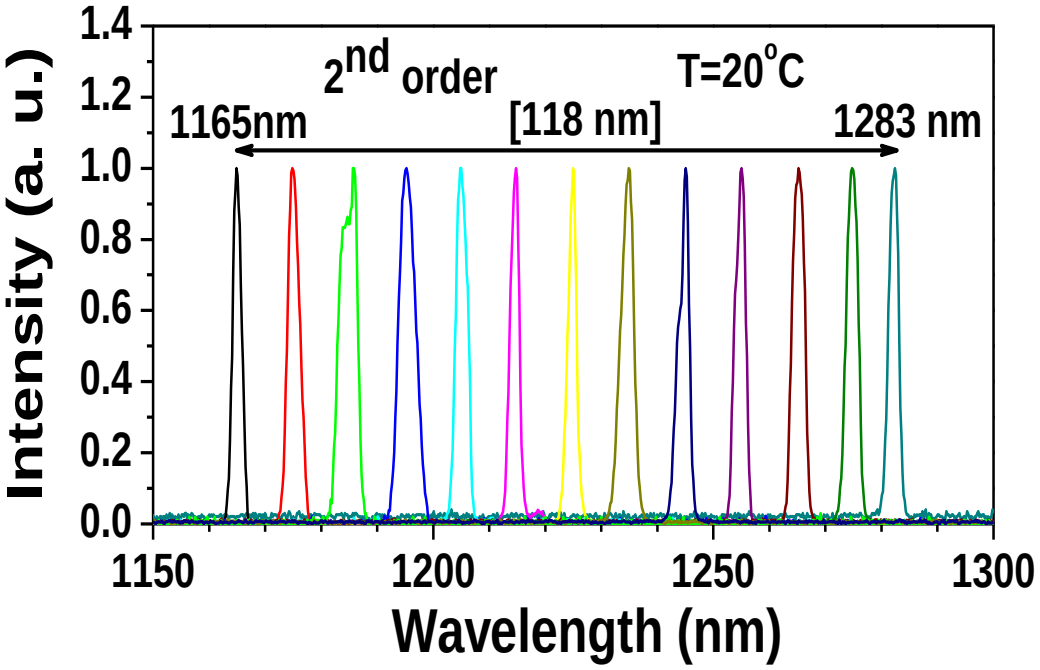

Figure 6-19 Optical spectra of tunable gain chip in mode-locked operation with gain chip current of 1 A, reverse bias of 0 V to 4 V.

In principles, the output power from the configuration with a 1st-order diffraction grating should be higher than that from the configuration with a 2nd-order one, whereas, we did not find any obvious difference between the two configurations with the different DG orders. As shown in Figure 6-20, the highest peak power of 4.39 W was obtained from the MOPA with a 2nd-order diffraction grating at 1226 nm wavelength for gain chip and SOA currents of 600 mA and 2185 mA respectively.

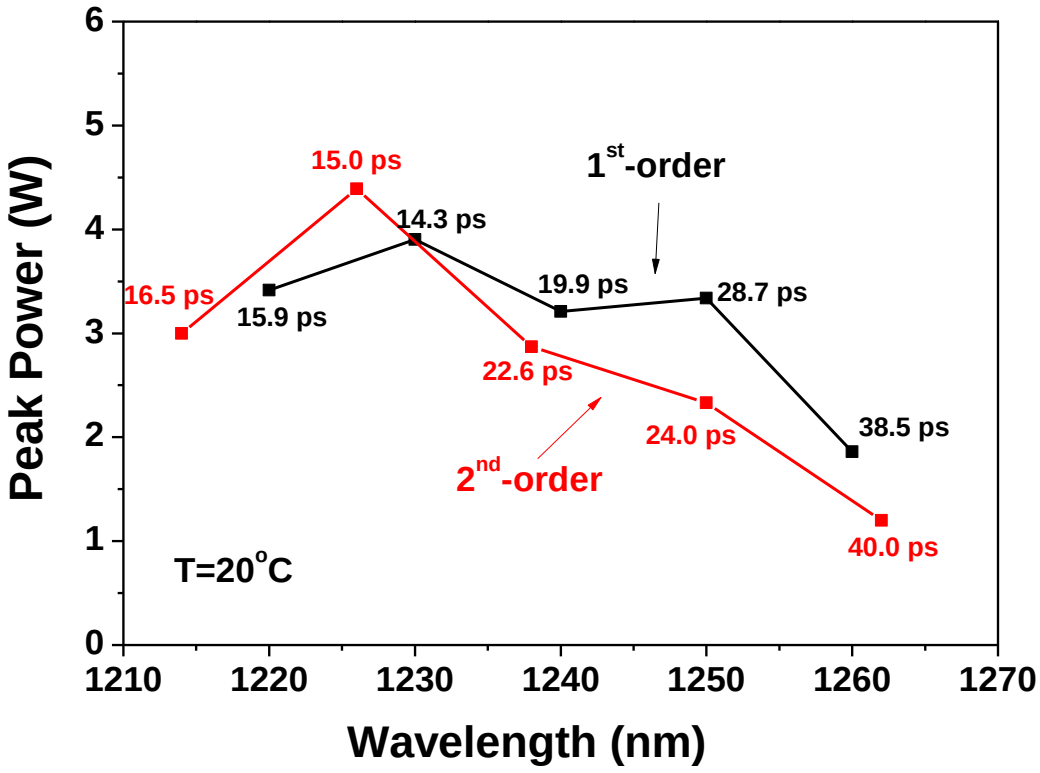

Figure 6-20 Dependence of the MOPA output peak power on wavelength for the 1st (black curve) and the 2nd (red curve) diffraction grating orders. Gain chip and SOA currents are 600 mA and 2185 mA, respectively.

The peak power from the configuration with a 1st-order DG is, however, higher than that from the configuration with a 2nd-order DG for the longer wavelength side (over 1230 nm). The peak power does not changes very much when an increasing current is applied to the gain chip because the pulse duration increases with the increasing current and offsets the increase of average output power with the increasing current.

For the 2nd-order DG configuration, this can be treated as a stricter filter as a bigger angle is required, so that the optical spectra should be narrower than those for the 1st-order DG configuration. Correspondingly, the pulse duration from the setup with the 1st-order DG should be somewhat narrower than that from the setup with the 2nd-order DG. As expected, we found a full-width at high maximum (FWHM) of the optical spectra from the setup with the 2nd-order DG was found to be much narrower than that from the setup with the 1st-order DG within the whole tuning range from the experiments. On the

other hand, the pulse durations from the two cases are similar although slightly broader pulse duration from the 2nd-order diffraction can be observed. The narrowest pulse of approximately14 ps was found from the set-up with the 1st-order DG. The dynamic contrast of RF spectra from the 1st-order DG is better than that from the 2nd-order DG, which indicates the mode-locking stability from a 1st-order DG is better and each case has its own merits.

The peak power spectral density which describes how the peak power of a pulse is distributed with wavelength is very important for some applications [10]. In Figure 6-21 it can be seen that the peak power spectral density obtained with the 2nd-order DG is much higher than that from the 1st-order DG under similar conditions, which can be attributed to the obvious difference in the FWHM of optical spectra.

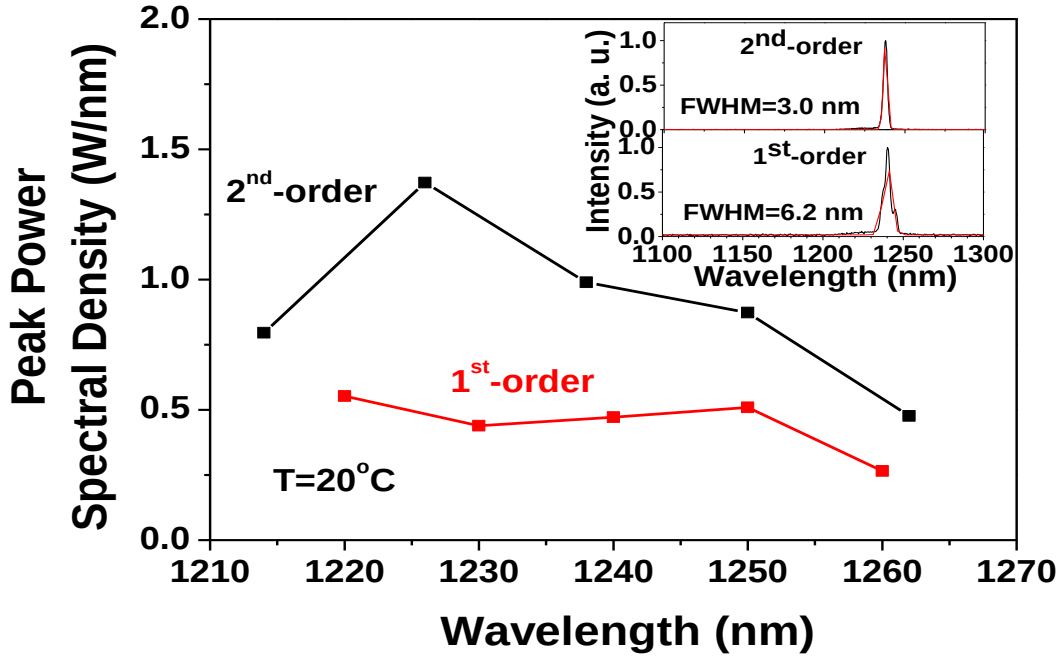

Figure 6-21 Comparison of the peak power spectral density of the MOPA at different wavelengths for the 1st (black curve) and the 2nd (red curve) diffraction grating orders. Gain chip and SOA currents are 600 mA and 2185 mA, respectively. Inset: the optical spectra from the two configurations with the different DG orders.

6.8 Conclusions

Our experiment demonstrates a comparison of the two configurations with 1st-order and the 2nd-order DG. The following conclusions were drawn. Although the tuning range in both cases can be improved by increasing the injection current of the gain chip, a broader tuning range, a narrower optical spectra and higher peak power spectral density (maximum of 1.37 W/nm) can be achieved in a configuration with the 2nd-order DG. The advantage of the narrowest pulse (~14 ps) can be found from the 1st-order DG, however and the dynamic contrast of RF spectra in the 1st order diffraction is also better. It is evident that there are advantages to be found in both cases depending on the chosen outcome i.e. a broad tuning range or a narrow pulse.

In terms of potential applications, the peak power spectral density obtained with the 2nd-order DG is much higher than that in the 1st-order DG under similar conditions, which suggests that the 2nd-order DG is more promising.

6.9 References

[1] Y. Ding, R. Aviles-Espinosa, M. Cataluna, D. Nikitichev, M. Ruiz, M. Tran, Y. Robert, A. Kapsalis, H. Simos, C. Mesaritakis, T. Xu, P. Bardella, M. Rossetti, I. Krestnikov, D. Livshits, I. Krestnikov, D. Syvridis, M. Krakowski, P. Loza-Alvarez, and E. Rafailov, "High peak-power picosecond pulse generation at 1.26 μm using a quantum-dot-based external-cavity mode-locked laser and tapered optical amplifier," *Optics Express*, vol. 20, pp. 14308-14320, 2012.

[2] H. Yokoyama, A. Sato, H.-C. Guo, K. Sato, M. Mure, and H. Tsubokawa, "Nonlinear-microscopy optical-pulse sources based on mode-locked semiconductor lasers," *Optics Express*, vol. 16, pp. 17752-17758, 2008.

[3] A. Alhazime, Y. Ding, D. Nikitichev, K. Fedorova, I. Krestnikov, M. Krakowski, and E. Rafailov, "Broadly tunable quantum-dot based ultra-short pulse laser system with different diffraction grating orders," *Electronics Letters*, vol. 49, pp. 364-366, 2013.

[4] K. A. Fedorova, M. A. Cataluna, I. Krestnikov, D. Livshits, and E. U. Rafailov, "Broadly tunable high-power InAs/GaAs quantum-dot external cavity diode lasers," *Optics Express*, vol. 18, pp. 19438-19443, 2010.

[5] A. Kovsh, I. Krestnikov, D. Livshits, S. Mikhrin, J. Weimert, and A. Zhukov, "Quantum dot laser with 75nm broad spectrum of emission," *Optics Letters*, vol. 32, pp. 793-795, 2007.

[6] S. E. Haggett, M. Krakowski, I. Montrosset, and M. A. Cataluna, "High-Power 1230-nm Quantum-Dot Tapered External Cavity Laser, with 100 nm Tunability," in *CLEO: Science and Innovations*, 2014, p. JTu4A. 123.

[7] Y. Ding, A. Alhazime, D. Nikitichev, K. Fedorova, M. Ruiz, M. Tran, Y. Robert, A. Kapsalis, H. Simos, C. Mesaritakis, T. H. Xu, P. Bardella, M. Rossetti, I. Krestnikov, D. Livshits, I. Montrosset, D. Syvridis, M. A. Cataluna,

M. Krakowski, and E. Rafailov, "Tunable Master-Oscillator Power-Amplifier Based on Chirped Quantum-Dot Structures," *IEEE Photonics Technology Letters*, vol. 24, pp. 1841-1844, Oct 2012.

[8] Z. I. Alferov, V. M. Andreev, E. L. Portnoi, and M. K. Trukan, "AlAs-GaAs heterojunction injection lasers with a low room-temperature threshold," *Sov. Phys*, vol. 3, pp. 1107-1110 1970.

[9] Y. Ding, D. Nikitichev, I. Krestnikov, D. Livshits, M. Cataluna, and E. Rafailov, "Quantum-dot external-cavity passively modelocked laser with high peak power and pulse energy," *Electronics Letters*, vol. 46, pp. 1516-1518, 2010.

[10] J. Hagen, R. Engelbrecht, B. Lins, B. Schmauss, and L. Gruner-Nielsen, "Optimization of the power spectral density of Raman-MOPAs using fiber Bragg gratings with tunable chirp," in *Optical Fiber Communication/National Fiber Optic Engineers Conf, 2008. OFC/NFOEC 2008. Conference on*, 2008, pp. 1-3.

Chapter 7. **High-Power Electrically Pumped Vertical External-Cavity Surface-Emitting Lasers (EP- ECSELs)**

7.1 Introduction

The most recent achievement was mode-locked EP-VECSELs with average output power up to 40 mW at a repetition rate of 15 GHz and pulses as short as 14.8 ps [1-2]. In the present experiment the focus was on different parameters with the finding that a significant reduction of laser repetition rate occurred with a subsequent increase of peak power. A quantum dot based semiconductor saturable absorber mirror (QD-SESAM) was used to mode-lock the laser, resulting in a low pulse fluence and a relieved cavity design. Average output power of 8 mW during the mode-locked operation was achieved at a repetition rate of 216 MHz, which corresponds to an optimised cavity length with a pulse duration of 24 ps at emission wavelength of 980 nm. Subsequent optimisation of all parameters enabled significant peak power scaling with values up to tens of watts.

7.2 EP-VECSEL Sample 1

The EP-VECSEL samples were designed and fabricated by Sheffield University for experimental testing, with an active region consisting of six quantum wells $Ga_{0.9}AsP_{0.1}$. N-DBR had 12 pairs of graded GaAs/$Al_{0.8}Ga_{0.2}As$. The samples were grown on the n-DBR GaAs substrate in reverse order. P-DBR had 32 pairs of graded

GaAs/$Al_{0.8}Ga_{0.2}As$. The samples had a 100-µm diameter ring contact, and were designed for 980 nm emission. Figure 7-1 shows a photograph of the device.

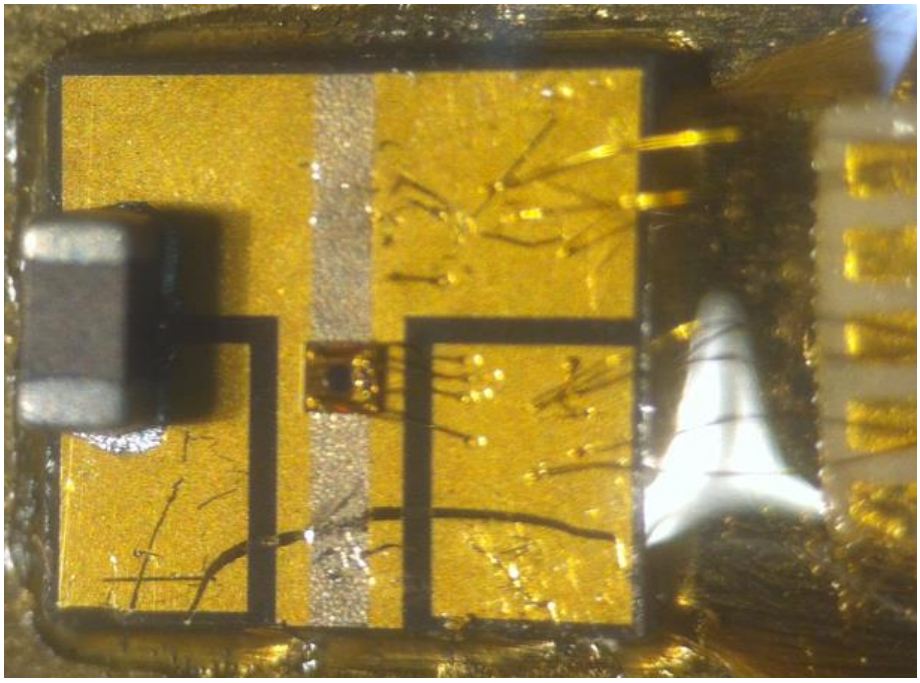

Figure 7-1 Photograph of EP-VECSEL sample.

A semiconductor saturable absorber mirror (SESAM) designed for 980 nm was grown by Molecular Beam Epitaxy (MBE). The absorbing section contained two layers of InGaAs quantum dots (QDs) sandwiched between GaAs barriers. The absorbing structure was resonant and grown on top of a DBR which had 28 pairs of ¼ lambda thick GaAs/AlGaAs layers resulting in peak absorption at 967 nm. QD SESAMs were previously successfully used to mode-lock solid state, fibre lasers and OP-VECSELs [3-4]. QD-SESAMs typically feature low saturation fluence, fast recovery times and low loss compared with QW absorbers [5].

7.2.1 Experimental Set-up

The EP-VECSEL device was operated under two different methods, (1) continuous wave (CW) and, (2) mode-locked operation. For these experiments, the device was

mounted on a copper heat sink, with its temperature controlled by a thermoelectric cooler.

The EP-VECSEL was first tested in CW regime, where a straight external cavity was formed using an output coupler with a RoC = -50 mm, with OC reflectances of 90 %, 96 % and 98 %. A maximum output power up to 30 mW was achieved under pump currents of 350 mA, from the device with 100 µm aperture and a 13-pair n-DBR. In general, devices with 100 µm aperture demonstrated the best performance, which suggests that this is the optimum size of ring contact aperture for such devices.

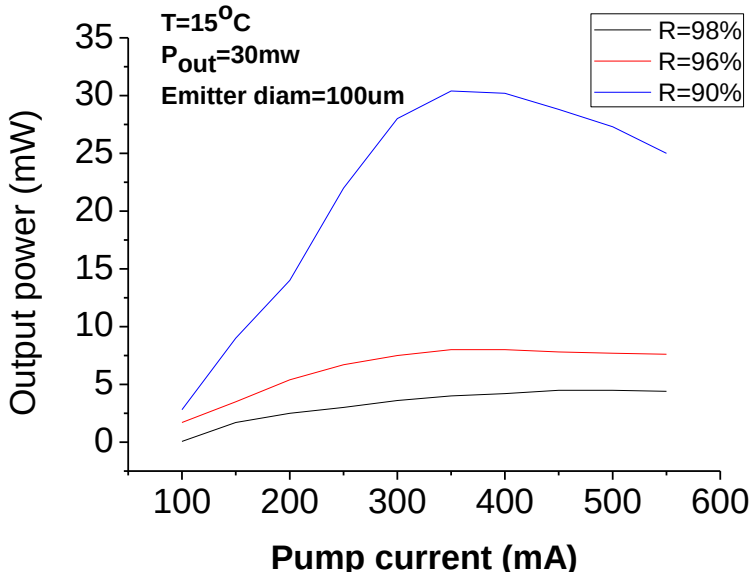

Figure 7-2 Pump output power characteristics.

The current-output power characteristics curve of the device is shown in Figure 7-2 for different transmissions. The highest output power was found with an OC reflectance of 90%. The EP-VESCEL was held at a temperature of 15 °C by the use of the temperature controller for the various OC transmission experiments. The wavelength of the EP-VESCEL was measured to be approximately 980 nm (Figure 7-3).

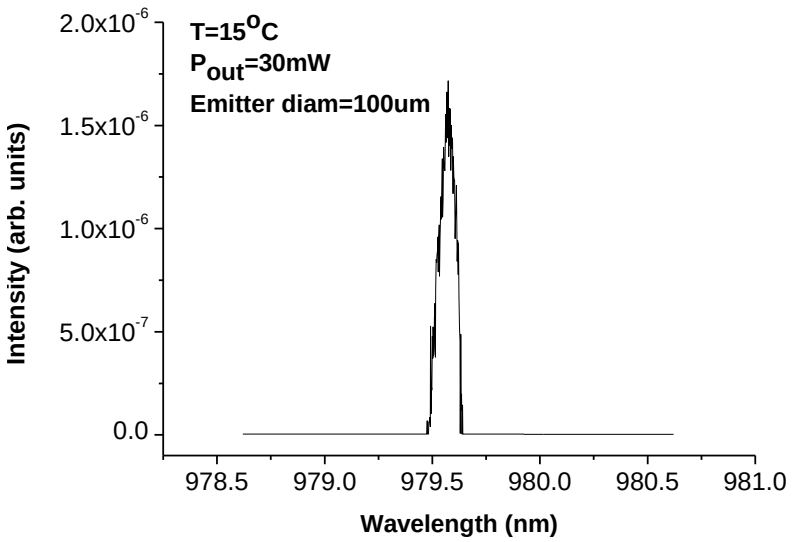

Figure 7-3 Optical spectrum of the EP-VECSEL sample.

For the mode-locking measurements; a multi-folded cavity was built using plano-concave and plane mirrors. The multi-folded cavity has a much longer length in order to, reach the lowest repetition rates. An output coupler with a RoC= -50 mm and 10 % transmission formed one end of the cavity whilst the SESAM closed the other end. The SESAM designed for optical spectra 980 nm and a saturated transmission of 6 %. The SESAM was mounted on temperature-controlled copper mounts. The temperature of QD-SESAM was set to 25 °C for the most stable operation. The experimental setup for the mode locking measurements is shown in Figure 7-4.

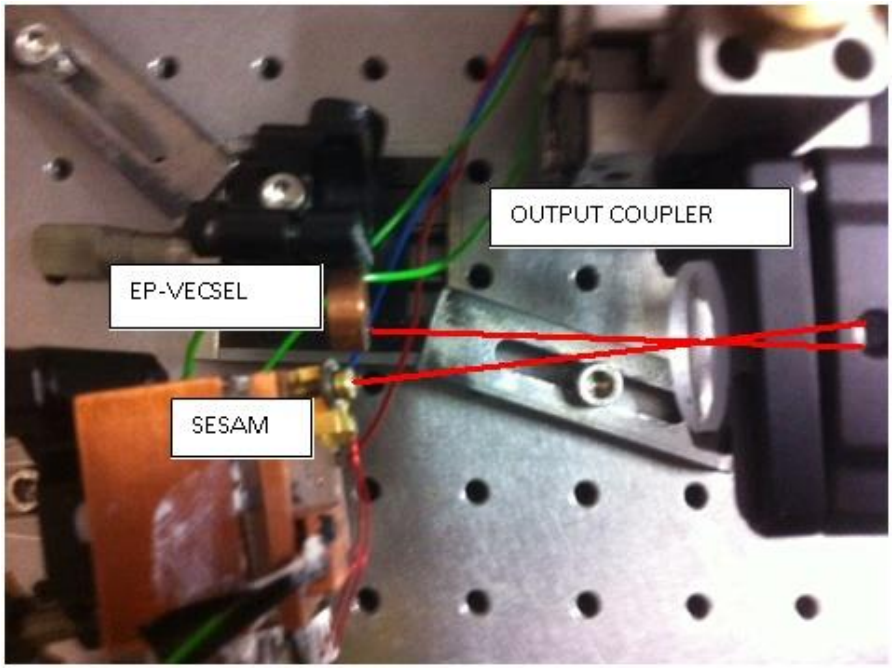

Figure 7-4 Top view of the EP-VECSEL cavity for mode-locking.

RF characteristics for the operation wavelength of 1230 nm are presented in Figure 7-5 from which it can be seen that at this wavelength there is a high signal to noise ratio and that the fundamental repetition rate was 1.46084 GHz which exhibits a dynamic range of 45 dB. Furthermore it can be seen from the inset that mode-locking is indeed occurring for the operating wavelength of 980 nm.

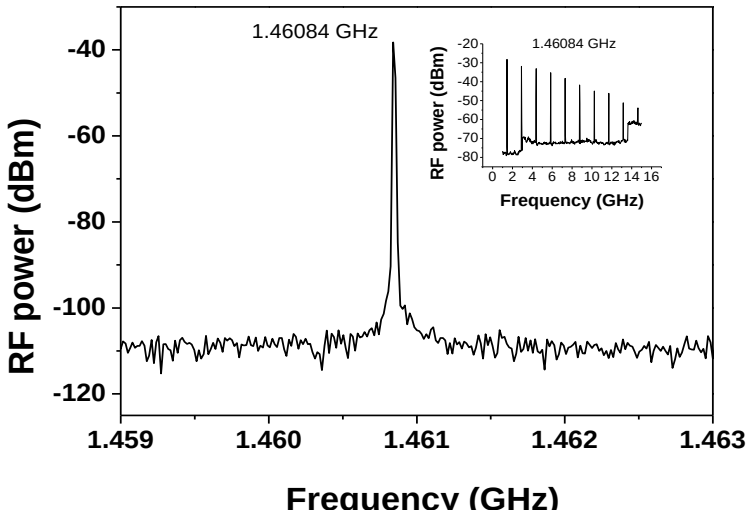

Figure 7-5 RF spectrum of mode-locked EP-VECSEL. The inset shows a number of subsequent harmonics of the spectrum.

In order to determine the pulse characteristics for the laser, the outputted light was passed into an autocorrelator and a trace obtained for the pulse shown in Figure 7-6, the results for optical spectrum peaks of 980 nm are shown in Figure 7-3. A Gaussian curve fit to the data results in a FWHM of the autocorrelation trace (Δt) of 36 ps and a deconvolved pulse duration (Δτ) of 23.3 ps. The peak power was calculated to be 3W at the wavelength of 980 nm.

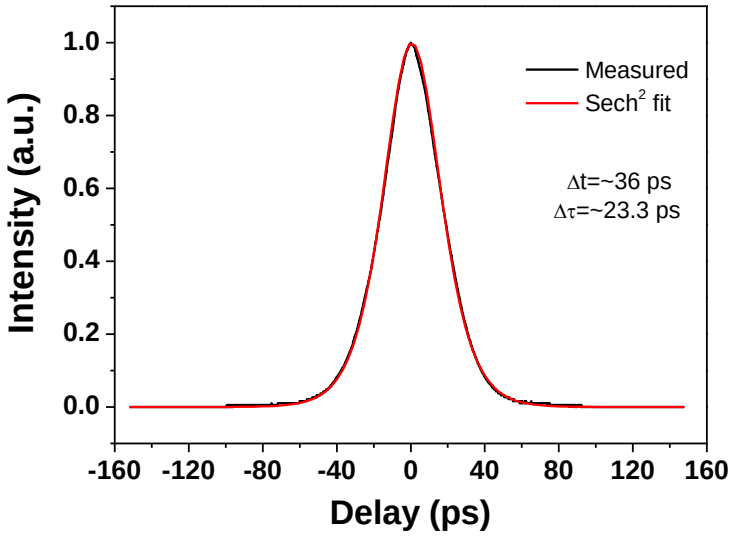

Figure 7-6 Autocorrelation at 280 mA gain current for mode-locking regime.

In summary, a quantum dot saturable absorber was used to passively mode lock an EP-VECSEL which was received from project partners for experimental testing. The devices was first tested in the CW configuration, the highest output powers achieved from such devices was up to 30 mW. The device was then tested in mode-locking experiments and pulsed operation was observed from the devices. The measurements indicated 23.3 ps pulse width with 10 mW average output power at 1.46 GHz repetition for the device operated at 980 nm.

7.3 EP-VECSEL Sample 2

Another EP-VECSEL used in this work was produced by Novalux, US and both its optical mode and wavelength was controlled by an extended compound optical cavity. The active region of the VECSEL was composed of several strain compensated InGaAs/GaAsP MQWs, grown by organometallic vapour deposition on top of an n-type multilayer GaAs/AlGaAs Bragg reflector (DBR, R ~0.7) and n-GaAs substrate. A MQW structure with strain may give a higher material gain. A high reflectivity p-type DBR completed the epitaxial structure that was bonded through a dielectric layer with an aperture providing electrical contact to a heatsink. The n-contact defined an optical aperture within the device to help stabilise the output into a TEM_{00} mode. The n-DBR was to partly offset finite absorption losses for light travelling through the n-GaAs substrate, as well as to stabilise the frequency output of the VECSEL [6]. Figure 7-7 shows a photograph of the device.

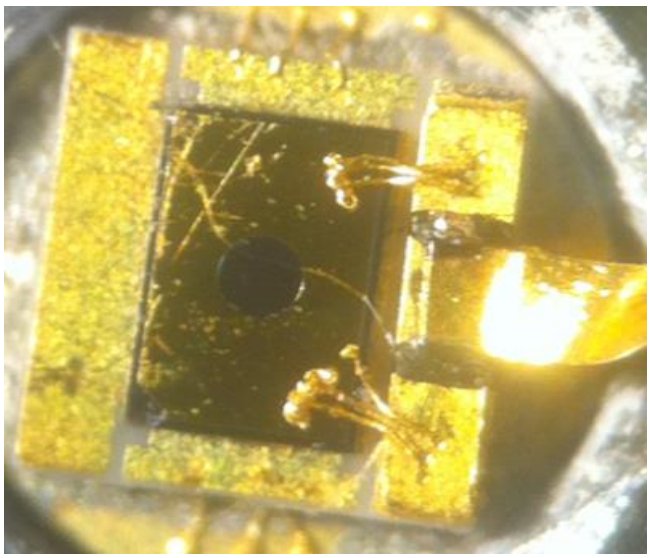

Figure 7-7 Top view of EP-VECSEL showing active region of the device. Diameter: 150 µm.

A semiconductor saturable absorber mirror (SESAM) designed for 980 nm was grown by Molecular Beam Epitaxy (MBE). The absorbing section contained two layers of InGaAs quantum dots (QDs) sandwiched between GaAs barriers. The absorbing

structure was resonant and grown on top of a DBR which had 28 pairs of ¼ lambda thick GaAs/AlGaAs layers with peak absorption at 967 nm. QD SESAMs have been successfully used to mode-lock solid-state fibre lasers and OP-VECSELs [3-4]. Compared with QW absorbers QD-SESAMs typically feature lower saturation fluence, faster recovery times and lower loss [5]. Luminescence spectra of both EP-VECSEL and SESAM are shown in Figure 7-8.

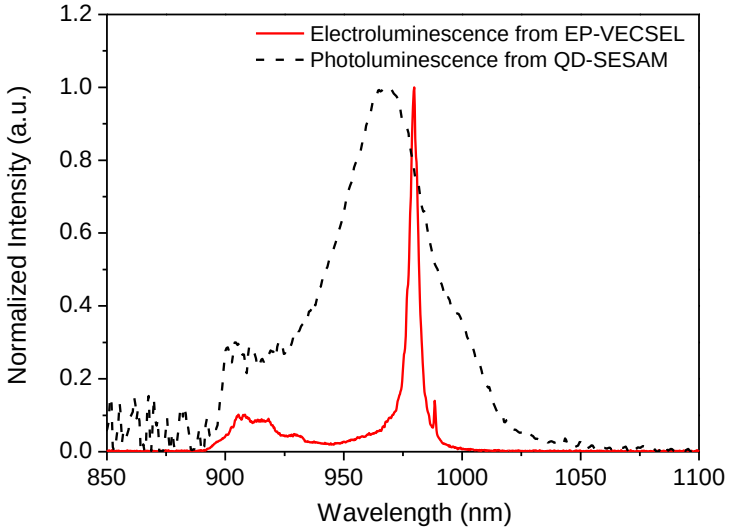

Figure 7-8 Red line shows electroluminescence measured from EP-VECSEL. Black line indicates the photoluminescence spectrum measured from the top of the QD-SESAM.

7.3.1 Experimental Set-up

The EP-VECSEL was first tested in CW regime with a straight two-mirror cavity formed from a RoC = -75 mm output coupler with 10 % transmission at 980 nm. In this configuration, output power up to 218 mW was achieved under a pump current of 850 mA. The current output power characteristic curve of the device is shown in Figure 7-9. For mode-locking experiments, a multi-folded cavity was built with plano-concave and plane mirrors. An output coupler with a RoC = -100 mm and 10 % transmission formed one end of the cavity and a SESAM closed the other end. The gain and SESAM were

mounted on temperature-controlled copper mounts. The temperature of QD-SESAM was set to 25 °C and the QW gain structure was 15°C for the most stable operation. Mode spot sizes on gain and SESAM were set to 75 µm in radius. A schematic drawing of the experimental laser cavity is shown in Figure 7-10.

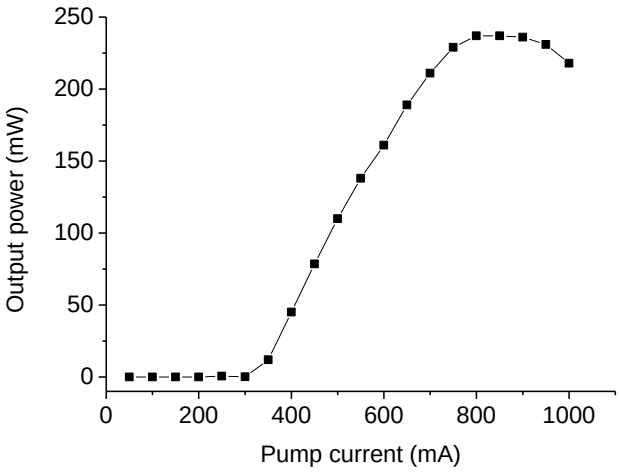

Figure 7-9-Light characteristics of EP-VECSEL operated in CW regime.

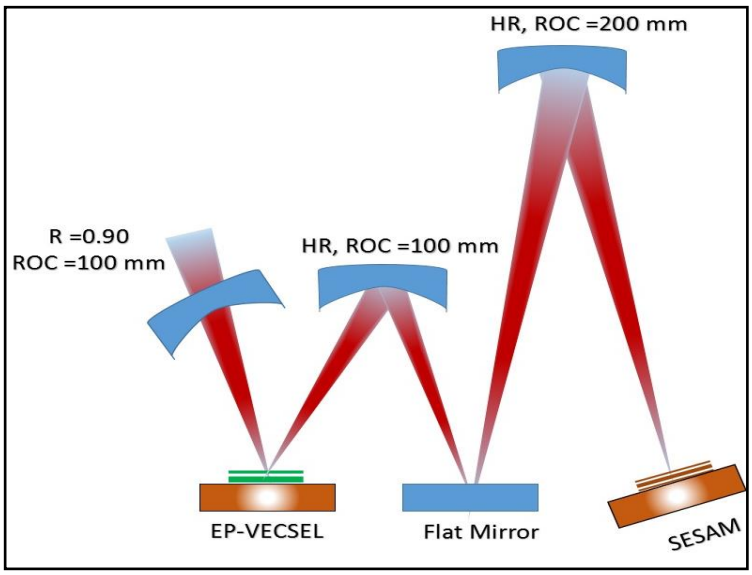

Figure 7-10 A schematic diagram of optical cavity layout for 980-nm mode-locked EP-VECSEL.

RF characteristics for the operation wavelength of 980 nm are presented in Figure 7-11 from which it can be seen that at this wavelength there is a high signal to noise ratio and the fundamental repetition rate was 216 MHz which exhibited a dynamic range of 45 dB. Furthermore it can be seen from the inset that mode-locking occurs at the operating wavelength of 980 nm. The spectrum was measured with a resolution bandwidth of 10 kHz.

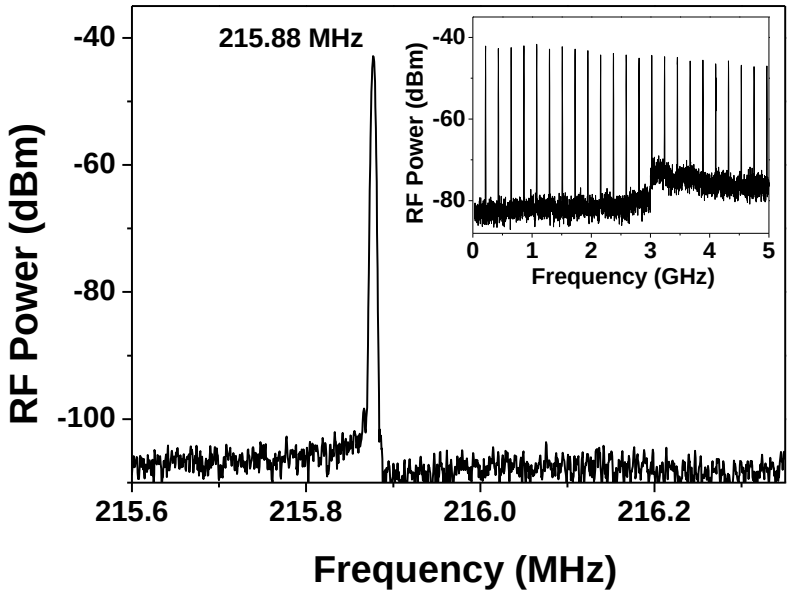

Figure 7-11 RF spectrum of mode-locked EP-VECSEL. The inset shows a number of subsequent harmonics of the spectrum.

The average output power of 8 mW was achieved with a direct pump current value of 730 mA.

For the operation wavelength of 980 nm (Figure 7-12) a $sech^2$ curve fitted to the data resulted in an FWHM of the autocorrelation trace (Δt) of 37 ps and a deconvolved pulse duration ($\Delta \tau$) of 24 ps. The output spectrum of the sample was centred at approximately 980 nm with FWHM = 0.07 nm and is shown in the inset of Figure 5-16. The pulses were 1.66 times transform-limited and the peak power was calculated to be 1.56 W.

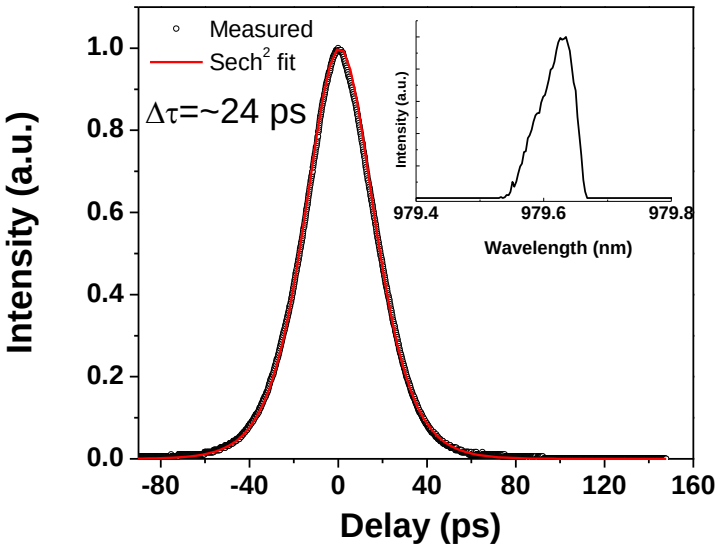

Figure 7-12 Autocorrelation trace of mode-locked EP-VECSEL indicating 24 ps pulse duration. The inset shows optical spectrum centred at 979.6 nm.

Slightly improved average output power could be achieved in the shorter cavity configuration where the output power was measured as 34 mW with pulse duration of 42 ps at a repetition rate of 499 MHz. Beam quality parameter M^2 was measured as approximately 1.23 in this configuration, as shown in Figure 7-13. It is believed that the increase in output power in the 499 MHz repetition rate set-up was a result of more efficient energy storage in the laser's upper state and a reduction of losses in the shorter cavity because of divergence and reflection losses. Furthermore, the pulse energy required to saturate the absorber should be constant, which implies that a higher repetition rate should correspond to a higher average output power [7].

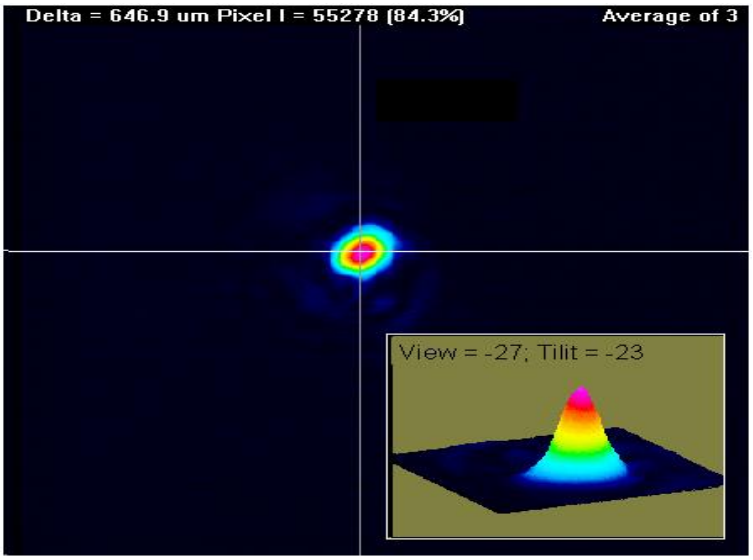

Figure 7-13 Beam quality parameter M^2 was measured as ~1.23 in this configuration.

The 216 MHz repetition rate was the minimum that could be achieved in this experiment because operation in a longer cavity would become unstable or would switch to harmonic mode-locking. For the stable mode-locking, the fundamental mode peak should be higher than other harmonics. On the other hand, the harmonics are sometimes higher than the fundamental peak and at other times the fundamental peak is higher than the harmonics if the mode-locking is unstable [8-9]. Although OP-VECSELs were mode-locked in similar and lower repetition rates, it is considered hardly achievable as cavity round-trip time becomes significantly longer than upper-state lifetime in the gain. Recently it was suggested that the phase amplitude effect could play a role in addition to the classical mode-locking image of interplay between gain and saturable absorber [10], especially when structures based on QW and QD are integrated, thus providing different alpha factors [11]. A deeper understanding of VECSEL dynamics is therefore necessary to explore the lower limit of repetition rate in this type of laser.

7.4 Conclusions

A quantum dot saturable absorber was used to passively mode-lock an EP-VECSEL at a record low repetition rate of 216 MHz. EP-VECSELs need higher repletion rate probably because they need to have the same power from a smaller volume. Furthermore, the laser produced 8 mW average output power with 24 ps pulse width at 980-nm emission wavelength and a peak power of 1.56 W was achieved. This low repetition rate demonstrates potential peak power scalability - further scaling of average output power and pulse duration will increase the peak power of the EP-VECSEL to more than 10 W. The increase of peak power has direct biomedical application in the form of nonlinear imaging techniques.

7.5 References

[1] K. Jasim, Q. Zhang, A. Nurmikko, E. Ippen, A. Mooradian, G. Carey, and W. Ha, "Picosecond pulse generation from passively modelocked vertical cavity diode laser at up to 15 GHz pulse repetition rate," *Electronics Letters,* vol. 40, pp. 34-36, 2004.

[2] K. Jasim, Q. Zhang, A. Nurmikko, A. Mooradian, G. Carey, W. Ha, and E. Ippen, "Passively modelocked vertical extended cavity surface emitting diode laser," *Electronics Letters,* vol. 39, pp. 373-375, 2003.

[3] A. A. Lagatsky, C. G. Leburn, C. T. A. Brown, W. Sibbett, S. A. Zolotovskaya, and E. U. Rafailov, "Ultrashort-pulse lasers passively mode locked by quantum-dot-based saturable absorbers," *Progress in Quantum Electronics,* vol. 34, pp. 1-45, 2010.

[4] K. G. Wilcox, M. Butkus, I. Farrer, D. A. Ritchie, A. Tropper, and E. U. Rafailov, "Subpicosecond quantum dot saturable absorber mode-locked semiconductor disk laser," *Applied Physics Letters,* vol. 94, Jun 2009.

[5] A. Lagatsky, F. Bain, C. Brown, W. Sibbett, D. Livshits, G. Erbert, and E. Rafailov, "Low-loss quantum-dot-based saturable absorber for efficient femtosecond pulse generation," *Applied Physics Letters,* vol. 91, pp. 231111-231111-3, 2007.

[6] E. U. Rafailov, W. Sibbett, A. Mooradian, J. G. McInerney, H. Karlsson, S. Wang, and F. Laurell, "Efficient frequency doubling of a vertical-extended-cavity surface-emitting laser diode by use of a periodically poled KTP crystal," *Opt. Lett.,* vol. 28, pp. 2091-2093, 2003.

[7] A. G. Vladimirov and D. Turaev, "Model for passive mode locking in semiconductor lasers," *Physical Review A,* vol. 72, p. 033808, 2005.

[8] Y. Ding, D. Nikitichev, I. Krestnikov, D. Livshits, M. A. Cataluna, and E. Rafailov, "Fundamental and harmonic mode-locking with pulse repetition rate between 200 MHz and 6.8 GHz in a quantum-dot external-cavity laser," in *The European Conference on Lasers and Electro-Optics*, 2011, p. CF_P23.

[9] M. Xia, M. G. Thompson, R. V. Penty, and I. H. White, "External-cavity mode-locked quantum-dot laser diodes for low repetition rate, sub-picosecond pulse generation," *IEEE Journal of Selected Topics in Quantum Electronics*, vol. 17, pp. 1264-1271, 2011.

[10] M. Butkus, E. Viktorov, T. Erneux, C. Hamilton, G. Maker, G. Malcolm, and E. Rafailov, "85.7 MHz repetition rate mode-locked semiconductor disk laser: fundamental and soliton bound states," *Optics Express*, vol. 21, pp. 25526-25531, 2013.

[11] A. Alhazime, M. Butkus, C. Hamilton, and E. Rafailov, "216 MHz repetition rate passively mode-locked electrically-pumped VECSEL," in *SPIE LASE*, 2014, pp. 89660K-89660K-5.